SURROGATE-ENABLED SEISMIC PERFORMANCE ANALYSIS OF

SPATIALLY DISTRIBUTED BRIDGES

JING QIAN

PhD

The Hong Kong Polytechnic University

2022

The Hong Kong Polytechnic University

Department of Civil and Environmental Engineering

Surrogate-enabled Seismic Performance Analysis of Spatially Distributed Bridges

Jing QIAN

A thesis submitted in partial fulfilment of the requirements for the degree of Doctor of

Philosophy

August 2022

Certificate of Originality

I hereby declare that this thesis is my own work and that, to the best of my knowledge and belief, it reproduces no material previously published or written, nor material that has been accepted for the award of any other degree or diploma, except where due acknowledgement has been made in the text.

_____   _____ (Signed)

Jing QIAN (Name of student)

Abstract

Transportation networks are crucial for the development of society. The spatially distributed bridges are vulnerable components within transportation networks. Earthquakes can occur stochastically within the service life of the bridges, damage the bridges, disrupt the functionality of transportation networks, and cause social, economic, and environmental consequences. Performance-based earthquake engineering (PBEE) is a new-generation philosophy for the assessment and decision-making of bridges. In this context, the bridges are expected to satisfy different performance objectives concerned by the stakeholders.

Due to the existence of dependence and uncertainty from multiple sources within PBEE, improving the confidence of seismic performance analysis of bridges is an essential task to aid effective design and management. It is necessary to develop an integrated framework dealing with uncertainty and dependence to jointly improve the confidence of PBEE. Besides, the occurrence of earthquakes is associated with stochastic time and intensity, and deterioration can continuously affect the performance of structures over time. Carbon neutrality and resilience are emerging goals of society. To contribute to a sustainable and resilient city, an approach of life-cycle sustainability and resilience assessment is needed. Novel structures should be developed to mitigate the seismic hazards considering life-cycle performance.

In this thesis, a surrogate-enabled performance analysis framework is developed for spatially distributed bridges against earthquakes. The confidence of seismic

performance assessment is jointly improved by appropriate IM selection, advanced demand surrogate model, multi-criteria global sensitivity analysis, and complex dependence capture. An approach for seismic intensity measure (IM) selection incorporating the trade-off among multiple criteria is proposed. An acceleration algorithm is formulated to develop the seismic demand surrogate model for performance assessment. A two-stage multi-criteria global sensitivity analysis approach coupling surrogate model and decision technique is developed to identify the holistic sensitive parameters to the system. A vine-copula-based approach is proposed to capture the complex dependence within the assessment. The historical data and artificially generated data from numerical models are used to develop the predictive models.

Then, the performance assessment is extended to a life-cycle context. An approach for life-cycle sustainability and resilience assessment of bridges is introduced incorporating the compound effects of earthquakes and deterioration. The time-dependent performance is computed based on the deterioration process. The stochastic renewal process is used to model the stochastic occurrence of the earthquake. The life-cycle sustainability and resilience can be computed by accumulating the consequences arising from potential hazards within an investigated time horizon. Finally, the life-cycle performance of a potential hazard mitigation solution (steel-shape memory alloy reinforced bridge) is assessed. New insights into the life-cycle cost and benefit of the novel bridge in terms of sustainability and resilience are provided.

Overall, the developed framework provides technical foundations of confident seismic performance analysis to aid the design and management of spatially distributed bridges against earthquakes.

Publications Arising from the Thesis

Journal papers:

Qian, J., & Dong, Y. (2020). Multi-criteria decision making for seismic intensity measure selection considering uncertainty. *Earthquake Engineering & Structural Dynamics*, *49*(11), 1095-1114. **(JCR Q1; Top journal identified by Chinese Academy of Sciences)**

Qian, J., & Dong, Y. (2022). Uncertainty and multi-criteria global sensitivity analysis of structural systems using acceleration algorithm and sparse polynomial chaos expansion. *Mechanical Systems and Signal Processing*, *163*, 108120. **(JCR Q1; Top journal identified by Chinese Academy of Sciences)**

Qian, J., & Dong, Y. (2022). Surrogate-assisted seismic performance assessment incorporating vine copula captured dependence. *Engineering Structures*, *257*, 114073. **(JCR Q1; Top journal identified by Chinese Academy of Sciences)**

Qian, J., Dong, Y., & Frangopol, D. M. (2022). Probabilistic long-term resilience of bridges under seismic and deterioration processes. In *Proceedings of the Institution of Civil Engineers-Bridge Engineering (Ahead of Print).*

Qian, J., Zheng, Y., Dong, Y., Wu, H., Guo, H., & Zhang, J. Sustainability and resilience of steel-SMA reinforced concrete bridge under compound earthquakes and functional deterioration within entire life-cycle **(JCR Q1; Top journal**

identified by Chinese Academy of Sciences)

Chen, L., **Qian, J.**, Tu, B., Frangopol, D. M., & Dong, Y. (2021). Performance-based risk assessment of reinforced concrete bridge piers subjected to vehicle collision. *Engineering structures*, *229*, 111640. **(JCR Q1; Top journal identified by Chinese Academy of Sciences)**

Li, Y., Dong, Y., & **Qian, J.** (2020). Higher-order analysis of probabilistic long-term loss under nonstationary hazards. *Reliability Engineering & System Safety*, *203*, 107092. **(JCR Q1; Top journal identified by Chinese Academy of Sciences)**

Zhang, N., Gu, Q., Dong, Y., **Qian, J.**, & Zheng, Y. (2021). Seismic performance of bridges with ECC-reinforced piers. *Soil Dynamics and Earthquake Engineering*, *146*, 106753.

Conference papers and presentations:

Qian, J., Yan, B., Zhang, Y., & Dong, Y. Eurasian Conference on OpenSees, Hong Kong, China (2019). Effects of simplified modeling on bridge seismic vulnerability and risk assessment.

Qian, J., & Dong, Y. The 7th International Symposium on Reliability Engineering and Risk Management, Beijing, China (2020). Efficient seismic vulnerability and risk assessment of highway bridges using surrogate models.

Qian, J., & Dong, Y. The 10th International Conference on Bridge Maintenance, Safety and Management Hokkaido, Japan (2020). Seismic intensity measure selection

under multiple criteria and uncertainty.

Qian, J., & Dong, Y. The Engineering Mechanics Institute Conference, New York, USA (2021). Surrogate-assisted performance-based earthquake engineering incorporating vector intensity measure and complex dependence.

Qian, J., & Dong, Y. The second ZHITU symposium on advances in civil engineering (2021). Surrogate-assisted efficient multi-criteria global sensitivity analysis of structural systems.

Qian, J., & Dong, Y. The 13th International Conference on Structural Safety & Reliability, Shanghai, China (2022). Sparse polynomial chaos expansion-aided resilience assessment of bridges under seismic hazards.

x

Acknowledgments

During my Ph.D. study at the Hong Kong Polytechnic University, I received vital support from many people and organizations. In this regard, I would like to express my appreciation to all of them.

First and foremost, I would like to express my sincere gratitude to my chief supervisor, Prof. You Dong, for his continuous support, professional guidance, and invaluable inspiration throughout my Ph.D. study. This work has been progressively directed, motivated, advanced, and reviewed by Prof. Dong. I believe this work could not exist without Prof. Dong's contribution and supervision. Prof. Dong's keen insights, creative thinking, and art of leadership show me the path to an outstanding scholar. Beyond the research, Prof. Dong is a life mentor who provides enlightening ideas. The things I learned from Prof. Dong are important assets and will benefit my future life and career. I am looking forward to collaborating more and learning more from Prof. Dong in the future.

I would like to express my sincere gratitude to my co-supervisor Prof. Yong Xia, for his encouragement, help, and support during my study. I would like to thank the members of my doctoral board of examiners Prof. Songye Zhu, Prof. Hao Zhang, and Prof. C.W. Lim for their time, efforts, and comments on my research. My thanks also go to Prof. Dan M. Frangopol and Prof. Yue Zheng for their support during the collaboration.

My sincere appreciation is expressed to my current and former colleagues in Prof.

Dong's group including Dr. Peng Yuan, Dr. Ruiwei Feng, Dr. Hongyuan Guo, Dr. Xiaoming Lei, Dr. Yaohan Li, Dr. Bing Tu, Dr. Anastasios Giouvanidis, Dr. Junlin Heng, Mr. Ghazanfar Ali Anwar, Miss. Menghan Zhao, Mr. Deming Zhu, Mr. Fuhao Deng, Miss. Qian Wu, Mr. Li Lai, Mr. Yu Zhang, Mr. Jiaxin Zhang, Mr. Jingyao Hu, Mr. Wingwai Cheng, and Mr. Chenbo Wang for their warm help and friendship.

Last but not least, I deeply appreciate my family for their constant encouragement and unconditional support throughout my whole life.

Table of Contents

List of Figures

List of Tables

CHAPTER 1
INTRODUCTION

1.1   Background

In the context of regional seismic performance assessment, bridges with different geometry and material parameters are spatially distributed in a region. Different bridges can be associated with different behavior under seismic hazards. The uncertainties associated with the spatially distributed bridges should be taken into consideration to develop a unified model to facilitate regional performance assessment. The probabilistic bridge parameters can be determined from the inventory data in a region. The spatially distributed bridges within the transportation networks play an important role in the development of society and the economy. It facilitates access to human activities at both the normal operational stage and post-hazard stage (e.g., emergency response, rescue, and restoration). Over the past decades, bridges have experienced damage under earthquakes, leading to severe consequences. During the 2008 Wenchuan earthquake in China, 46 bridges experienced severe damage, and 128 bridges experienced moderate damage. The total loss of the transportation system in that event is over 10 billion dollars (Han et al., 2009; Xie, 2017). After the 1994 Northridge earthquake, around 150 million dollars were spent on repairing 230 damaged bridges, and 120 million dollars were spent on recovering 6 collapsed bridges (Kiremidjian & Basöz, 1997). During the 1989 Loma Prieta earthquake, 144 highway bridges were damaged (Gordon, 2002), and 42 people were killed due to the collapse

of the Cypress Street Viaduct of Interstate 880 in West Oakland (Tarakji, 1992). From the lessons of previous events, the earthquake can cause damage to the transportation network, resulting in consequences associated with social, environmental, and economic aspects. (Han et al., 2009; Stanford, 1998; Tierney, 1997; Wakabayashi & Kameda, 1992).

At the early stage, bridges are designed to prevent different damage levels under different seismic severity levels. After the 1994 Northbridge and 1995 Kobe earthquakes, it is found that the indirect loss (e.g., downtime) and direct loss (e.g., repair cost) are tremendous, even though the bridges were designed to satisfy conventional safety requirements (Lee & Mosalam, 2006). Performance-based earthquake engineering (PBEE) was then developed to aid the design and decision-making of structures considering performance objectives (e.g., economic loss, fatality, and downtime) concerned by stakeholders (Anwar, Dong, & Li, 2020; Asadi et al., 2019; Mosalam et al., 2018). In this engineering philosophy, the structures are expected to satisfy different performance objectives. PBEE generally involves probabilistic hazard analysis, seismic demand prediction, damage analysis, and consequence evaluation (Baker & Cornell, 2008). There exist uncertainties associated with hazards, structures, and consequences. A probabilistic approach was developed by the Pacific Earthquake Research (PEER) center considering a wide range of uncertainties. In FEMA P-58, a general approach was introduced for seismic performance assessment of structures, and the performance can be assessed in terms of casualties, repair cost, repair time, and environmental impacts (FEMA). Sustainability is a multi-dimensional measure of

performance assessment including social, economic, and environmental metrics (Dong et al., 2013). Resilience measures the capability of a system for maintaining safety and recovering from extreme events. Improving confidence in performance assessment is an emerging task.

Due to the existence of uncertainties, selecting an appropriate seismic intensity measure (IM) and developing an advanced demand prediction model can improve assessment confidence. An earthquake ground motion contains complex time-series information. A measure to describe the intensity of the hazard is required in PBEE. It can link the hazard to structural vulnerability and further connect to consequences. An appropriate seismic IM can reduce the uncertainty of the assessment (Padgett et al., 2008). Bridges contain multiple components resulting in multiple failure modes. The optimal IMs may not be consistent for different components and failure modes (Wang et al., 2018). Another important concern in improving the confidence of assessment is seismic demand prediction. In traditional cloud analysis, a linear regression between the logarithmic space of seismic IM and demand is used to predict the probabilistic seismic demand. Some advanced surrogate models for seismic performance assessment were developed to improve the accuracy (Ghosh et al., 2013; Jeon et al., 2019; Mangalathu, Heo, et al., 2018; Mangalathu, Jeon, et al., 2018; Wang et al., 2022). There is a need to refine the seismic IM selection approach by incorporating multiple criteria and components. It is an essential trend to further explore the advanced surrogate models within PBEE for confident assessment.

As complex dependence exists within PBEE, modeling dependence is a key component to ensure a confident assessment. Dependence modeling can affect the results of performance analysis under natural hazards (Wang *et al.*, 2020; Zeng, Zhang and Wang, 2020). Dependence can result from multiple IMs and multiple demands. The dependence should be modeled for multiple demands to formulate the joint probabilistic seismic demand models. The dependence should be modeled for probabilistic hazard analysis to identify the probabilistic vector IMs. The assumption of the joint lognormal distribution of IMs and demands is widely used in previous studies for dependence modeling (FEMA). The linear correlation coefficients among multiple IMs and demands are used to compute the joint distributions. Nonlinear and complex dependence characteristics (e.g., central-, lower-, and upper-tail dependence) can appear for multivariant variables. Neglecting the complex dependence can cause unrealistic joint probabilistic distributions and may lead to biased performance assessment. It is necessary to introduce a more flexible and general data-inferred approach to develop the model capturing complex dependence characteristics within PBEE. The effects of dependence modeling on seismic performance should be investigated.

The uncertainties can be from multiple sources and understanding the influence of the probabilistic input on output is necessary to aid the treatment of uncertainty and refine the database. The global sensitivity analysis can be used to assess the effects of the whole variations of input variables on the output. The Monte Carlo method can be used to compute the global sensitivity index by running a large number of simulations

(Sobol, 2001). The high computational time hinders the application in complex physical models. Bridges are associated with multiple components and failure modes. Most of the existing sensitivity analysis approaches can only identify the sensitive parameters of the individual outcome. However, the critical parameters may be different considering different structural performance criteria (Jeon et al., 2019). There is a need to reduce the computational time of the global sensitivity analysis and advance the approach to identify the holistic sensitive parameters considering multiple performance criteria.

Bridges can suffer multiple earthquakes and continuous deterioration within the service life, the performance assessment including sustainability and resilience should be extended to a life-cycle perspective. The occurrence of multiple earthquakes is stochastic in time, and it can be modeled using a stochastic process. Besides, in a marine environment, chloride can penetrate concrete cover, contact with reinforcing steel and initiate corrosion. The chloride-induced deterioration can cause the area loss of reinforcing steel and continuously affect the performance of bridges. The deterioration can increase the seismic vulnerability of bridges (Ghosh & Padgett, 2010). The compound effects on structural performance can be caused by earthquakes and deterioration. The consequences can be accumulated within the lifespan. The framework of life-cycle seismic sustainability and resilience assessment should be developed by incorporating stochastic earthquake and deterioration processes.

Overall, the confidence of PBEE can be jointly improved by selecting an appropriate IM, developing an advanced demand prediction model, performing global

sensitivity analysis, and capturing complex dependence. To provide a holistic understanding of seismic performance within the entire lifespan, sustainability and resilience should be assessed in a life-cycle context incorporating stochastic earthquake and deterioration processes.

1.2   Objectives

The goal of this research work is to develop a confident probabilistic seismic performance analysis framework for spatially distributed bridges under seismic hazards. To achieve this goal, the specific objectives are summarized as follows:

- ✧ To propose a seismic IM selection approach for structural systems considering the trade-off among multiple criteria and components.

- ✧ To develop efficient surrogate models for confident seismic demand prediction and an efficient algorithm for global sensitivity analysis incorporating multiple criteria.

- ✧ To propose a data-inferred approach to model the complex dependence from multiple sources within PBEE.

- ✧ To propose an approach for assessing the life-cycle sustainability and resilience of bridges under compound earthquakes and deterioration, and then apply it to assess the seismic hazard mitigation measures.

1.3   Thesis Organization

This thesis consists of 8 chapters. The framework of the thesis is illustrated in Figure 1.1

Chapter 1 introduces the background, objectives, and outline of the thesis.

Chapter 2 presents the literature review and the identified research gap.

Chapter 3 proposes a multi-criteria seismic intensity measure (IM) selection framework. The performance criteria of IM alternatives on different structural components are computed. A compromise decision-making process is involved in the seismic IM selection considering the trade-off among multiple components and criteria. The selected IM can aid the confident performance assessment.

Chapter 4 introduces an approach for developing the seismic demand surrogate model. The sparse polynomial chaos expansion (SPCE) is used to develop the surrogate demand model of structures by using the simulated data from numerical models. The developed surrogate model can be used for performance assessment confidently and efficiently.

Chapter 5 proposes a two-stage multi-criteria global sensitivity analysis approach to efficiently identify the holistic sensitive parameters of the bridge system. The SPCE is used to compute the global sensitivity indices with respect to different performance criteria efficiently. A decision model is employed to compute the holistic global sensitivity indices considering the trade-off among multiple performance criteria.

Chapter 6 develops a vine copula-based approach for seismic performance assessment incorporating complex dependence. The historical data and simulated data

7

sets are used to infer the vine copula model for multiple dependence sources. The developed vine copula model capturing complex dependence can be used in seismic performance assessment.

Chapter 7 proposes an approach to assess the life-cycle sustainability and resilience of bridges under compound earthquake and deterioration processes. The stochastic renewal process is used to model the stochastic occurrence of earthquakes. The deterioration process is used to compute the time-dependent performance. The life-cycle sustainability and resilience are computed by accumulating the consequences within a life span. The life-cycle sustainability and resilience of a potential hazard mitigation alternative (steel-shape memory alloy (SMA) reinforced concrete bridge) under earthquakes and deterioration are investigated. The new insights into the life-cycle cost and benefit of the steel-SMA reinforced concrete bridge in terms of sustainability and resilience are provided.

Chapter 8 contains conclusions and future work.

The PBEE framework includes hazard analysis, structural analysis, damage analysis, and performance analysis. The approaches in chapters 3-6 can jointly improve the confidence of seismic performance assessment from different aspects including the robust multi-criteria decision for IM selection, the surrogate model for uncertainty quantification, holistic multi-criteria global sensitivity analysis, and complex dependence modeling. Then, the PBEE framework is extended in a life-cycle context in chapter 7.
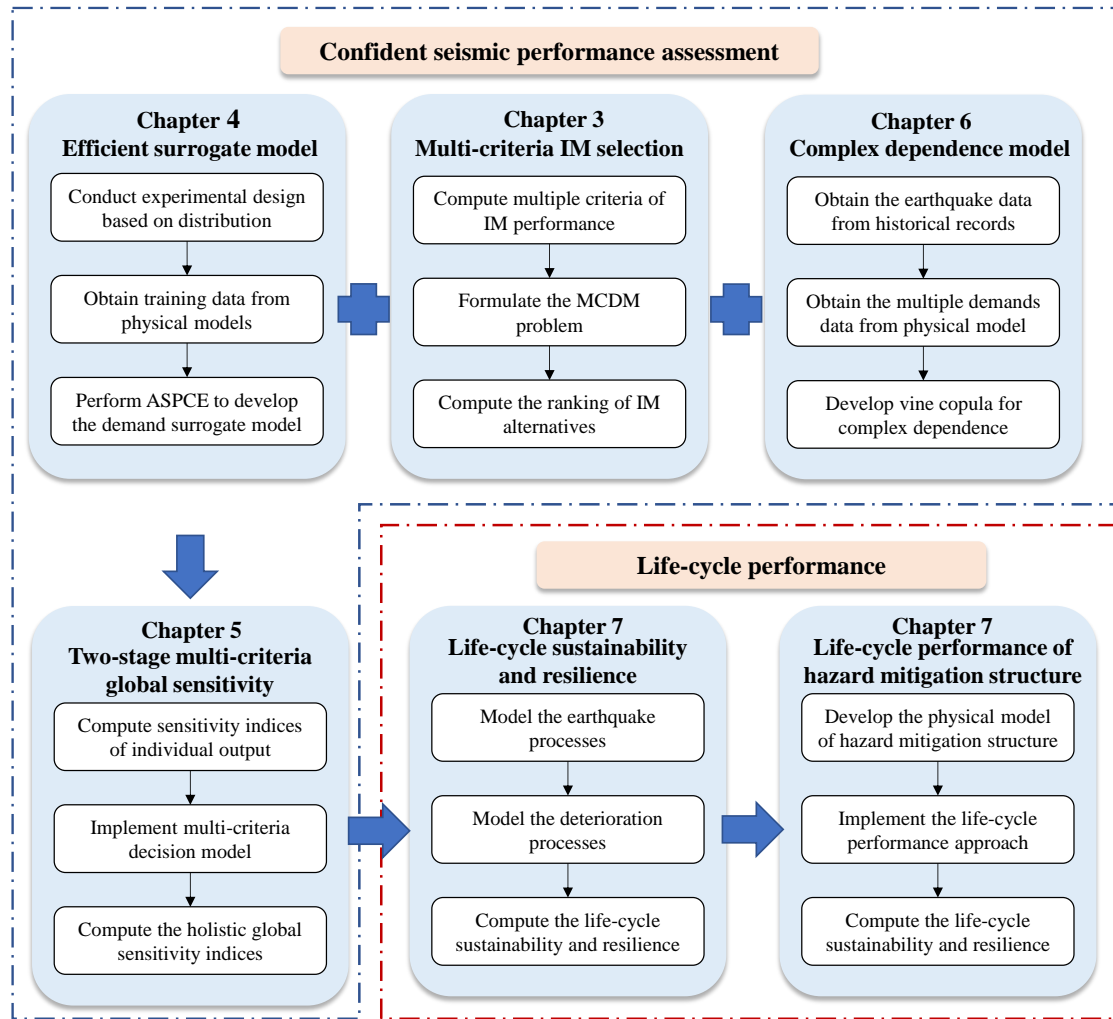
Figure 1.1 Proposed framework of the thesis

CHAPTER 2
LITERATURE REVIEW

2.1 Introduction

Within the scope of this research, this chapter reviews the development of approaches toward a confident PBEE assessment. Specifically, the studies regarding seismic IM selection, surrogate demand model, dependence modeling, sensitivity analysis, life-cycle performance, and performance of the hazard mitigation measure (steel-SMA reinforced concrete bridge) are summarized. Based on the literature, the research gaps are identified.

2.2 Seismic Intensity Measure Selection for Structural Systems

The probabilistic seismic demand model (PSDM), linking the structural demand with seismic intensity measure (IM), is a basic tool for PBEE. The PSDM is described as the probabilistic distribution of structural responses under the given seismic IM. The uncertainty reduction and efficiency improvement in PBEE are of great importance and can be accomplished by selecting an appropriate IM.

Selecting an IM is a necessary task to facilitate engineering applications and system-level analysis. For instance, to assess the regional risk, a ground motion intensity map should be generated. The ground motion intensity map is generally described by an IM such as (Miller & Baker, 2015). For engineering applications, an IM, which is systematically optimal on all the components and failure modes, can be

used to connect the intensity map. In addition, the system-level performance assessment also requires an optimal IM. A single IM is used to connect the demands of different components so that the joint PSDM can be formulated. The seismic fragility is then computed at a system level to link the performance quantification.

Studies have been conducted on the evaluations of different IMs for PSDM. For instance, Shome (Shome, 1999) assessed the performance of IMs on a building structure and found that spectral acceleration at the fundamental period is more efficient compared with peak ground acceleration (PGA). Hariri-Ardebili and Saouma (Hariri-Ardebili & Saouma, 2016) studied the optimal IM for concrete dams and found that spectral-based IMs have higher efficiency and proficiency. In addition to the conventional IMs, some novel IMs were proposed. Du et al. (Du et al., 2019) investigated the performance of posterior optimal IMs based on hysteretic single-degree-freedom systems in terms of efficiency and sufficiency. Baker and Cornell (Baker & Cornell, 2005) analyzed a vector-valued IM considering spectral acceleration and epsilon. Besides individual structure, Kazantzi and Vamvatsikos (Kazantzi & Vamvatsikos, 2015) conducted IM selection for building classes and concluded that the geometric mean of spectral accelerations is the optimal IM for the studied building classes. Some other studies further investigated the superiority of average spectral acceleration (Adam et al., 2017; Eads et al., 2015). Giovenale et al. (Giovenale et al., 2004) indicated that the performance criteria of an IM are sufficiency, efficiency, and hazard computability. Moreover, the IM selection process needs to consider practicality

and proficiency (Padgett et al., 2008). To ensure the capacity and accuracy of the PSDM, the performance properties of an IM should meet the above requirements.

In the bridge community, some studies assessed the performance of different IMs based on selected bridge component engineering demand parameters. For instance, Padgett et al. (Padgett et al., 2008) evaluated the performance of ten IMs over several components for highway bridge portfolios and pointed out that PGA was the optimal IM for the considered bridge inventory. Dong et al. (Dong et al., 2014) also used PGA as the IM to compute the sustainability of highway bridge networks at a regional scale. Some studies extended the IM performance assessment for bridges in a complex geotechnical context (Wang et al., 2018). The optimal IMs may not be consistent for different components and failure modes. For instance, Wang et al. (Wang et al., 2018) found the IM, which obtains the largest p-value (sufficiency), is not consistent for different structural demand parameters. Baker (Baker, 2011) pointed out that higher-mode (or shorter-period) excitation could contribute to the seismic demand for some structural elements of upper-story shear forces.

Triantaphyllou (Triantaphyllou, 2000) indicated that the problems are considered as multi-criteria decision problems when the following situations appear in the problems: a goal or multiple goals need to be achieved; the decision-makers are involved in the selection process; multiple alternatives act as the selection elements; multiple criteria are used to evaluate the performance of the alternatives; the preferences of the decision-makers are expressed as the weighting factors applied to the criteria; and the criterion with respect to each alternative can be quantitatively assessed.

According to the above definition, the IM selection process can be considered as a multi-criteria decision problem and the different IMs are considered as alternatives.

Overall, most of the existing studies selected the optimal IM only based on some specific criteria without considering the systematic performance over all the criteria. The trade-off among all components and criteria for selecting an optimal IM has not been well considered. The multi-criteria decision-making framework of IM selection has not been well developed.

2.3   Surrogate Demand Models

Developing fragility models serves as the basic step in PBEE and directly affects the accuracy of performance assessment. The incremental dynamic analysis (Vamvatsikos & Cornell, 2002) and multi-stripe analysis (Jalayer & Cornell, 2009) can be standardly used for fragility computation. Within these methods, the nonlinear time history analyses are performed repeatedly for different levels of ground motion intensity, causing high computational expense. Cloud analysis is an efficient approach for fragility computation, as a set of ground motions can be used and relatively fewer time history analyses are performed (Jalayer et al., 2015; Nielson, 2005).

In the context of cloud analysis, the surrogate model, representing the relationship between the input and output, can be used to emulate the output of a model efficiently. The uncertainty quantification can be conducted efficiently by using surrogate models. Using a surrogate model such as a power law model (linear regression in the logarithmic space) is the norm when employing cloud analysis (Cornell et al., 2002; Jalayer et al.,

2015; Padgett & DesRoches, 2008). The advanced surrogate models representing the complex relationship between input and response can be adopted based on a training process. In this way, multiple predictors (e.g., IMs and structural parameters) can be incorporated into surrogate models to perform an accurate performance assessment. Advanced surrogate models have been applied to engineering problems and seismic vulnerability analysis with satisfying accuracy. For instance, Ebad Sichani and Padgett (Ebad Sichani & Padgett, 2019) assessed the collision between vertical concrete dry casks using surrogate models, and the polynomial response surface with stepwise regression was found to be suitable among the investigated surrogate models. Mangalathu *et al*. (Mangalathu et al., 2018) compared the performance of different regression techniques on bridge seismic demand modeling, and Lasso regression was found to be the most effective one in terms of mean square error and absolute error. Ghosh *et al.* (Ghosh et al., 2013) investigated four surrogate models, and the parameterized fragility models were developed by employing logistic regression. The artificial neural network and Bayesian approach were also considered as alternative surrogate models to facilitate structural performance assessment (Jeon et al., 2019; Mangalathu, Heo, et al., 2018). Deep learning was employed for seismic fragility analysis (Wang et al., 2022).

The PCE is another type of surrogate model, which has been applied to several engineering problems for efficient uncertainty quantification (Guo et al., 2018; Hariri-Ardebili & Sudret, 2020; Wu & Law, 2012). The other usage of PCE is global sensitivity analysis, once the PCE is developed, the global sensitivity index can be

computed efficiently by post-processing the coefficients. The PCE utilizes the spectral representation on an appropriately established basis of polynomial functions (Marelli & Sudret, 2015; Wiener, 1938). The number of significant terms of PCE is relatively small due to the negligible high-order interaction effects and different effects of input variables on output (Blatman & Sudret, 2010). Hence, the sparse PCE which only contains a small number of significant terms was introduced. Under the same accuracy level, the required number of model evaluations for establishing sparse PCE is found to be smaller than full PCE, thus computational burden can be saved significantly by using sparse PCE (Blatman & Sudret, 2010). Some greedy algorithms such as orthogonal matching pursuit (OMP) (Doostan & Owhadi, 2011) and least-angle regression (Blatman & Sudret, 2011) were proposed to establish the sparse PCE. Additionally, algorithms were developed to establish sparse approximations using the techniques of reweighting coefficients (Candès et al., 2008) and adapting the dictionary of basis functions (Jakeman et al., 2015). One challenging issue within conventional greedy algorithms is the high computational burden for high-dimension input problems. The number of candidate basis functions increases significantly with the input dimension, and the computational cost of developing sparse PCE can increase subsequently since a complete evaluation of the candidate set is needed to identify the appropriate basis functions at each iteration. The degree of the polynomial can have a significant influence on the system response, the computation cost is high for high-degree cases, and an acceleration algorithm is needed in such cases (Sinou & Jacquelin, 2015). Considering the advantages of sparse PCE in both uncertainty quantification and

global sensitivity analysis, there is a need to formulate efficient algorithms for sparse PCE to aid the efficient and confident assessment in PBEE.

2.4   Dependence modeling within PBEE

Within the PBEE, there exists dependence from multiple sources (e.g., the demand side and IM side). Different dependence models can directly affect the joint distribution of multivariant variables thus affecting confidence in performance assessment. Multiple components and failure modes are associated with bridge systems. The dependence associated with multiple structural components should be modeled effectively to compute the vulnerability at a system level. When vector IM is used, the dependence among multiple IMs should be modeled to perform the probabilistic hazard analysis.

The assumption of the joint lognormal distribution of IMs and demands is widely used in FEMA P-58 and some other studies for dependence modeling (FEMA; Nielson, 2005; Faouzi and Nasser, 2014; Kohrangi, Bazzurro and Vamvatsikos, 2016a). This assumption may not be the optimal dependence structure for IMs and demands if another dependence modeling approach is applicable. A copula is a flexible approach for modeling the dependence of variables. In this approach, the joint distribution is decomposed as marginal distributions and dependence models (Nelsen, 2006). Compared with the assumption of multivariate normality, the copula can incorporate more dependence characteristics (e.g., central-, lower-, and upper-tail dependence) and reflect more realistic dependence features (Goda & Tesfamariam, 2015; Wang et al., 2018; Wang et al., 2020). However, for multivariate variables, the conventional copula

approach uses the same dependence structure for modeling all pairs of random variables. This constraint limits the modeling of multiple structures and characteristics of dependence among multivariate variables. Vine copula was then proposed to address this issue (Aas et al., 2009; Okhrin et al., 2017). In the vine copula approach, the joint distribution is decomposed into marginal distributions, and the multiple dependence structures among multivariate variables are captured using a system of pair copulas. The widely used assumption of multivariate normality of logarithmic IMs and demands can be considered as a specific case in the vine copula approach, where the pair copulas are all Gaussian copulas (Wang et al., 2020). To the authors' best knowledge, the vine copula approach has not been adopted for the dependence modeling of both IMs and demand surrogate models within an integrated seismic performance assessment framework.

There exists uncertainty within the seismic performance of structures (Dong & Frangopol, 2015, 2016a). The decisions obtained based on the expected performance values may not be optimal considering uncertainty (Goda & Hong, 2006). Using only expected seismic performance may not be appropriate when risk attitudes are considered within the decision-making of structures (Cha & Ellingwood, 2013). The decisions obtained based on expected seismic performance are only optimal for the risk-neutral decision-maker (Goda & Hong, 2006). The higher-order moments of loss (e.g., variance, skewness, and kurtosis) reflecting the information of probabilistic distribution are essential for decision-makers to incorporate different decision attitudes (Goda & Hong, 2006; Li, Dong, & Qian, 2020). Different decision solutions can be obtained if

18

the higher-order moments of seismic performance are different (Li, Dong, & Qian, 2020). Therefore, a confident assessment of higher-order moments of seismic performance is important to aid rational decisions. The effects of dependence modeling on higher-order moments of seismic performance should be investigated.

2.5   Sensitivity Analysis

Structural performance assessment is associated with uncertainties from different sources (Dong and Frangopol 2015; Anwar, Dong, and Zhai 2020; Li et al. 2020a). The sensitivity analysis could aid the rational treatment of uncertainties in the modeling process. The sensitivity analysis can be categorized as local sensitivity analysis and global sensitivity analysis. The local sensitivity analysis reveals the local impact of input on the model by computing the gradient of the response associated with its parameters around a nominal value (Sudret, 2008). The local sensitivity analysis can only provide the information at the point where local sensitivity is computed, the rest of the input space could not be explored (Saltelli et al., 2008).

The global sensitivity analysis aims to quantify the effects of the whole variations of input variables on the output. Compared with local sensitivity analysis, the global sensitivity analysis could avoid the limited exploration of the input space and take the interaction of different factors into consideration (Saltelli et al., 2008). The global sensitivity analysis is preferred, when the model is associated with nonlinearity, a large level of uncertainty, and interactions among input parameters (Wan et al., 2020). It is worth noting that the global sensitivity index is based on the decomposition of variance.

It uses the information of output variance without the full information of the probability density function of the output. Additionally, it only reflects the amplitude of the global sensitivity without the direction of influence of the input variable. It may not be applicable when the sensitivity information from other aspects is concerned. Decision-makers could choose different sensitivity analysis approaches based on the information of interest. This study focuses on global sensitivity analysis.

The Monte Carlo methods were developed by Sobol (Sobol, 2001) to compute the global sensitivity index. In this approach, running a large number of physical models is needed, and the computational time is high especially for complex structural systems. Then, Sudret (Sudret, 2008) derived the sensitivity index using the coefficients of the PCE. Once the PCE model is established, the PCE-based global sensitivity index can be computed analytically by post-processing the PCE coefficients with negligible computational cost. For a structural system, the responses associated with multiple performance criteria are of interest, the developed sensitivity analysis can only identify the sensitive parameters on an individual structural performance criterion. The critical parameters could be different considering different structural performance criteria (Jeon et al., 2019). Based on traditional global sensitivity analysis, it is challenging to identify the sensitive parameters considering all performance objectives. There is a need to develop an efficient global sensitivity analysis incorporating multiple criteria in the context of PBEE.

2.6   Life-cycle Seismic Performance Assessment

To assess the life-cycle performance, the performance metrics should be defined. The

stochastic hazards occurring within the entire life span of the bridges should be identified.

It is crucial to ensure that the infrastructural systems are environmental-friendly and sustainable. Carbon dioxide is a global greenhouse gas emitted from human activities (e.g., construction and traffic emissions) and it is the driver of climate change (Wang et al., 2021). The global warming of climate change has adverse effects on food security, resource, ecosystems, and among others, worsening the living condition of humans (Chu et al., 2021; Zhao et al., 2020). It can also increase the risk of natural hazards such as floods, droughts, storms, and sea-level rise (Zhao et al., 2022). Responding the climate change by achieving carbon neutrality has become an urgent need for society. On December 12, 2015, several countries reached the "Paris agreement" at Paris Climate Change Conference, to reduce greenhouse gas emissions, achieve carbon neutrality, and mitigate climate change (Anderson & Peters, 2016; Wang et al., 2021). For the structural performance assessment, attention should be paid to the consequences related to the environment (e.g., carbon dioxide emission). Sustainability is a comprehensive measure to understand the seismic performance of structures incorporating environmental, social, and economic metrics (Dong & Frangopol, 2016a). The methods for quantifying sustainability have been developed (Dong et al., 2014, 2015). The environmental metric is considered to be carbon dioxide emission. Since the social metric can be regarded as fatality, the safety of humans should be given a top priority. The economic metric can be quantified as the monetary values of direct loss (e.g., repair cost) and indirect loss (e.g., running cost and time loss)

(Dong et al., 2014, 2015). The approach to assessing time-variant sustainability has been developed considering multiple hazards (Dong et al., 2013). Sustainability has been used as the criterion for bridge network retrofit planning and building design under earthquakes (Asadi et al., 2019; Dong et al., 2015). Different structure systems may have different sustainability metrics. The social sustainability measures in schools include security, well-being, accessibility, income, service provision, and community organizations (Santa-Cruz et al., 2016).

Resilience is defined as the ability of systems to absorb disruptions and recover to a satisfying functionality state (Timmerman, 1981). Frangopol and Bocchini (2011) defined the resilience index as the ratio of integration of time-variant functionality over investigated time horizon to the total investigated time. Decò, Bocchini and Frangopol, (2013) developed a probabilistic approach to quantify the time-variant functionality and resilience of bridges considering uncertainties within the recovery process. Dong and Frangopol (2016) developed a framework to assess the seismic resilience of bridges under flood effects. Minaie and Moon (2017) developed a multistage framework to assess the resilience of bridges by incorporating expert knowledge and lessons from previous experience. The effects of different seismic intensity measures (IM) on probabilistic resilience have been assessed to support IM selection (Qian & Dong, 2020). Dong and Frangopol (2015) proposed a framework to quantify seismic resilience under mainshock and aftershock sequences. Kong and Simonovic (2019) developed an approach for assessing the resilience of infrastructure systems considering interdependence among infrastructure systems, multiple hazard interactions, and

restoration strategies. A framework was proposed to assess the resilience of a hospital system in terms of quality of service (Cimellaro et al., 2010). Argyroudis et al. (2020) proposed a framework to quantify the resilience of infrastructure under multiple hazards incorporating vulnerability, recovery rapidity, and temporal variability.

Within the service life of structures, earthquakes can occur with stochastic occurrence time and intensity. The occurrence of earthquakes can be modeled using stochastic process models (Pandey & Van Der Weide, 2017). The homogeneous Poisson process (HPP) is widely adopted for computing long-term damage costs (Liu et al., 2004). In HPP, the mean occurrence rate is assumed to be constant, and the occurrence of hazards is considered as independent from time (Takahashi, Der Kiureghian and Ang, 2004). The simplicity of HPP may not well capture the stochastic characteristics of hazards (Pandey & Van Der Weide, 2017). Due to the mechanism of energy accumulation and release, the occurrence of earthquakes is associated with time-dependent features (Matthews et al., 2002). For instance, an earthquake can occur when energy accumulation meets a critical state. The energy is released after the earthquake, and a new cycle of rupture failure starts. Considering time-dependent characteristics, the Brownian passage-time (BPT) renewal process can be used to model the long-term occurrence of earthquakes (Matthews, Ellsworth, and Reasenberg 2002; Li et al. 2020b).

In addition to earthquakes, bridges can be exposed to chloride environments. Chloride can penetrate concrete cover and contact with reinforcing steel initiating corrosion (Stewart & Al-Harthy, 2008). The corrosion product from the deteriorated steel can expand the concrete, and cracks occur in the concrete, leading to the reduction

of concrete strength. The chloride-induced deterioration can affect the performance of structures time-dependently (Guo et al., 2021a; Guo et al., 2021b). The deterioration can affect the reliability and redundancy of concrete bridges at material, component, and system levels (Tu et al., 2019). The compound effects refer to the aggravated impact caused by two or more simultaneously or sequentially occurred mechanisms of hazards (Towhata, 2013). Compound events can be categorized into three types: two or more simultaneous or successive extreme events; extreme events combined with the conditions that amplify the influences; and the combinations of non-extreme events that cause extreme events or influences (Catto & Dowdy, 2021). As an example of compound effects, a flood after an earthquake can aggravate the damage to structures and lifelines (Gautam & Dong, 2018). Compared with sole earthquake hazard, the deterioration and earthquake coupled scenarios are associated with higher seismic vulnerability and severer consequences (Shekhar et al., 2018). The deterioration and earthquake can have compound effects on structures. Assessing and mitigating the tremendous consequences induced by compound earthquakes and functional deterioration are essential. The compound effects of earthquakes and corrosion should be incorporated into life-cycle performance assessment.

From a long-term perspective, the consequences can be accumulated due to multiple disruptions. To ensure the safety and functionality of bridges within their prescribed service life, it is of vital importance to understand the long-term performance. Studies have been conducted on life-cycle performance. The performance assessment has been extended to a life-cycle context (Gencturk, Hossain, and Lahourpour 2016;

Padgett and Tapia 2013; Anwar, Dong, and Li 2020; Zheng, Dong, and Li 2018; Li, Dong, and Qian 2020). Yang and Frangopol (2019) introduced the concept of lifetime resilience. An integrated probabilistic framework to assess life-cycle sustainability and resilience under deterioration and earthquakes has not been well developed.

2.7 Performance of Seismic Hazard Mitigation Measure Using SMA

During the service life, reinforced concrete (RC) bridges may be subjected to extreme events (e.g., earthquakes) and environmental pollution (e.g., carbonization and corrosion), causing tremendous consequences to the economy and society. This study adopts shape memory alloy (SMA)-steel RC bridge as a promising solution to mitigate the consequences induced by earthquakes and functional deterioration. Thus, the gap between long-term sustainability and resilience assessment and novel steel-SMA RC bridges due to earthquake and functional deterioration needs to be filled.

The smart material SMA can be an alternative to mitigate the consequences of compound earthquakes and functional deterioration. The SMA is associated with flag-shaped hysteretic behavior, presenting self-centering and energy dissipation characteristics. The SMA can recover to its original shape after suffering large deformation (Fang et al., 2014, 2017; Fang, Wang, et al., 2022; Xiang et al., 2020). Additionally, SMA has satisfying corrosion resistance (Billah & Alam, 2012), and such property is vital for coastal structures which expose to a chloride environment yet to maintain their functionality over the lifespan. The pier is a critical component of the

bridge system, the failure of the pier caused the collapse of the whole bridge (Padgett, 2007). Therefore, the SMA bar can be arranged in the plastic hinge of the pier to mitigate seismic damage (Billah & Alam, 2015). Experiments demonstrated that SMA reinforced concrete pier could recover to its original position after the shaking table test (Zheng & Dong, 2019).

To understand the seismic performance of SMA-steel reinforced concrete piers, the seismic vulnerability was assessed (Billah & Alam, 2015; Shrestha & Hao, 2016). The seismic vulnerability of the SMA-steel reinforced concrete bridge and the bridge equipped with both SMA reinforced concrete pier and the SMA cable restrainer were compared (Li et al., 2021). The seismic loss of SMA-steel reinforced concrete bridges has been assessed under performance-based earthquake engineering, and the advantage of SMA in terms of mitigating economic loss was illustrated (Fang et al., 2021; Xiang et al., 2020; Zheng & Dong, 2019). Other applications of SMA in bridges include rocking foundation piers (Fang et al., 2020; Zheng et al., 2021) and isolation bearings (Fang, Liang, et al., 2022; Liang et al., 2020). A novel type of superelastic SMA angles was developed as self-centering device (Wang et al., 2020). The cyclic behavior and deformation mechanism of superelastic SMA U-shaped dampers (SMA-UDs) were investigated (Wang et al., 2021). The bridge can suffer multiple earthquakes and continuous deterioration within its lifetime, and the performance should be assessed from a long-term perspective. The long-term performance of SMA-steel reinforced concrete bridges incorporating broader metrics has not been well assessed under the compound earthquakes and functional deterioration.

Considering multiple sudden and continuous disruptions within the service life of structures, the sustainability and loss of resilience can be time-dependent and accumulated. The accumulated long-term sustainability and resilience loss of SMA-steel reinforced bridges under compound earthquakes and functional deterioration has not been well assessed.

2.8　　　　Research Gaps

This study focuses on confident seismic performance analysis of spatially distributed bridges. The relevant components including seismic IM selection, surrogate demand model, dependence modeling, sensitivity analysis, life-cycle performance, and performance of the hazard mitigation measure are reviewed. The research gaps are identified.

- The trade-off of the IM performance on the components and criteria has not been well considered within the IM selection process. A robust multi-criteria decision-making process has not been involved in IM selection.

- An efficient SPCE-based framework has not been developed to aid the uncertainty quantification of PBEE. The efficient global sensitivity analysis approach incorporating multiple criteria has not been developed within the PBEE framework.

- The nonlinear complex dependence from multiple sources has not been well modeled and incorporated in PBEE. The advanced techniques (e.g., advanced surrogate model for demand prediction and vine copula for dependence

modeling) have not been well interconnected to formulate an integrated framework to jointly improve the confidence of PBEE.

- An integrated framework of life-cycle sustainability and resilience assessment under compound earthquakes and deterioration has not been well developed. The life-cycle cost-benefit analysis in terms of sustainability and resilience of a hazard mitigation measure (steel-SMA reinforced bridge) under compound earthquakes and deterioration has not been investigated.

The procedures of PBEE include hazard analysis, structural analysis, damage analysis, and performance analysis. Related to these procedures, the seismic IM selection, uncertainty quantification, global sensitivity analysis, complex dependence modelling, and life-cycle performance assessment under compound earthquakes and deterioration are challenging tasks. Each of these tasks can affect the confidence of PBEE. These challenges motivate the author to develop a confident PBEE framework by improving the components in different stages.

CHAPTER 3
SEISMIC INTENSITY MEASURE SELECTION UNDER MULTIPLE CRITERIA AND UNCERTAINTY

3.1   Introduction

Earthquake ground motions contain complex time-series information. Within seismic performance assessment, PSDM is used to predict the probabilistic demand conditioned on seismic IM. Selecting an appropriate seismic IM can reduce uncertainty and serves as the basis of a confident performance assessment. Considering the multiple failure modes of the systems and IM performance objectives, seismic IM selection is associated with the consideration of multiple criteria. Besides, there are uncertainties within the selection process.

According to the definition (Triantaphyllou, 2000) of decision-making, the IM selection process can be considered as a multi-criteria decision problem and the different IMs are considered as alternatives. However, few studies selected the IM incorporating the multi-criteria decision process. One of the most widely used multi-criteria decision-making (MCDM) methods so-called TOPSIS, is adopted herein. The TOPSIS is a deterministic process, the rank computed by the TOPSIS model for each alternative is a single value. However, when uncertainties exist in criteria and weighting factors as limited information is available, the rank of each alternative provided by TOPSIS becomes random. It is impossible to make reliable decisions based on the TOPSIS technique only, as the presence of uncertain rank. Therefore, probabilistic

29

models should be incorporated into TOPSIS to support decision-making under uncertainties (Lahdelma & Salminen, 2001; Wu et al., 2019). The uncertainty and trade-off among multiple criteria have not been well incorporated in seismic IM selection. The importance of different components has not been well incorporated in seismic IM selection. There is no existing MCDM framework that can be directly adopted to solve the IM selection by considering multiple criteria and uncertainties.

In this chapter, an MCDM framework coupling SMAA-2 and TOPSIS is proposed to address the IM selection under uncertainty. The IM selection criterion values at structural components are first computed, and a decision matrix is formulated based on all the criterion values of each IM alternative. With the consideration of probabilistic seismic scenarios, the importance of the component to the system reliability is then quantified in a probabilistic manner and used as the input of weighting factors in the MCDM stage. After performing the MCDM process using the decision matrix and probabilistic weighting factors, the acceptability of each IM for each rank is computed, and the overall acceptability levels of the IM alternatives are presented based on the holistic acceptability indices. Additionally, the effects of IM selection on loss and resilience are investigated in this chapter.

3.2   Seismic Intensity Measure Alternatives and Performance Criteria

Based on previous studies (Bianchini et al., 2009; Padgett et al., 2008), ten IMs are considered in this chapter and are summarized in Table 3.1. The directionality of ground motions is also defined. In general, there exist several directionality definitions in the

literature (e.g., (Beyer & Bommer, 2006; Boore & Kishida, 2017)). Boore (Boore, 2010) introduced the seismic intensity using RotD50 values that is orientation-independent without calculating the geometric means. The RotD50 is defined as the 50-percentile (median) value of response spectra of the two horizontal components protected onto all nonredundant azimuths (Boore, 2010). The RotD50 is used in the Pacific Earthquake Engineering Research Center's (PEER) Next Generation Attenuation (NGA)-West2 project. Herein, the PGV, PGA, and spectral accelerations are computed using the RotD50 values.

Table 3.1 Seismic intensity measure alternatives

No.	IM	Definition	Units
1	PGV	Peak ground velocity	cm/s
2	PGA	Peak ground acceleration	g
3	Sa-0.2s	Spectral acceleration at the period of 0.2 s	g
4	Sa-$1s$	Spectral acceleration at the period of 1 s	g
5	Sa-$T1$	Spectral acceleration at the first mode period	g
6	Sa-$gmTLT$	Spectral acceleration at the geometric mean of the fundamental periods of the longitudinal and transverse directions (calculated by Eq. 3-1)	g
7	Sa-$gmT12$	Spectral acceleration at the geometric mean of the first and second mode periods (calculated by Eq. 3-1)	g
8	$S_{a,C}$	Composite IM (calculated by Eq. 3-2)	g
9	Sa$_{avg}$	Average spectral acceleration (defined in Eq. 3-3)	g
10	GeoSa-TLT	Geometric mean of the spectral accelerations at the fundamental periods of the longitudinal and transverse directions (calculated by Eq. 3-4)	g

The Sa-*gmTLT* and Sa-*gmT12* are computed as

$$Sa - gmTLT = Sa(\sqrt{T_L T_T}) \ , \quad Sa - gmT12 = Sa(\sqrt{T_1 T_2}) \tag{3-1}$$

where T_L and T_T are the fundamental periods associated with the longitudinal and transverse directions of the structure; T_1 and T_2 are the first and second mode periods of the structure respectively; and $Sa(\sqrt{T_L T_T})$ is the spectral acceleration at the period $\sqrt{T_L T_T}$.

The composite IM $S_{a,C}$ is expressed as follows (Cordova et al., 2000)

$$S_{a,C} = Sa(T_1) \left[\frac{Sa(2T_1)}{Sa(T_1)} \right]^{0.5} = \sqrt{Sa(T_1)Sa(2T_1)} \tag{3-2}$$

The average spectral acceleration is represented by the geometric mean of spectral accelerations at the periods between $\zeta_1 T_1$ and $\zeta_{Np} T_1$ (Bianchini et al., 2009)

$$Sa_{avg}(\zeta_1 T_1, ..., \zeta_{Np} T_1) = (\prod_{i=1}^{Np} Sa(\zeta_i T_1))^{1/Np} \tag{3-3}$$

where Np is the number of periods used to compute Sa_{avg} and ζ_i is a non-negative value. In this study, ten equally spaced periods between $0.25T_1$ to $3T_1$ are used to compute the Sa_{avg}.

The GeoSa-*TLT* is expressed as

$$GeoSa - TLT = \sqrt{Sa(T_L)Sa(T_T)} \tag{3-4}$$

To sum up, the GeoSa-*TLT* and $S_{a,C}$ can be regarded as two variants of Sa_{avg}. Herein, the Sa_{avg} is computed as the geometric mean of spectral accelerations (using the RotD50 values) at ten periods, while GeoSa-*TLT* is computed as the geometric mean of spectral accelerations at T_L and T_T of the structure, and $S_{a,C}$ is the geometric mean of

spectral accelerations at T_1 and $2T_1$. The RotD50 value is used for all the spectral accelerations to compute these IMs. Given the structural information, the T_L, T_T, T_1, and T_2 can be obtained.

The widely used power law PSDM is used to demonstrate the developed framework in this chapter. A power law is generally used in the PSDM to estimate the median value of the demand under a given IM (Cornell et al., 2002)

$$\ln(S_D) = \ln(a) + b\ln(IM) \tag{3-5}$$

where S_D is the median of the demand and the coefficients a and b are obtained from regression analysis. Then, the conditional probability of demand exceeding structural capacity under a given IM is computed as

$$P\left[D \geq Cap \mid \text{IM}\right] = \Phi\left[\frac{\ln\left(S_D / Cap\right)}{\sqrt{\beta_{D|\text{IM}}^2 + \beta_C^2}}\right] = \Phi\left[\frac{\ln(\text{IM}) - \dfrac{\ln(Cap) - \ln(a)}{b}}{\dfrac{\sqrt{\beta_{D|\text{IM}}^2 + \beta_C^2}}{b}}\right], \quad \beta_{D|IM} \cong \sqrt{\frac{\sum_1^{Na} (\ln(S_D) - \ln(d_i))^2}{Na - 2}}$$

$$\tag{3-6}$$

in which $\Phi(.)$ is the standard normal cumulative distribution function; Cap is the defined limit state; $\beta_{D|IM}$ and β_C are the dispersions of the demand and capacity, respectively; d_i is the demand of ith analysis; and Na is the number of analysis.

The six criteria namely, efficiency, practicality, sufficiency to magnitude, sufficiency to distance, proficiency, and correlation are assessed. The structural demand parameters considered in this study include column curvature ductility, bearing longitudinal and transverse displacement, abutment active displacement, passive displacement, and transverse displacement. Counting six performance criteria for each

structural demand parameter, thus a total of thirty-six criteria are assessed in this study. The criteria are explained as follows.

Efficiency describes the variability of the peak demand computed under a certain level of seismic intensity. The efficiency is represented by $\beta_{D|IM}$. The IM associated with lower $\beta_{D|IM}$ is considered to be more efficient, as an efficient IM can reduce the dispersion of the demand under a given IM.

The practicality is examined by the slope of the linear regression between ln IM and ln demand. The practicality is represented by coefficient b, as indicated in Eq. 3-5. A high slope value indicates the engineering demand is strongly dependent on IM (Padgett et al., 2008), therefore, the IM is considered as practical. The IM cannot be used for demand estimation if the slope of the linear regression between ln IM and ln demand is close to zero indicating an impractical IM.

An IM, which is highly independent on other ground motion characteristics such as earthquake magnitude (M) and distance (R), is considered as sufficient. When a sufficient IM is used, the results from PSDM are conditionally independent of M and R. Given an intensity level, the probability of exceeding a damage state produced by a sufficient IM is not affected by the M and R. To compute the sufficiency, the regression is first conducted between residuals from PSDM and other seismic parameters (e.g., M, R). The sufficiency is quantified by the p-value of the regression. A lower p-value indicates a higher statistical significance of the regression, resulting in a reasonable decision to reject the IM.

The correlation coefficient describes the level of interdependency between two variables. As the linear relationship is assumed between ln demand and ln IM, an appropriate IM should be highly correlated with demand. A higher correlation coefficient indicates less variable and more accurate demand estimation. The correlation coefficient $Cor(\ln IM, \ln D)$ is expressed as follows

$$Cor(\ln IM, \ln D) = \frac{Cov(\ln IM, \ln D)}{\sqrt{Var[\ln IM]Var[\ln D]}} \tag{4-7}$$

where $Cov(\ln IM, \ln D)$ is the covariance of ln IM and ln *demand D* and $Var[.]$ is the variance function.

Proficiency refers to the composite performance of efficiency and practicality and is expressed as the modified dispersion. An IM with lower modified dispersion is considered as more proficient. The proficiency Pr is computed as

$$\Pr = \frac{\beta_{D|IM}}{b} \tag{3-8}$$

3.3 Novel Multi-criteria Decision-making Model Considering Uncertainty

This study proposes a novel MCDM method incorporating uncertainties within the decision process. When the input of the decision process is deterministic, the MCDM technique such as TOPSIS outputs the deterministic rank of the alternatives. It is visible for decision-makers to choose the best solution based on rank. However, when the decision matrix and weighting factors are associated with uncertainties, the rank of each alternative becomes probabilistic. Each alternative may rank at any place with a certain

acceptability level. This study combines TOPSIS and SMAA-2 to address decision-making under uncertainties.

3.3.1 MCDM Technique: TOPSIS

This study adopts one of the MCDM methods so-called TOPSIS. The basic idea of this method is to determine the optimal alternative with the shortest distance to the ideal solution (A^+) and the longest distance to the negative ideal solution (A^-) (Hwang & Yoon, 1981). In the TOPSIS procedure, the performance criteria for each alternative should be quantified first, thus, a decision matrix is formulated. The decision matrix **D** is expressed as follows

$$\mathbf{D} = \begin{pmatrix} x_{1,1} & \cdots & x_{1,ncr} \\ \vdots & \ddots & \vdots \\ x_{nal,1} & \cdots & x_{nal,ncr} \end{pmatrix} \tag{3-9}$$

where x_{ij} is the value of the jth criterion with respect to the ith alternative; ncr is the number of criteria; and nal is the number of alternatives.

The normalization of the decision matrix is conducted as

$$\mathbf{R} = \begin{pmatrix} r_{1,1} & \cdots & r_{1,ncr} \\ \vdots & \ddots & \vdots \\ r_{nal,1} & \cdots & r_{nal,ncr} \end{pmatrix}, \quad r_{i,j} = \frac{x_{i,j}}{\sqrt{\sum_{k=1}^{nal} x_{k,j}^2}} \tag{3-10}$$

where **R** is the normalized decision matrix and x_{kj} is the original value of the jth criterion with respect to the kth alternative.

The weighting factors for each criterion determined by the decision-makers are then applied to the normalized decision matrix, the normalized and weighted decision matrix is finally obtained as

$$\mathbf{V} = \begin{pmatrix} v_{1,1} & \cdots & v_{1,ncr} \\ \vdots & \ddots & \vdots \\ v_{nal,1} & \cdots & v_{nal,ncr} \end{pmatrix}, \quad v_{i,j} = w_j \times r_{i,j} \tag{3-11}$$

where $\mathbf{V}$ donates the weighted and normalized decision matrix and w_j represents the weighting factor for the jth criterion.

The criteria, which are expected to maximize or minimize to achieve the satisfied objectives, are defined as "benefit" or "cost" criteria, respectively. The best performance values among all alternatives are determined by the maximum values of the "benefit" criterion and the minimum values of the "cost" criterion. The ideal solution and the negative-ideal solution are computed by extracting the best and worst performance values among all the alternatives respectively

$$A^+ = \{v_{1+},...,v_{ncr+}\} = \{(\max v_{i,j} \mid j \in J^b),(\min v_{i,j} \mid j \in J^c)\},$$
$$A^- = \{v_{1-},...,v_{ncr-}\} = \{(\min v_{i,j} \mid j \in J^b),(\max v_{i,j} \mid j \in J^c)\} \tag{3-12}$$

where J^b and J^c are the "benefit" and "cost" criteria, respectively; and v_{j+} and v_{j-} are the jth criterion values of the ideal solution and negative ideal solution.

The distance of each solution to the ideal solution and negative ideal solution can be calculated by Eq. 3-13. The final alternative rank is determined by the relative closeness defined in Eq. 3-14. The best alternative should have the highest value of relative closeness.

$$D_{i+} = \sqrt{\sum_{j=1}^{ncr}(v_{i,j} - v_{j+})^2} \; ; D_{i-} = \sqrt{\sum_{j=1}^{ncr}(v_{i,j} - v_{j-})^2} \qquad (3\text{-}13)$$

$$C_{i+} = \frac{D_{i-}}{D_{i+} + D_{i-}} \qquad (3\text{-}14)$$

where D_{i+} and D_{i-} are the distances of alternative i to the ideal solution and negative solution respectively and C_{i+} is the relative closeness to alternative i.

3.3.2 Incorporating Uncertainties in MCDM by SMAA

SMAA is an MCDM method for assessing alternatives when the criterion values and criterion weightings are uncertain or inaccurate. Lahdelma and Salminen (Lahdelma & Salminen, 2001) proposed the SMAA-2 method to assess the overall acceptability of the alternatives based on the conventional SMAA methods. In SMAA, the weighting factors and the criterion values are described as probabilistic distributions, the acceptability indices are the outputs of SMAA. The acceptability index indicates the variety of different preferences that give an alternative a specific rank place. The holistic acceptability index representing the overall acceptability of an alternative can be calculated by assigning meta-weighs to the acceptability indices of that alternative associated with all passible rank places. In this study, the uncertainties within the MCDM problem are addressed by coupling the SMAA-2 with TOPSIS.

The SMAA-2 procedure is presented as follows. The distributions of the random criterion values and weighting factors are described by the probability density functions (PDFs) $f_X(c)$ and $f_W(w)$, respectively. To ensure the sum of the weighting factors equals 1, the distribution of the random weighting factors should be within the random variable space W defined as follows

$$W = \left\{ \mathbf{w} \in R^{ncr} : w_j \geq 0, \sum_{j=1}^{ncr} w_j = 1 \right\} \qquad (3\text{-}15)$$

where $\mathbf{w}$ is the weight vector.

The random decision matrix realization $\mathbf{X}$ is expressed as

$$\mathbf{X} = \begin{pmatrix} c_{1,1} & \cdots & c_{1,ncr} \\ \vdots & \ddots & \vdots \\ c_{nal,1} & \cdots & c_{nal,ncr} \end{pmatrix} \qquad (3\text{-}16)$$

where the variable c_{ij} represents the random j^{th} criterion value with respect to the ith alternative.

The favorable rank weight $W_i^r(c)$ can be defined as the weights that ensure the alternative i ranking at r

$$W_i^r(c) = \left\{ \mathbf{w} \in W : rank(\mathbf{c_i}, \mathbf{w}) = r \right\} \qquad (3\text{-}17)$$

where $\mathbf{c_i}$ is the random criterion vector of alternative i; and $rank$ ($\mathbf{c_i}$, $\mathbf{w}$) is the ranking function that returns the rank of alternative i, given the random criterion vector $\mathbf{c_i}$ and random weight vector $\mathbf{w}$.

The rank acceptability index rar_i^r represents the variety of preferences that yields the alternative i ranking at r and is computed as

$$rai_i^r = \int_X f_X(c) \int_{W_i^r(c)} f_W(\mathbf{w}) d\mathbf{w} dc \qquad (3\text{-}18)$$

The holistic acceptability index hai_i for alternative i combines the acceptability for each possible rank and represents the overall acceptability of this alternative. The holistic acceptability index hai_i for alternative i is expressed as

$$hai_i = \sum_{r=1}^{nal} \frac{rai_i^r}{r} \qquad (3\text{-}19)$$

The procedures of the novel MCDM model are indicated in Figure 3.1. In SMAA-2, the uncertainties associated with the decision matrix and weighting factors are assessed and the probabilistic distributions are formulated. The TOPSIS model is then implemented with the input of a stochastic decision matrix and weighting factor samples generated from the predetermined distributions. The probabilistic closeness coefficients and rank are therefore computed. These probabilistic outputs serve as the input in SMAA-2 to compute acceptability indices. The holistic acceptability index of an alternative is calculated by applying the meta-weights to the acceptability indices of that alternative associated with all possible rank places. The overall rank of the alternatives considering uncertainties is determined based on the holistic acceptability indices. The proposed approach can be applied to a wide range of MCDM problems considering uncertainties.
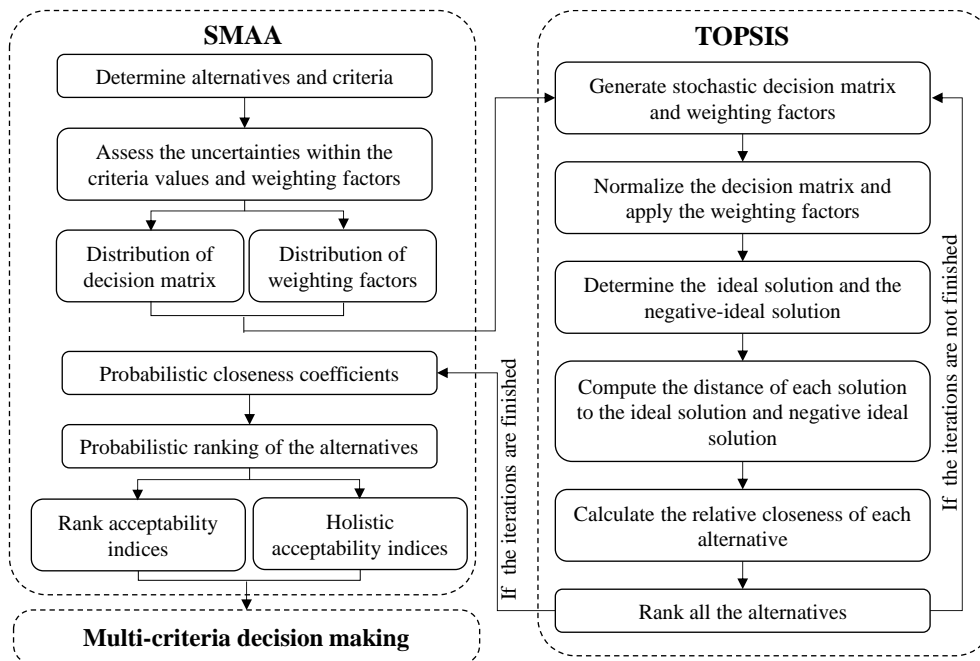
Figure 3.1 Computational process of the novel MCDM model

3.3.3 Component Importance Measures

The IM selection process involves the consideration of the importance of single-component performance to the system reliability, which means the performance criteria associated with a relatively more critical component should be weighted with a larger factor in the MCDM process. Kang et al. (Kang et al., 2008) indicated that the conditional failure probability of a component given the system failure can be considered as the importance of the component to the system reliability. The component importance measure (CIM) is computed as follows

$$CIM_i^j(IM) = P(F_i^j \mid F_{system}^j, IM) = \frac{P(F_i^j F_{system}^j \mid IM)}{P(F_{system}^j \mid IM)} \tag{3-20}$$

where $CIM_i^j(IM)$ is the importance measure of the ith component under the hazard intensity IM for the jth limit state; $P(F_i^j \mid F_{system}^j, IM)$ is the conditional failure probability of ith component given the system failure considering j^{th} limit state; $P[F_{system}^j/IM]$ is the probability of the system exceeding the jth limit state under a given IM; and $P(F_i^j F_{system}^j \mid IM)$ is the probability of both the ith component and system exceeding j^{th} limit state under IM.

The Monte Carlo simulation (MCS) can be used within bridge vulnerability analysis considering the joint PDFs of the demands of multiple components (Dueñas-Osorio & Padgett, 2011; Nielson & DesRoches, 2007). The approach is adopted in this study to compute the system fragility and component importance measures considering multiple components.

3.4   Framework of Seismic Intensity Measure Selection Under Multiple Criteria and Uncertainty

This study develops an integrated IM selection framework to assess the overall IM acceptability using the proposed MCDM method. A flowchart of the proposed framework is shown in Figure 3.2. As indicted, there are four computational modules within the framework: PSHA, vulnerability analysis, MCDM, and loss and resilience quantification. The PSHA is conducted for the bridge location, thus the probabilistic distributions of IMs are obtained. The vulnerability analysis is then performed to compute the IM performance criteria, CIMs, and system fragility. The CIMs are quantified in a probabilistic manner by incorporating the probabilistic IMs distributions from PSHA. The MCDM model is used to provide the rank of the alternatives under uncertainty. To formulate an MCDM problem, the decision matrix and weighting factors need to be obtained. Therefore, the decision matrix is formulated based on the criterion values quantified for the ten alternatives. The probabilistic weighting factors are calculated by normalizing the CIMs. Once the two main inputs (decision matrix and probabilistic weighting factors) of MCDM are obtained, following the procedures of MCDM, the overall acceptability levels of the alternatives are determined based on the holistic acceptability indices. Finally, the effects of IM selection on risk and resilience assessment are investigated by considering both the mean and standard deviation.

In summary, several IMs are determined as alternatives for the IM selection. Multiple criteria are considered in the selection. Different structural components are

associated with different importance to system safety. Thus, a multi-criteria decision-making model is implemented. This decision model incorporates the trade-off among multiple criteria and the different importance of structural components. Based on the holistic acceptability index, the ranking of the IM alternatives can be determined. The effects of IMs on probabilistic loss and resilience are investigated to further support IM selection.
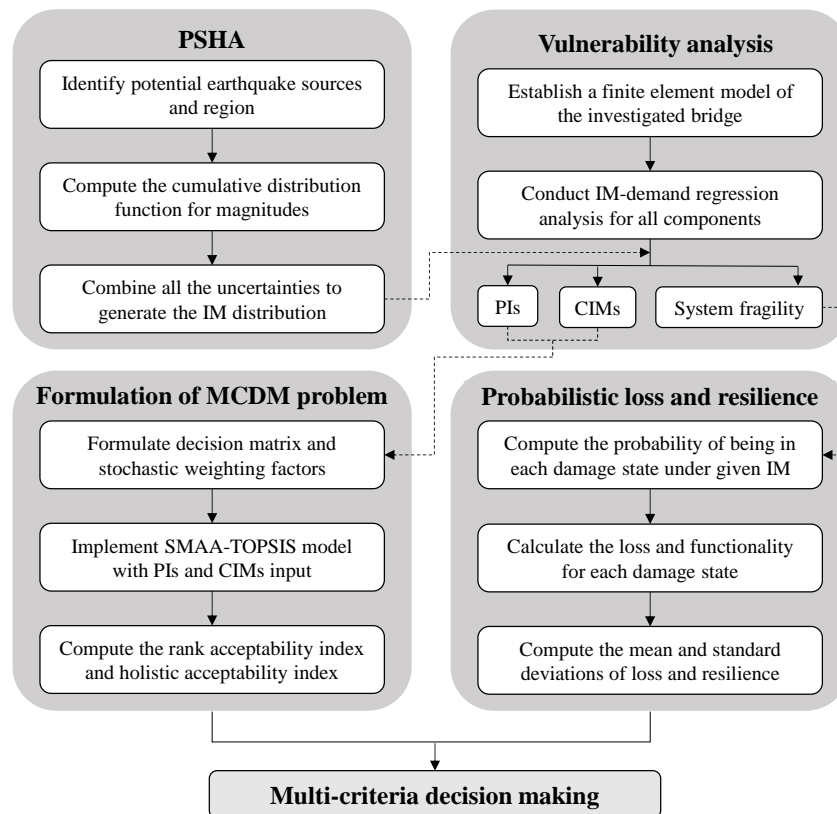
Figure 3.2 Proposed IM selection framework

3.5　　　Illustrative Example

3.5.1　Hazard Analysis and Bridge Modeling

The uncertainty associated with seismic hazards is considered in this study. The hazard analysis is performed in a probabilistic manner. A bounded cumulative distribution function (CDF) for the earthquake magnitudes can be derived as (Baker, 2013)

$$F_M(m) = \frac{1-10^{-h(m-m_{\min})}}{1-10^{-h(m_{\max}-m_{\min})}}, \quad m_{\min} < m < m_{\max} \tag{3-21}$$

where $F_M(m)$ is the CDF for earthquake magnitudes; m_{max} is the maximum earthquake magnitude that a given source can produce; m_{min} is the minimum magnitude considered in the analysis; and h is the coefficient.

The ground motion prediction models (GMPMs) can be used to predict the IM levels with the medians and standard deviations. The GMPMs are described as a function of some seismic characteristic parameters (e.g., earthquake magnitude, distance, rupture mechanism). The GMPM (Boore et al., 2014) is given by

$$\ln Y = F_E(M, mech) + F_P(R_{JB}, M, region) + F_S(V_{S30}, R_{JB}, M, region, z_1) + \varepsilon\sigma(M, R_{JB}, V_{S30}) \tag{3-22}$$

where $\ln Y$ is the natural logarithm of a ground-motion IM; F_E, F_P, and F_S are functions of source, path, and site parameters respectively; M is magnitude; $mech$ is the mechanism of the event; R_{JB} is the Joyner-Boore distance; $region$ represents the investigated region; V_{S30} is the shear wave velocity averaged over top 30 m; z_1 is the basin depth; ε is the fractional number of standard deviations of a single value of $\ln Y$ away from the mean; and σ is the total standard deviation of the model.

The total standard deviation is the combination of between-event and within-event variability, given by

$$\sigma(M, R_{JB}, V_{S30}) = \sqrt{\phi^2(M, R_{JB}, V_{S30}) + \tau^2(M)} \tag{3-23}$$

where τ is the *M*-dependent between-event standard deviation and ϕ is the *M*-, R_{JB}-, and V_{S30}- dependent within-event standard deviation.

The lognormal distribution parameters of spectral acceleration-based IMs can be computed directly from the GMPMs, while distribution parameters of ln Sa$_{avg}$ are estimated as follows (Baker & Jayaram, 2008)

$$\ln Sa_{avg}(\zeta_1 T_1,...,\zeta_{Np} T_1) = \frac{1}{Np}\sum_{i=1}^{Np}\ln Sa(\zeta_i T_1) \tag{3-24}$$

$$\mu_{\ln Sa_{avg}(\zeta_1 T_1,...,\zeta_{Np} T_1)} = \frac{1}{Np}\sum_{i=1}^{Np}\mu_{\ln Sa(\zeta_i T_1)} \tag{3-25}$$

$$\sigma^2_{\ln Sa_{avg}(\zeta_1 T_1,...,\zeta_{Np} T_1)} = \frac{1}{Np^2}\sum_{i=1}^{Np}\sum_{j=1}^{Np}\rho_{\ln Sa(\zeta_i T_1),\ln Sa(\zeta_j T_1)}\sigma_{\ln Sa(\zeta_i T_1)}\sigma_{\ln Sa(\zeta_j T_1)} \tag{3-26}$$

where $\mu_{\ln Saavg(\zeta 1 T1,..., \zeta Np T1)}$ and $\mu_{\ln Sa(\zeta i T1)}$ are the mean values of ln Sa$_{avg}(\zeta_1 T_1,...,\zeta_{Np}T_1)$ and ln Sa$(\zeta_i T_i)$ respectively; $\sigma_{\ln Saavg(\zeta 1 T1,..., \zeta Np T1)}$ and $\sigma_{\ln Sa(\zeta i T1)}$ are the standard deviations of ln Sa$_{avg}(\zeta_1 T_1,..., \zeta_{Np}T_1)$ and ln Sa$(\zeta_i T_1)$ respectively; and $\rho_{\ln Sa(\zeta i T1), \ln Sa(\zeta j T1)}$ is the correlation coefficient of ln Sa$(\zeta_i T_1)$ and ln Sa$(\zeta_j T_1)$ (Baker & Bradley, 2017). As mentioned previously, the GeoSa-*TLT* and S$_{a,C}$ can be regarded as two variants of Sa$_{avg}$. The distribution parameters of these two IMs can be calculated similarly with respect to Sa$_{avg}$ as indicated in Eqs. 3-25 and 3-26, where *Np* equals 2 and the periods in the equations change accordingly. Based on the probabilistic distribution of magnitudes and GMPM, the probabilistic distributions of IMs can be computed.

The proposed approach is illustrated on a highway bridge as indicated in Figure 3.3. The investigated bridge is a 62 *m* length two-equal-span continuous RC bridge with two columns per bent. The height and width of the box girder are 2 and 10 *m*,

respectively. The height and the diameter of the circular columns are 10 and 1.5 *m*, respectively.

The detailed finite element model of the bridge is established in OpenSees. The finite element model is developed based on previous studies (Nielson, 2005; Zheng et al., 2018). Elastic beam-column elements are used for superstructure modeling, as the superstructure is expected to behave elastically under seismic effects. The zero-length element is used for modeling the bearing. The Steel01 material can be used to model the elastomeric pad. The columns are expected to behave nonlinearly and can be developed using nonlinear beam-column elements with fiber sections representing the actual column section configuration. Three types of material models are utilized to describe the constitutive behavior of the column section namely unconfined concrete, confined concrete, and steel rebar. The concrete and steel are modeled using the materials Concrete01 and Steel01. The abutment actions are modeled using zero-length elements. In the longitudinal direction, the passive action includes the soil and pile contributions, and a parallel system consisting of quad-linear and tri-linear materials is used. The active action is related to the contribution of the pile. In the transverse direction, the action of the abutment is related to the pile contribution. The boundary condition is assigned to the foundation. Three types of springs are created along the foundation namely, *p-y*, *t-z,* and *q-z* springs to represent the soil-structure interactions in lateral and vertical directions. The detailed foundation modeling procedure is based on (Wang et al., 2014). For the mesh assignment, the deck is discretized into a number of elements with a length of 1 m. The displacement increment test can be used for the

convergence test. A set of 80 ground motion records identified by (Baker et al., 2011) is used in this study to conduct PSDM.

3.5.2 IM Selection

The regression analysis is performed for each pair of natural logarithm IM and structural component responses. Six IM performance criteria (i.e., efficiency, practicality, proficiency, correlation, sufficiency to magnitude, and sufficiency to distance) over six engineering demand parameters, thus, a total of thirty-six criteria are assessed for each IM alternative. Some comparison results are presented in Figures 3.4 – 3.6. As illustrated, Sa-*T1* is more efficient than Sa-*0.2s* in bearing longitudinal displacement, Sa-*gmTLT* is more sufficient than Sa-*0.2s* related to magnitude in bearing transverse displacement, and PGA is more practical than $S_{a,C}$ in column curvature ductility. The selected IMs performance criteria for different bridge components are visualized in Figure 3.7. The optimal criterion values are marked by cycle. For column curvature ductility, PGA is the optimal alternative by considering both efficiency and practicality. However, with respect to the bearing longitudinal displacement and abutment active displacement, there does not exist a sole alternative consistently optimal in both efficiency and practicality. Moreover, for a specific criterion (e.g., efficiency or practicality), there is not an alternative IM, which consistently yields optimal criterion values over all components. It is necessary to use a single IM to connect the demands of different components so that the joint PSDM can be formulated for system-level fragility, loss, and resilience assessment. These results further

demonstrate the necessity of implementing the proposed MCDM approach to address

the trade-off of IM performance among the criteria and components.
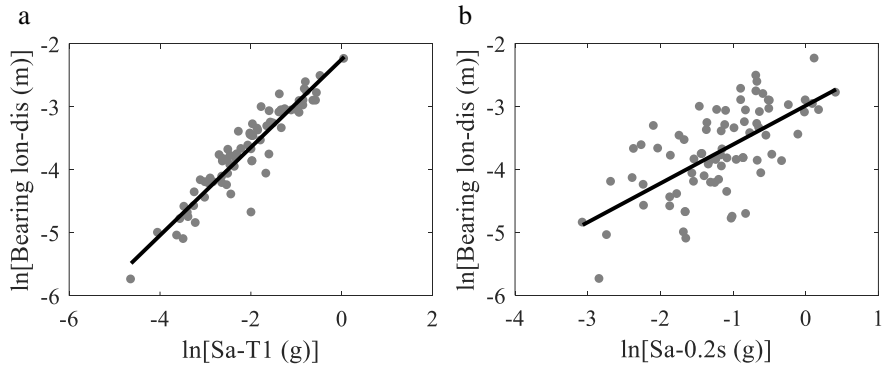
Figure 3.3 Comparison of efficiency in bearing longitudinal displacement for (a) Sa-

T1 and (b) Sa-*0.2s*.
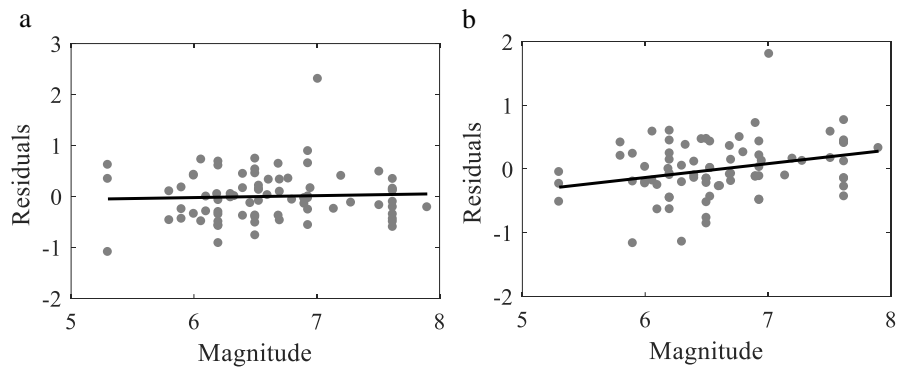
Figure 3.4 Comparison of sufficiency related to magnitude in bearing transverse

displacement for (a) Sa-*gmTLT* and (b) Sa-*0.2s*.
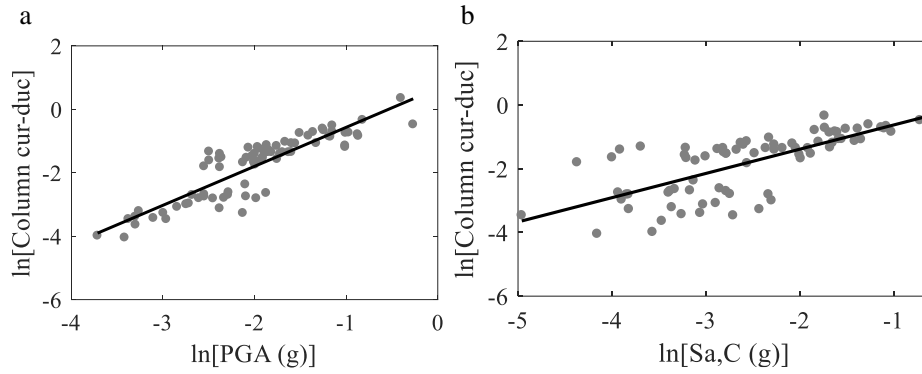
Figure 3.5 Comparison of practicality in column curvature ductility for (a) PGA and

(b) $S_{a,C}$.
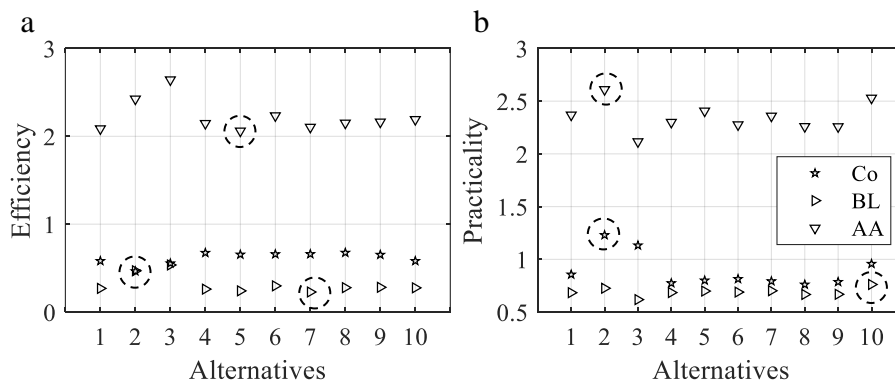
Figure 3.6 IMs performance for different bridge components in terms of (a)

efficiency and (b) practicality (the order of the IMs is indicated in Table 3.1).

Considering thirty-six criteria for ten alternatives, a ten-by-thirty-six transposed

decision matrix is formulated. Selecting an optimal IM considering the trade-off among

all criteria and components becomes a challenge when facing a large number of

alternatives and criteria. This issue is addressed by using the proposed MCDM process

to assess the integrated IM performance. To determine the weighting factors in MCDM,

the system fragility of the bridge and CIMs are calculated, as presented in Figures 3.8 – 3.9. As illustrated in Figure 3.9, the contributions of bridge components to the system reliability vary from the IM levels, which indicates the necessity of considering the uncertainties of seismic hazards to compute the weighting factors. For a slight damage state, the bearing longitudinal and transverse displacement and abutment transverse displacement seem to have similar importance to the system reliability under the high IM levels. The importance measure of the column increases with the IM levels. For the moderate damage state, the importance of abutment transverse displacement stands out at low IM levels, the importance measures of the bearing transverse displacement and the column increase significantly with the IM levels. The importance of the abutment passive and active displacement is relatively lower compared with other demands under all the investigated IM levels.
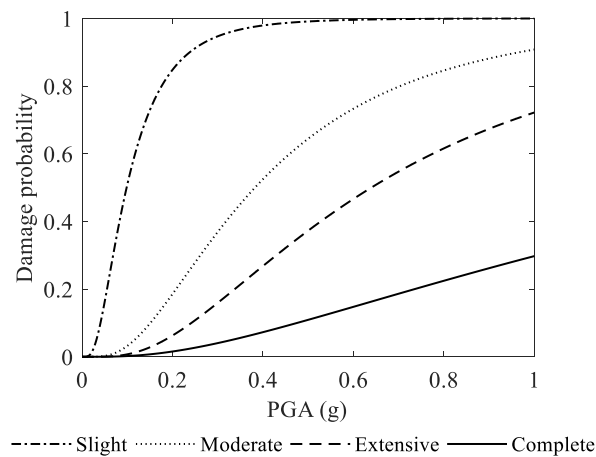
Figure 3.7 System fragility curves for the four damage states
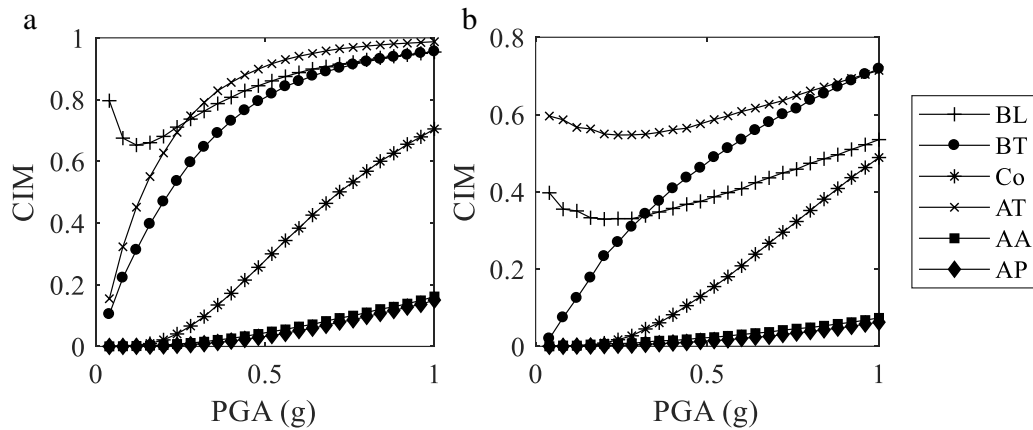
Figure 3.8 Component importance measures for (a) slight and (b) moderate damage

states

Considering the uncertainties associated with seismic hazards, the weighting

factors are computed in a probabilistic context. Following the procedures of PSHA, the

probabilistic IM distributions given the occurrence of the earthquake are computed. As

the CIM is conditioned on IM levels, the probabilistic CIM samples can be generated

based on the IM distributions. Each set of the CIM samples is first normalized to ensure

the sum of them equals one. Considering six criteria are assessed for each engineering

demand parameter, the probabilistic weighting factors are finally computed based on

the normalized CIMs. The density of the component weighting factors (normalized

CIMs to ensure the sum of the six component weighting factors is equal to 1) is

presented in Figure 3.10.

Once the decision matrix and probabilistic weighting factors are obtained,

following the procedure of the proposed MCDM framework, the rank acceptability

indices representing the acceptability levels of each alternative ranking at different

places are computed and shown in Figure 3.11(a). The results illustrate that the alternative can obtain an arbitrary rank with certain acceptability when uncertainties are incorporated into the decision-making process. The rank acceptability indices provide a preliminary identification of satisfactory or unsatisfactory alternatives. Satisfactory alternatives are associated with high acceptability values for the best rank. In contrast, alternatives with high acceptability values for the worst rank are identified as unsatisfactory alternatives and should be eliminated in decision-making. From the preliminary identification, Sa_{avg}, PGV, and Sa-*0.2s* are determined as satisfactory alternatives, as they have high acceptability values for best ranks. The holistic acceptability indices aggregating all rank acceptability indices indicate the overall acceptability of alternatives and are presented in Figure 3.11(b). The overall ranking of the alternatives is determined based on holistic acceptability indices. The results show the Sa_{avg} is the most acceptable IM for the investigated bridge followed by PGV and Sa-*0.2s*. In previous studies, the IM, which is associated with the most optimal criterion values and maintains satisfactory performance on other criteria, was determined as the appropriate IM. Following this consideration, the PGA stands out among all the IMs. Based on the proposed method, the overall acceptability of PGA computed by the MCDM model is not ranked in the first place. The reason why the overall acceptability of Sa_{avg} stands out may be interpreted as follows. By taking the geometric mean of the spectral accelerations at multiple periods, Sa_{avg} contains more information associated with the ground motion than a single-period spectral acceleration-based IM. Besides

the determined single period, the response at other periods may be important to compute

the nonlinear behavior of the structural system.
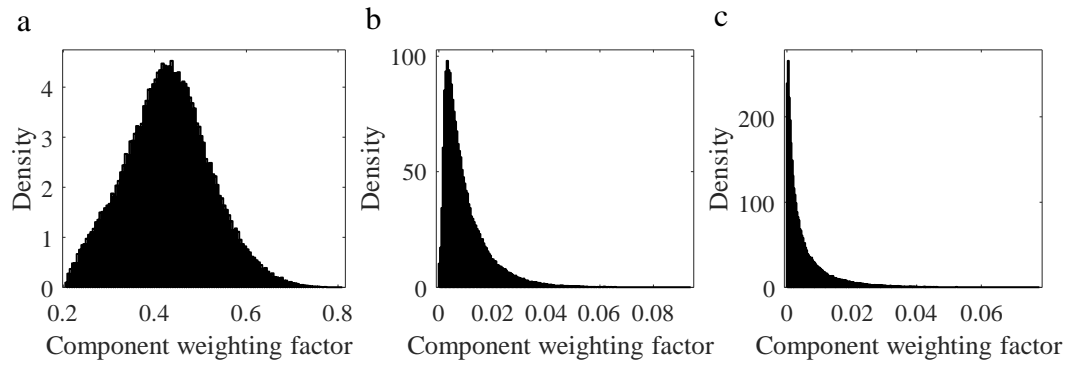
Figure 3.9 Distributions of component weighting factors for (a) bearing longitudinal

displacement; (b) abutment active displacement; and (c) abutment passive

displacement
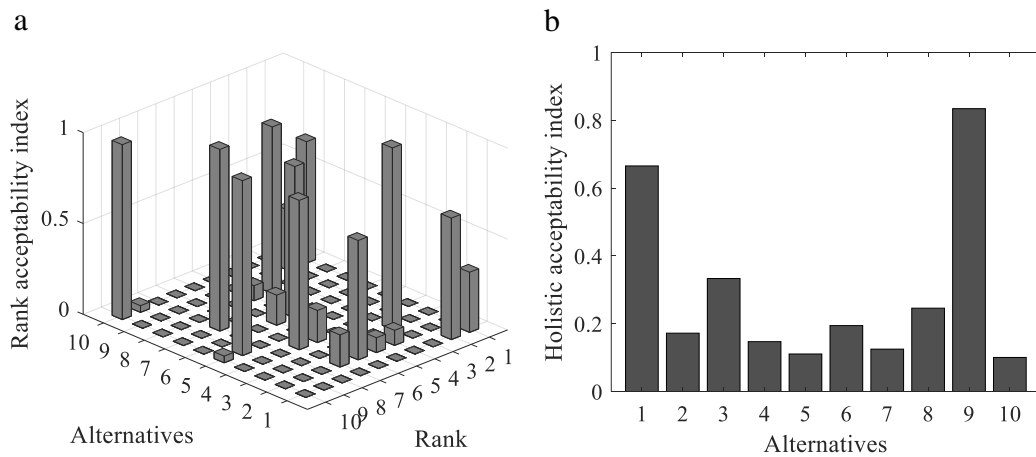
Figure 3.10 (a) Rank acceptability indices and (b) holistic acceptability indices for

the ten alternatives (the order of the IMs is indicated in Table 3.1)

3.5.3   Effects of IMs on Probabilistic Loss and Resilience

This study further investigates the effects of selected IMs on probabilistic loss and resilience. The top three IM alternatives Sa$_{avg}$, PGV, and Sa-$0.2s$ ranked from the MCDM model are chosen to perform the loss and resilience assessment. The repair cost of the bridge given a damage state is assumed proportional to the rebuilding cost of the bridge (Stein et al., 1999). To quantify the seismic loss associated with each damage state, the repair cost ratios representing the ratios of the repair cost to the rebuilding cost need to be defined. Werner et al. (Werner et al., 2006) proposed the repair cost ratios for different damage states, in which 0, 0.03, 0.25, 0.75, and 1 are associated with none, slight, moderate, major, and complete damage states, respectively. Given the above information, the seismic loss for the four damage states can be calculated. Based on the total probability theorem, the expected loss under a given seismic hazard is computed as the sum of the weighted loss for all damage states. The weighting factors are the probabilities of the bridge being in different damage states. The direct loss is considered within the assessment process and the indirect loss (e.g., downtime and fatality loss) could also be incorporated within the evaluation process (Dong et al., 2013).

The concept of resilience is used by decision-makers to assess the sustained function of infrastructure systems subjected to new challenges. The resilience can be quantified as follows (Frangopol & Bocchini, 2011)

$$R = \frac{\int_{t_0}^{t_0+t_h} Q(t)dt}{t_h} \tag{3-27}$$

where R is the resilience index; t_0 is the time of occurrence of the extreme event; t_h is

the investigated time interval; and $Q(t)$ is the time-variant functionality of the structure.

The expected time-variant functionality is expressed as the sum of the weighted

functionalities for all damage states (Dong & Frangopol, 2015; Zheng et al., 2018).

Given the IM distribution from the PSHA, the probabilistic seismic loss and resilience

can be computed correspondingly.

The density of repair loss is presented in Figure 3.12. The distribution parameters

are listed in Table 3.3. The Sa$_{avg}$ provides the lowest standard deviations for loss and

resilience. There exists a large difference in the expected loss when using three different

IMs, the expected loss computed using Sa-*0.2s* is near 3.5 times that using Sa$_{avg}$. The

results of expected resilience using the three IMs are similar, the difference between

the highest and lowest expected resilience is 0.07, Sa$_{avg}$ provides the highest value of

expected resilience followed by PGV and Sa-*0.2s*. Different types of structures can be

associated with different optimal IMs. The developed framework can be generally

applied to different types of structures to determine the appropriate IM. More studies

are needed for the IM selection for different types of structures.
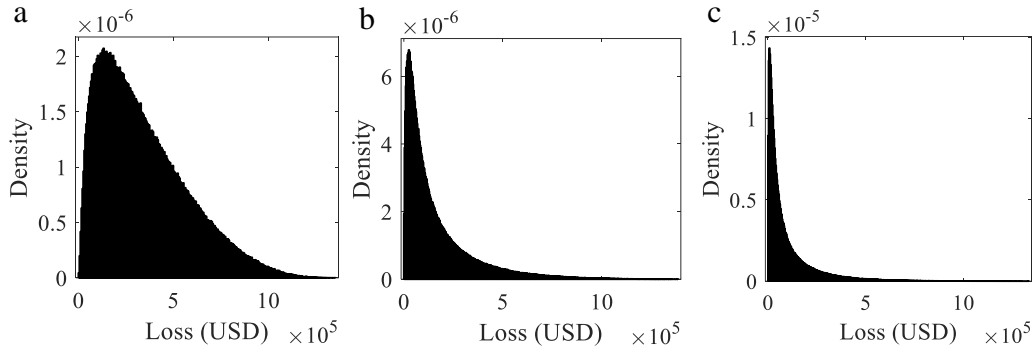
Figure 3.11 Distributions of loss using different IMs: (a) Sa-*0.2s;* (b) PGV; and (c)

Sa$_{avg}$

Table 3.2 Distribution parameters of loss and resilience

IM	Rank$_{MCDM}$	μ_L (10^4 USD)	μ_{res}	σ_L (10^4)	σ_{res}
Sa-*0.2s*	3	34.19	0.91	23.06	0.08
PGV	2	16.06	0.96	17.39	0.05
Sa$_{avg}$	1	9.85	0.98	12.84	0.04

3.6 Summary

In this chapter, a novel multi-criteria decision-making (MCDM) approach by incorporating stochastic multi-criteria acceptability analysis (SMAA) with the technique for order preference by similarity to ideal solution (TOPSIS) is proposed to solve the stochastic decision-making problem. TOPSIS provides an alternative rank function and the SMAA is used to address the uncertainties within the IM selection. The performance criteria (e.g., efficiency, proficiency, practicality, sufficiency, and correlation) are evaluated for the investigated structural components, and the decision matrix is formulated based on the criteria of each IM alternative. Furthermore, the

importance of the component to system reliability is quantified in a probabilistic manner using nonlinear time history analysis and serves as the weighting factor in the MCDM stage. The holistic acceptability indices indicating the overall acceptability levels of IM alternatives are computed by the proposed approach. Additionally, the effects of different IMs (e.g., average spectral acceleration, peak ground velocity, spectral acceleration) on probabilistic seismic loss and resilience are investigated to further support the IM selection. The proposed approach is illustrated on a highway bridge and the results are presented. In addition to the bridge system, the IM selection framework can be applied to the IM selection problems on other types of infrastructural systems. Furthermore, the proposed decision-making framework can deal with a wide range of decision-making problems in multiple disciplines considering multiple criteria and uncertainty. The following conclusions are drawn.

- For the investigated case, the optimal performance criterion values are separately distributed within the IM alternatives. Selecting an optimal IM considering the trade-off among all criteria and components becomes a challenge when facing a large number of alternatives and criteria. The proposed novel MCDM approach can be used to solve the issues and account for the uncertainties within the decision-making process.

- The contributions of bridge components to the system reliability measured by the conditional failure probability vary from the IM levels, which indicates the necessity of considering the uncertainties of seismic hazards to compute the weighting factors. The results of the component importance measure show that

the bearing displacement, column curvature ductility, and abutment transverse displacement have major contributions to the system reliability, and other component engineering demand parameters have minor contributions.

- The holistic acceptability indices indicate the Sa_{avg} is the most acceptable IM for the investigated bridge followed by PGV and Sa-*0.2s*. In general, Sa_{avg} contains more information on ground motion than a single-period spectral acceleration-based IM. Besides the determined single period, the response at other periods may be important to compute the nonlinear behavior of the investigated structural system.

- Among the top three investigated IMs, Sa_{avg} provides the lowest standard deviations for loss and resilience. There exists a large difference in the expected loss when using three different IMs, the expected loss computed using Sa-*0.2s* is near 3.5 times that using Sa_{avg}.

CHAPTER 4

SURROGATE-ASSISTED SEISMIC DEMAND PREDICTION

4.1   Introduction

There exists uncertainty within structural systems and the environment, resulting in a stochastic response. It is essential to perform uncertainty quantification accurately and efficiently for seismic performance analysis. The Monte Carlo simulation (MCS) can be used for uncertainty quantification. However, the computational time of MCS can become unaffordable if the computational time of the original model is high. The surrogate model can be obtained from a training process using a relatively small size of data. It represents the complex relationship between the input and output and can be used to emulate the output of a physical model efficiently.

Sparse polynomial chaos expansion (SPCE) as one type of surrogate model can be used to emulate the stochastic model output where the original model is computationally expensive. Considering the advantages of both efficient uncertainty quantification and global sensitivity analysis, this study focuses on the implementation of SPCE. Structural systems are usually associated with high-dimensional and probabilistic input. The number of candidate basis functions increases significantly with input dimension, resulting in a high computational burden for establishing SPCE. Previous applications regarding sparse PCE mainly focus on relatively simple structures and loading scenarios. Few studies implement sparse PCE to assess the

seismic performance of bridges considering multiple components. There is a need to implement and investigate the acceleration algorithm and sparse PCE within seismic performance analysis of bridges.

In this study, acceleration techniques are integrated to formulate an algorithm for the efficient computation of sparse PCE (ASPCE). The integrated algorithm can improve the efficiency of the computational process compared with conventional greedy algorithms while ensuring satisfying predictive performance. Once the sparse PCE model is obtained, the uncertainty quantification can be performed efficiently. The sparse PCE from the acceleration algorithm is implemented to assess the vulnerability of multi-responses highway bridges under earthquake hazards. The performance of sparse PCE and acceleration algorithm for this engineering problem is investigated. These applications and investigations can provide new implications for the uncertainty quantification of highway bridges subjected to natural hazards.

A schematic diagram illustrating the ASPCE for uncertainty quantification is presented in Figure 4.1. The probabilistic distributions of the input variables are identified. Through the experimental design, a set of input samples can be generated, and the corresponding outputs are computed by physical models. Then, the acceleration algorithm is performed to establish the sparse PCE model using the training data. Based on the developed sparse PCE., the seismic vulnerability can be efficiently computed. The uncertainty propagation from the input to the output is accomplished through the ASPCE.
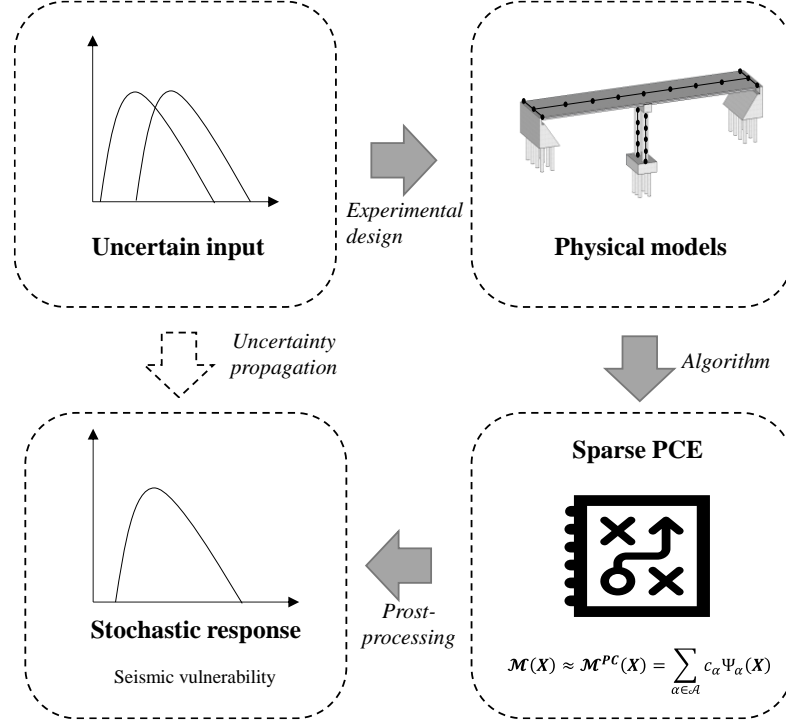
Figure 4.1 Illustration of uncertainty quantification and global sensitivity

analysis using ASPCE

4.2 Polynomial Chaos Expansion (PCE)

Let $\mathcal{M}$ represent a computational model. The random input vector $X \in \mathbb{R}^M$ of $\mathcal{M}$ is described by a joint PDF f_X. The response of the system $Y = \mathcal{M}(X)$ has a finite variance, the PCE of $\mathcal{M}(X)$ is expressed as follows (Marelli & Sudret, 2015)

$$Y = \mathcal{M}(X) = \sum_{\alpha \in \mathbb{N}^M} c_\alpha \Psi_\alpha(X) \tag{4-1}$$

where $\Psi_\alpha(X)$ are the multivariate polynomials orthonormal with respect to f_X; $\alpha \in \mathbb{N}^M$ is a set of indices mapping to the components of the $\Psi_\alpha(X)$; and c_α are the coefficients.

The multivariate polynomials are computed as

$$\Psi_\alpha(\mathbf{x}) = \prod_{i=1}^{M} \phi_{\alpha_i}^{(i)}(x_i) \tag{4-2}$$

where $\phi_{\alpha_i}^{(i)}$ is the univariate orthogonal polynomial with respect to the ith variable in degree α_i.

For practical purposes, original PCE is truncated to a finite sum and the truncated PCE is

$$\mathcal{M}^{PC}(X) = \sum_{\alpha \in \mathcal{A}} c_\alpha \Psi_\alpha(X) \tag{4-3}$$

where $\mathcal{A}$ is the truncated set of multi-indices of multivariate polynomials. The PCE is truncated by setting the total degree of all the polynomials associated with the input variables smaller than or equal to p as (Ni et al., 2019)

$$\mathcal{A}^{M,p} = \{\alpha \in \mathbb{N}^M : |\alpha| \leq p\}, card\mathcal{A}^{M,p} \equiv P = \frac{(p+M)!}{p!M!} \tag{4-4}$$

After the truncation, the coefficients can be computed using the least square solution as follows (Blatman & Sudret, 2010; Wan et al., 2020)

$$\widehat{\boldsymbol{C}} = (\boldsymbol{\Phi}^T \boldsymbol{\Phi})^{-1} \boldsymbol{\Phi}^T Y, \quad \boldsymbol{\Phi} = \begin{pmatrix} \Psi_0(\mathbf{x}^{(1)}) & \cdots & \Psi_{card\mathrm{A}^{M,p}-1}(\mathbf{x}^{(1)}) \\ \vdots & \ddots & \vdots \\ \Psi_0(\mathbf{x}^{(N)}) & \cdots & \Psi_{card\mathrm{A}^{M,p}-1}(\mathbf{x}^{(N)}) \end{pmatrix} \tag{4-5}$$

where $\widehat{\boldsymbol{C}}$ is the computed vector of coefficients; Y is the vector of the model evaluations at N input vectors $\mathbf{x}^{(1)}, \dots, \mathbf{x}^{(N)}$; and $\Psi_i(.), i = 0, \dots, card\mathcal{A}^{M,P} - 1$ are the basis functions.

Once the PCE is obtained, it could be used to compute the uncertainty features (e.g., PDF and statistic moments) of the output efficiently (Georgiou et al., 2012). The

sparse PCE models which exclude the insignificant terms perform better in some studies (Blatman & Sudret, 2010) and are introduced in the following section.

4.3   Orthogonal Matching Pursuit for Sparse PCE

Doostan and Owhadi (Doostan & Owhadi, 2011) presented a greedy algorithm orthogonal matching pursuit (OMP) for establishing sparse PCE. The OMP sequentially selects the basis functions and adds them to the approximation from the candidate set. For each iteration, the OMP selects a basis function which is most correlated with the residual from a dictionary set by solving (Salehi et al., 2017)

$$h(k) = \text{argmax}_{i \in \mathbb{C}_k} \frac{|\langle \psi_i, \mathbf{r}_{k-1} \rangle|}{\|\psi_i\|_2} \tag{4-6}$$

where $\Psi_{h(k)}$ is the selected basis function at iteration k; $\mathbb{C}_k$ is the updated dictionary at iteration k by excluding the basis function selected at iteration $k-1$; ψ_i represent the evaluations using basis function i; and $\mathbf{r}_{k-1}$ represents the residual from the PCE associated with iteration $k-1$.

At each iteration, the coefficients for currently selected basis functions are computed based on least square regression. The residual $\mathbf{r}_{k-1}$ is given by

$$\mathbf{r}_{k-1} = \mathbf{\Phi}_{k-1} C_{k-1} - Y \tag{4-7}$$

where $\mathbf{\Phi}_{k-1}$ is the matrix containing the evaluations using the basis functions at iteration $k-1$ and C_{k-1} are the coefficients obtained at iteration $k-1$.

The selection procedures are repeated and stopped until $\|\mathbf{r}\|_2$ is below the tolerance. This tolerance is predetermined through v-fold cross-validation technique.

4.4   Acceleration Algorithm for Computation of Sparse Polynomial Chaos Expansion (ASPCE)

To avoid the high computational burden associated with the conventional greedy algorithms for computation of sparse PCE, three techniques can be utilized within the acceleration algorithm (Baptista et al., 2019).

Technique 1: Probabilistic reduction of basis function candidates

A lemma presented by Smola and Schölkopf (Smola & Schölkopf, 2000) is applied herein to reduce the computational burden. Instead of selecting the basis functions from the full dictionary, it is possible to select the basis functions from the subsets of dictionary with satisfying performance. Let $\delta_1, \ldots, \delta_{ns}$ represent *ns* independent variables which follow identical distribution. The cumulative distribution function (CDF) of them is expressed as

$$\mathbb{P}(\delta_i \leq \tau) = F(\tau) \tag{4-8}$$

The CDF of $\delta := max_{i \in [ns]}\delta_i$ is expressed as

$$\mathbb{P}(\delta \leq \tau) = (F(\tau))^{ns} \tag{4-9}$$

Based on $\delta_i := (\boldsymbol{\psi}_i^T \mathbf{r}_k)^2 / \|\boldsymbol{\psi}_i\|_2^2$, by evaluating *ns* basis functions, the selection process at one iteration can guarantee a basis function within top $(1 - F(\tau)) \times 100\%$ of the full candidate set with probability ϑ. The number of evaluated basis functions is computed as

$$ns = \frac{log(1-\vartheta)}{log\, F(\tau)} \tag{4-10}$$

Technique 2: QR decomposition and efficient updating

The QR factorization based approach for solving the coefficients could satisfy efficiency requirement and is more numerically stable. The $\mathbf{\Phi}_k \in \mathbb{D}^{N \times k}$ is decomposed as

$$\mathbf{\Phi}_k = \mathbf{QR}, \mathbf{Q} \in \mathbb{D}^{N \times k}, \mathbf{R} \in \mathbb{D}^{k \times k} \tag{4-11}$$

where $\mathbb{D}^{N \times k}$ represents the dimension of the matrix is $N \times k$; and $\mathbb{D}^{k \times k}$ represents the dimension of the matrix is $k \times k$.

After performing a new iteration, a new basis function is selected and the Gram-Schmidt process with re-orthogonalization (Daniel et al., 1976) is used to update the QR factorization. Then, the coefficients of the PCE associated with current iteration are computed by solving

$$\mathbf{R}_k C_k = (\mathbf{Q}_k)^T Y \tag{4-12}$$

The conventional method for computing the residual requires to solve the PCE coefficients. By using the QR factorization, the residual can be updated efficiently without computing the coefficients as (Baptista et al., 2019)

$$\mathbf{r}_k = \mathbf{r}_{k-1} - (\mathbf{Q}_k(:,k))^T Y \mathbf{Q}_k(:,k) \tag{4-13}$$

Technique 3: Implementation of early stopping criterion

The trade-off between the complexity of the surrogate model and the number of experimental design points should be considered (Hariri-Ardebili & Sudret, 2020). By training a small number of points to obtain a complex sparse PCE model (e.g., a large

number of basis functions), the error of sparse PCE model using these trained points could be small. However, it may have large errors for the unseen data (e.g., generated new input data points). In this way, the surrogate model is over-fitted.

To avoid the over-fitting problem, the leave-one-out (LOO) cross-validation is used for model selection. The LOO error is computed as follows (Blatman & Sudret, 2010)

$$e_{\mathcal{X}}[\mathcal{M}_{\mathcal{X},S}] = \frac{1}{N}\sum_{i=1}^{N}\left(\mathcal{M}(\mathbf{x}^{(i)}) - \mathcal{M}_{\mathcal{X}\setminus i,S}(\mathbf{x}^{(i)})\right)^2 \tag{4-14}$$

where $e_{\mathcal{X}}[\mathcal{M}_{\mathcal{X},S}]$ is the LOO error; $\mathcal{X} = \mathbf{x}^{(1)}, \dots, \mathbf{x}^{(N)}$ represent N realizations of input vectors; $\mathcal{M}_{\mathcal{X},S}$ is the surrogate model S established using data set $\mathcal{X}$; $\mathcal{M}(\mathbf{x}^{(i)})$ is the evaluation at the input vector $\mathbf{x}^{(i)}$; $\mathcal{M}_{\mathcal{X}\setminus i,S}$ is the surrogate model S trained by leaving the ith data out of $\mathcal{X}$; and N is the number of samples.

For the PCE based methods, it is not necessary to train N PCE models to compute the LOO error, alternatively, the LOO can be computed with one analysis as (Blatman & Sudret, 2010)

$$e_{\mathcal{X}}[\mathcal{M}_{\mathcal{X},S}] = \frac{1}{N}\sum_{i=1}^{N}\left(\frac{\mathcal{M}(\mathbf{x}^{(i)}) - \mathcal{M}_{\mathcal{X},S}(\mathbf{x}^{(i)})}{1 - h_i}\right)^2 \tag{4-15}$$

where h_i is the ith term of the $diag(\mathbf{\Phi}(\mathbf{\Phi}^T\mathbf{\Phi})^{-1}\mathbf{\Phi}^T)$.

The LOO error can also be expressed as residual error as (Golub & Van Loan, 1996)

$$e_{\mathcal{X}}[\mathcal{M}_{\mathcal{X},S,k}] = \frac{1}{N}\sum_{i=1}^{N}\left(\frac{\mathbf{r}_{k,i}}{\partial \mathbf{r}_{k,i}/\partial Y_i}\right)^2 \tag{4-16}$$

Based on QR decomposition, the LOO error can be rewritten as (Baptista et al., 2019)

$$e_{\mathcal{X}}\left[\mathcal{M}_{\mathcal{X},S,k}\right] = \frac{1}{N}\sum_{i=1}^{N}\left(\frac{\mathbf{r}_{k,i}}{\mathbf{1}-\mathbf{Q}_k(i,:)\mathbf{Q}_k(i,:)^T}\right)^2 \tag{4-17}$$

As illustrated, the LOO error can be efficiently computed through the QR decomposition at each iteration. The LOO error can be adopted as a model selection criterion to overcome the over-fitting problem. Traditionally, a greedy algorithm can be used to perform all possible iterations and the LOO errors are recorded at each iteration. The sparse PCE model associated with the minimum LOO error is chosen as the final model. In this study, the evolution of LOO error from iterations is investigated in case study parts. To avoid unnecessary iterations, the LOO error-based criterion for early stopping the algorithm is proposed.

Overall, this study focuses on reducing the computational time of developing sparse PCE within high-dimensional engineering problems, by combining the three acceleration techniques: probabilistic reduction of basis function candidates; efficient updating using QR decomposition; and implementation of early stopping criterion. The three techniques accelerate the algorithm from different aspects, and each technique interacts with others. For instance, the leave-one-out error-based early stopping criterion is used to speed up the algorithm by avoiding unnecessary iterations, and QR decomposition is used to reduce the burden of computing this early stopping criterion. Within basis function selection, reduction of basis function candidates is adopted to reduce the computational burden, the residual, which is used in basis function selection,

can be efficiently updated by QR decomposition. Each of the three techniques interacts with others to jointly reduce the computational burden.

The computational process of the integrated ASPCE is illustrated in Table 4.1. The evolution of LOO error from iterations is investigated, and the LOO error-based criterion for stopping the algorithm is proposed. At each iteration, a subset of basis function candidates is sampled from the whole dictionary. From the subset candidates, the algorithm finds the basis function which is most correlated with the current model residual, and the identified basis function is then added to the active set. The residual and LOO error are updated using currently selected basis functions based on QR decomposition. These procedures are repeated, and the algorithm is stopped once meeting the stopping criterion. The coefficients of the sparse PCE are finally solved after stopping the iteration and the sparse PCE is established.

Table 4.1 Procedures of ASPCE

Acceleration algorithm for computation of sparse PCE
1. Initialization: determine the number of basis candidates in a subset; $\mathbb{C}_1 = \mathbb{C}$; $\mathbb{S}_0 = \emptyset$; $\mathbf{r}_0 = Y$; $k = 1$.
2. While: stopping criterion is not satisfied.
3. Probabilistic sampling of subset basis candidates $\mathbb{C}_s \subseteq \mathbb{C}_k$.
4. Find basis function $\Psi_{h(k)}$, so that $h(k) = \text{argmax}_{i \in \mathbb{C}_s} \frac{|\langle \psi_i, \mathbf{r}_{k-1} \rangle|}{\|\psi_i\|_2}$.
5. Remove selected basis from candidate set $\mathbb{C}_{k+1} = \mathbb{C}_k \backslash h(k)$.
6. Add selected basis to active set $\mathbb{S}_k = \mathbb{S}_{k-1} \cup h(k)$.
7. Compute residual $\mathbf{r}_k$ using QR decomposition.
8. Update LOO error.
9. $k = k+1$.
10. End.
11. Compute coefficients of PCE by solving $\mathbf{R}_m C = (\mathbf{Q}_m)^T Y$.

4.5   Illustrative Example

The computational procedures consist of three parts: initiation of training data; establishment of sparse PCE model; and post-processing of sparse PCE model. In the first stage, probabilistic distributions of the input variables are identified. A set of input samples is generated based on the experimental design, and the output parameters are computed by running the physical models. The sparse PCE model is obtained after performing the ASPCE. The uncertainty quantification can be accomplished efficiently.

In this section, the developed approach is applied to a frame structure firstly. Then, the presented framework is applied to spatially distributed bridges under seismic hazards. Within the investigated two examples, the performance of ASPCE is compared with OMP and other surrogate models: regression tree (RT), support vector machine (SVM), and Gaussian process regression (GPR). The basic ideas of these models are briefly introduced in this section.

The RT divides the data space into small sub-spaces and trains the models using each sub-space data. Since several data sub-spaces are produced by this approach, the interactions can be captured by the nonlinear model with several layers (Morgan & Sonquist, 1963; Rokach & Maimon, 2008). The SVM uses the kernels to convert the parameters into a high dimension space. The SVM model is expressed as the sum of weighted nonlinear functions and a constant parameter. The selection of kernel and nonlinear functions are very important (Ebad Sichani & Padgett, 2019). The GPR

surrogate model is regarded as nonparametric kernel-based probabilistic models (Rasmussen & Williams, 2006). The GPR model describes the outputs by explicit basis functions and latent variables from a Gaussian process. The basis functions map the input parameters to high dimension space.

4.5.1 Case 1: Uncertainty Quantification of a Frame Structure

A three-span three-story frame structure under lateral loads is selected as the example. The sketch of the structure is illustrated in Figure 4.2, and the uncertain parameters considered are listed in Table 4.2. Three different lateral loads are applied to the left part of the structure. The displacement at the top right corner is considered as the response of interest.
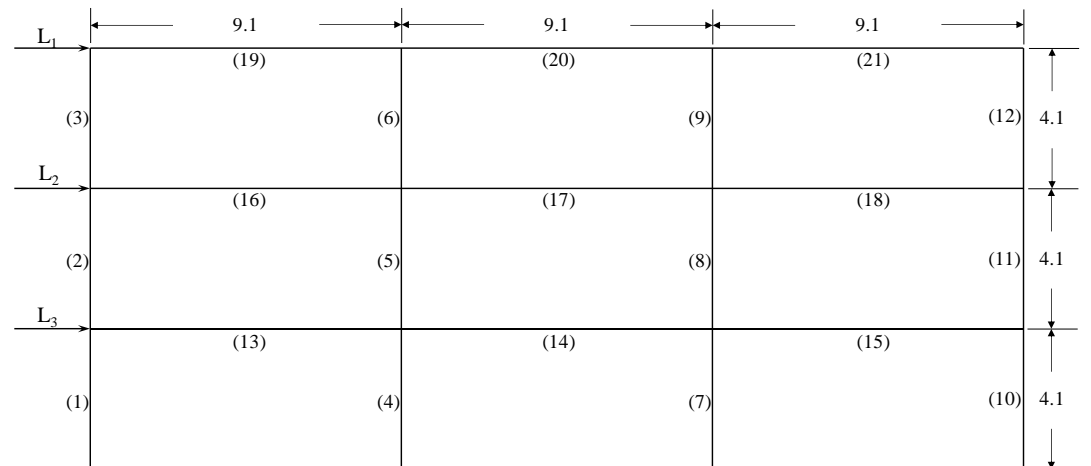
Figure 4.2 Investigated frame structure subjected to lateral loads (unit: m, the numbers indicate different elements and are mapped to the parameters in Table 4.2)

Table 4.2 Parameters used within the frame structure

Symbol	Parameter	Number	Units	Distribution type	μ	σ
L_1	Load 1	1	N	Lognormal	4.89×10^5	1.47×10^5
L_2	Load 2	2	N	Lognormal	4×10^5	1.6×10^5
L_3	Load 3	3	N	Lognormal	2×10^5	8×10^4
E_{13-21}	Young's modulus (material property of elements 13-21)	4	N/m^2	Lognormal	1.98×10^{11}	1.74×10^{10}
E_{1-12}	Young's modulus (material property of elements 1-12)	5	N/m^2	Lognormal	1.99×10^{11}	1.75×10^{10}
A_{1-3}	Cross-sectional area of elements 1-3	6	m^2	Lognormal	0.0488	0.0087
A_{4-9}	Cross-sectional area of elements 4-9	7	m^2	Lognormal	0.0590	0.0105
A_{10-12}	Cross-sectional area of elements 10-12	8	m^2	Lognormal	0.0476	0.0085
A_{13-18}	Cross-sectional area of elements 13-18	9	m^2	Lognormal	0.0224	0.004
A_{19-21}	Cross-sectional area of elements 19-21	10	m^2	Lognormal	0.0130	0.0023
I_{1-3}	Moment of inertia of elements 1-3	11	m^4	Lognormal	0.0014	1.86×10^{-4}
I_{4-9}	Moment of inertia of elements 4-9	12	m^4	Lognormal	0.0018	2.40×10^{-4}
I_{10-12}	Moment of inertia of elements 10-12	13	m^4	Lognormal	0.0015	2.00×10^{-4}
I_{13-15}	Moment of inertia of elements 13-15	14	m^4	Lognormal	0.0025	3.33×10^{-4}
I_{16-18}	Moment of inertia of elements 16-18	15	m^4	Lognormal	0.0021	2.80×10^{-4}
I_{19-21}	Moment of inertia of elements 19-21	16	m^4	Lognormal	7.617×10^{-4}	1.01×10^{-4}
M_f	Mass factor	17	-	Uniform	1	0.058

Note: μ = mean value and σ = standard deviation.

The performance of surrogate models under different sample sizes is investigated. Based on the statistic parameters in Table 4.2, 8 sets of frame structure and load realizations (with sample sizes of 100, 200, 400, 600, 800, 1000, 1200, and 1400) are generated using Latin hypercube sampling technique (Ayyub & Lai, 1989). The displacement at the top right corner can be computed using finite element model in OpenSEES. The 8 sets of input and output training data are obtained. As discussed previously, the LOO error is considered as the stopping criterion in ASPCE. In this study, the evolution of LOO error is investigated and an appropriate occasion for stopping the algorithm is proposed. The LOO errors changing with iterations are presented in Figure 4.3 The results show that the evolution of LOO error is convex and smooth for the investigated case. To avoid the possible local minima of LOO error, the proposed early stopping criterion is to stop the algorithm when the LOO error continuously increases for ten iterations.
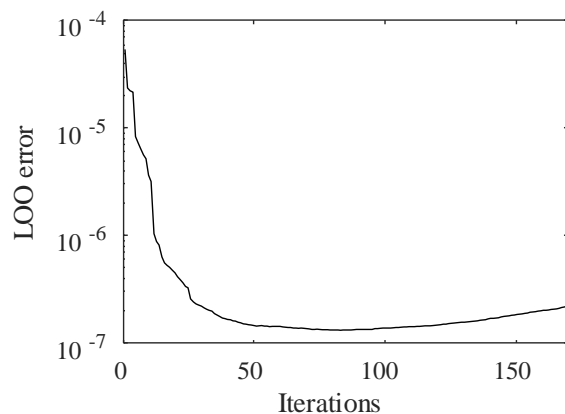
Figure 4.3 The evolution of the LOO error

The surrogate models are trained using ASPCE, OMP, SVM, RT, and GPR under the 8 sets of training data. The training time of OMP and ASPCE is presented in Figure

4.4. The training time of OMP increases significantly with the total degree of polynomials while the training time of ASPCE is independent with the total degree of polynomials. The ASPCE seems to be more efficient than OMP under high total degree of polynomials. The superiority of ASPCE in terms of efficiency is further demonstrated in the following example.
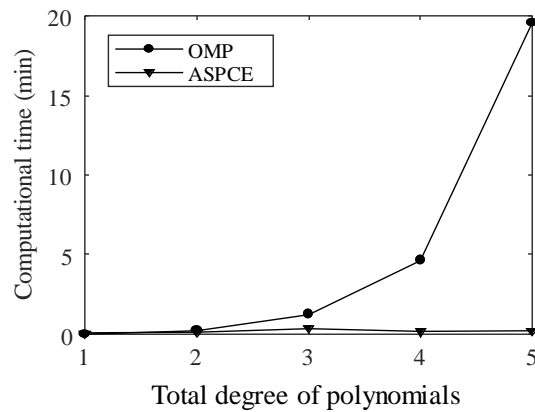
Figure 4.4 Training time of OMP and ASPCE associated with the investigated frame structure

The brute-force MCS is used to validate the results obtained from surrogate models (Yang et al., 2019). The statistic moments, PDF, and reliability indices computed from MCS serve as references to calculate the relative errors. Once the sparse PCE model is obtained, the statistic moments are computed efficiently. The relative errors in mean and standard deviation of the five surrogate models under different sample sizes are presented in Figure 4.5. With respect to predictive performance in mean, the ASPCE, OMP, and GPR are identified as suitable surrogate models. The relative errors in mean from these three models converge after the sample size of 400 and maintain at relatively lower level after convergence. For the relative errors in

standard deviation, the sparse PCE based methods ASPCE and OMP outperform other

models under all sample sizes, while the GPR produces higher relative errors.
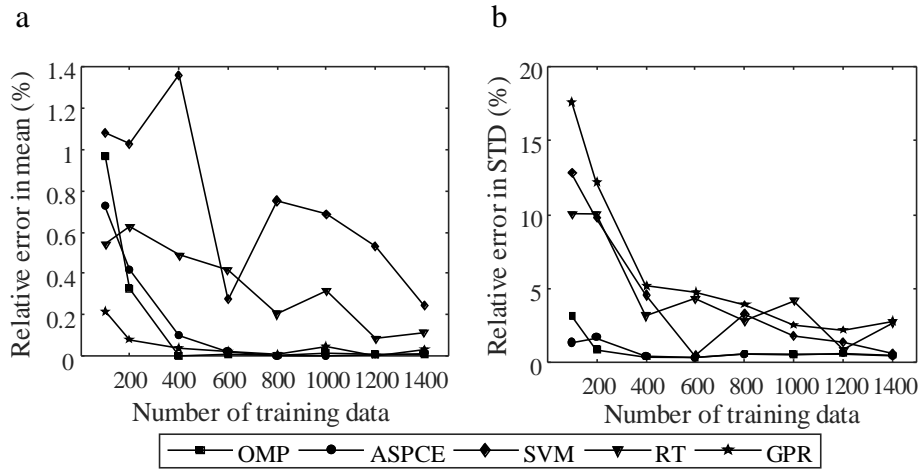
Figure 4.5 Relative errors in: (a) mean and (b) standard deviation under different

sample sizes

The relative errors in reliability indices for two different limit thresholds (e.g., 3

cm and 5 cm) are illustrated in Figure 4.6. For the case of limit threshold 3 cm, the

errors from ASPCE, OMP, and GPR converge after the sample size of 200 and these

three models stand out among the five. With respect to the limit threshold of 5 cm, the

convergence sample size for ASPCE and OMP is 400. These two models have

relatively lower errors than others in this scenario.
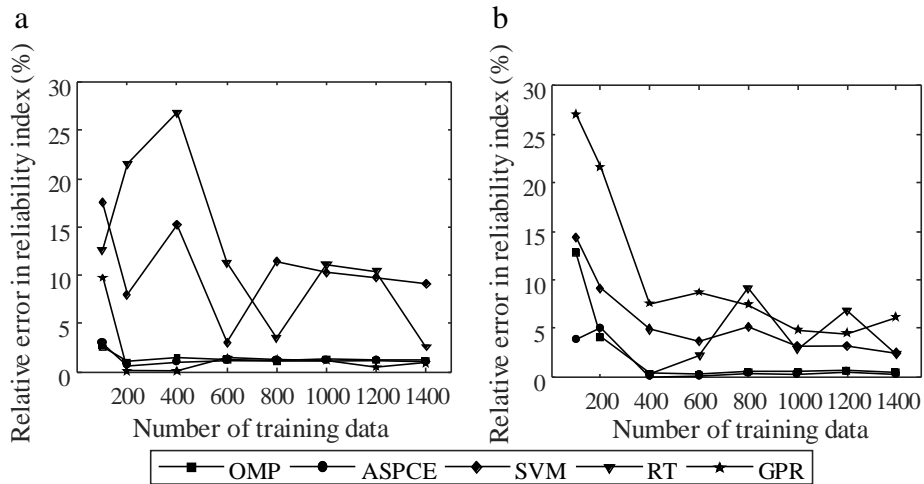
Figure 4.6 Relative errors of reliability indices under the limit thresholds of (a) 3 cm

and (b) 5 cm, respectively.

The PDFs of the displacement obtained by ASPCE, GPR, and MCS are shown in

Figure 4.7. The PDF from ASPCE matches perfectly with MCS. For the GPR, the errors

can be observed around the peak and tail of PDF curve.
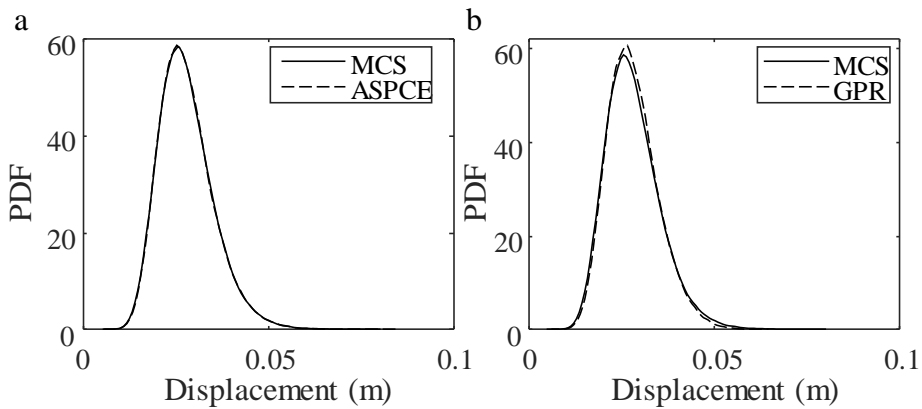
Figure 4.7 Comparisons of the PDFs computed by MCS and surrogate models of (a)

ASPCE and (b) GPR.

The confidence interval provides information on the confidence of estimated

statistical results in consideration of the uncertainties. The ASPCE derived 95%

confidence intervals for the mean of displacement and standard deviation of displacement are computed. The lower bound and upper bound for mean value are 2.797×10^{-2} and 2.802×10^{-2}, respectively. The lower bound and upper bound for standard deviation value are 7.346×10^{-3} and 7.413×10^{-3}, respectively. The confidence intervals are narrow for the statistical moments and reliability indices, indicating the computational confidence and stability of ASPCE.

The computational time of uncertainty quantification can be saved significantly by using the ASPCE. The data from running 400 finite element models (FEMs) is used in ASPCE, while the data from running 10^5 FEMs is used in MCS. The total computational time of MCS is 6 hours and computational time ASPCE is 2 minutes.

To sum up, the sparse PCE based methods ASPCE and OMP have satisfying predictive performance compared with other investigated surrogate models. The training time of ASPCE is less compared with OMP under high degree cases. By using ASPCE, the total time of uncertainty quantification can be reduced significantly compared with conventional MCS, in the meanwhile, this method provides satisfying accuracy.

4.5.2   Case 2: Seismic Vulnerability Analysis of Spatially Distributed Bridges

The spatially distributed RC bridges is selected for investigation. In regional risk assessment, the bridges distributed within a region could have different material and geometric parameters. Conventionally, it is impractical to develop the fragility curves

for each specific structure in a region, as the computational time is extensive. Developing bridge class level fragility, by incorporating material and geometric uncertainties within a class, can be one possible solution to address this challenge (Mangalathu et al., 2016). The bridge class level fragility is used to describe the damage probabilities for the bridges within a class under earthquakes. To facilitate the regional risk assessment, the bridge class level fragility should be developed and incorporate the uncertainties from hazards, material and geometric parameters (Mangalathu et al., 2016; Mangalathu, Jeon, et al., 2018). Thus, the uncertainties associated with material and geometric parameters should be considered in training of surrogate model (Jeon et al., 2019). The probabilistic parameters of these bridges are summarized in Table 4.3. Based on the probabilistic distributions of the bridge parameters, the bridge realizations are sampled using Latin hypercube sampling technique (Ayyub & Lai, 1989). The finite element models of the bridge realizations are established using the software OpenSEES (Dong et al., 2013; Li, Dong, & Qian, 2020; Qian & Dong, 2020). For each bridge sample, one ground motion from (Baker et al., 2011) is randomly selected and coupled with this bridge sample. So that the input data including bridge samples and ground motions are obtained. The number of the ground motions and that of the Latin hypercube sampling structures are identical. The ground motions used for coupling with bridge samples are associated with different intensities and characteristics. Thus, these input samples incorporate the uncertainties associated with bridge geometry, material, and ground motions. A set of nonlinear time history analyses using the input samples is performed to obtain the training data. The seismic demands of different components

can be computed using the developed finite element model (Giouvanidis & Dong, 2020;

Zheng & Dong, 2019).

Table 4.3 Parameters used within the bridges

Parameters	Number	Units	Distribution type	μ	σ	Ref.
Concrete compressive strength	1	MPa	Normal	29.03	3.59	(Mangalathu, Jeon, et al., 2018)
Reinforcing steel yield strength	2	MPa	Lognormal	465.0	37.30	(Mangalathu, Jeon, et al., 2018)
Span length	3	mm	Lognormal	31775	8738	(Mangalathu, Jeon, et al., 2018)
Deck width	4	mm	Lognormal	11970	2418	(Mangalathu, Jeon, et al., 2018)
Column height	5	mm	Lognormal	6625	865	(Mangalathu, Jeon, et al., 2018)
Abutment backwall height	6	mm	Lognormal	2186	441	(Mangalathu, Jeon, et al., 2018)
Bearing coefficient of friction	7	-	Normal	0.3	0.1	(Mangalathu, Jeon, et al., 2018)
Strength of a composite of two dowels	8	kN	Lognormal	116	9.28	(Nielson, 2005)
Abutment-deck gap	9	mm	Lognormal	23.5	12.5	(Mangalathu, Jeon, et al., 2018)
Backfill initial stiffness at the benchmark backwall height	10	N/m/cm	Lognormal	384	138	(Xie et al., 2019)
Backfill ultimate capacity at the	11	kN/m	Lognormal	475	111	(Xie et al., 2019)

benchmark backwall height						
Damping	12		Normal	0.045	0.0125	(Mangalathu, Jeon, et al., 2018)
Foundation translational spring stiffnesses	13	N/mm	normal	140101	105076	(Mangalathu, Jeon, et al., 2018)
Shear modulus of elastomeric pad	14	MPa	Uniform	1.365	0.407	(Nielson, 2005)
Mass factor	15	-	Uniform	1	0.058	(Nielson, 2005)
Longitudinal reinforcement ratio	16	(%)	Uniform	2.25	0.52	(Mangalathu, Jeon, et al., 2018)

Note: μ = mean value and σ = standard deviation.

The training for the surrogate model is carried out once using the data consisting of ground motions with different intensities, structure samples, and seismic demands from finite element models. The uncertainties associated with structures and ground motions are considered in uncertainty quantification. To further testify the applicability of the proposed LOO error-based stopping criterion, the evolution of LOO error is investigated in this case. To the authors' best knowledge, the evolution of LOO error on bridge seismic demands has not been investigated in previous studies. The results show that the evolution of LOO error of ASPCE is convex and smooth, and proposed LOO error-based stopping criterion is still applicable.

The predictive performance of surrogate model can be evaluated in terms of the mean squared error (MSE) on an independent test sample set (Mangalathu, Heo, et al., 2018). The MSEs of the investigated models on a test sample set are computed and

listed in Figure 4.8. The effects of the training sample sizes on predictive performance are also investigated. As indicated, the sparse PCE based methods (e.g., ASPCE and OMP) have satisfying performance for all considered sample sizes. The ASPCE provides similar predictive performance with OMP.
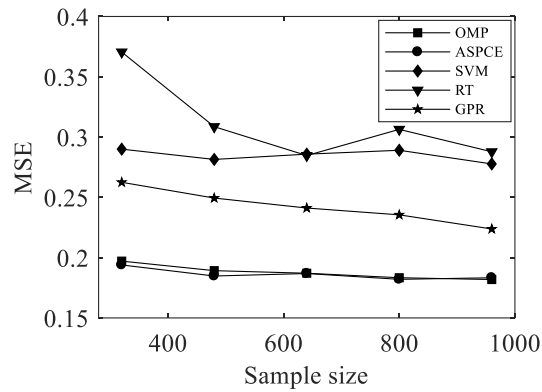
Figure 4.8 MSE of the seismic demands on a test sample set under different training sample sizes

The training time for each model is calculated as the sum of the training time for all the structural components. The training time for two sparse PCE based methods with increasing total degree of polynomials is illustrated in Figure 4.9. The training time of OMP increases significantly with total degree of polynomials, while the training time of ASPCE is negligible and independent with total degree of polynomials. The improved efficiency of the ASPCE can be interpreted through the three speeding-up techniques. As illustrated in Figure 4.10, the number of candidate basis functions increases significantly with total degree of polynomials and input dimensions. With the implementation of probabilistic reduction of basis function candidates, the ASPCE would evaluate a subset of polynomial candidates, while the OMP uses the whole

dictionary. Additionally, the number of evaluated candidates is constant at all degrees and input dimensions in ASPCE. This consistency ensures the training time of ASPCE is independent with the total degree of polynomials and input dimensions. This speeding-up technique ensures that the ASPCE can be performed for high degree and high dimension problems with negligible computational cost. With the implementation of QR decomposition, the residual and LOO error can be efficiently updated at each iteration without solving the PCE coefficients, while the OMP relies on solving the coefficients at each iteration. The implementation of stopping criteria aids the ASPCE to avoid unnecessary iterations and early stop at an appropriate occasion. The stopping of OMP needs the determination of an optimal error tolerance which is computed by cross-validation, and this process induces additional computational time.
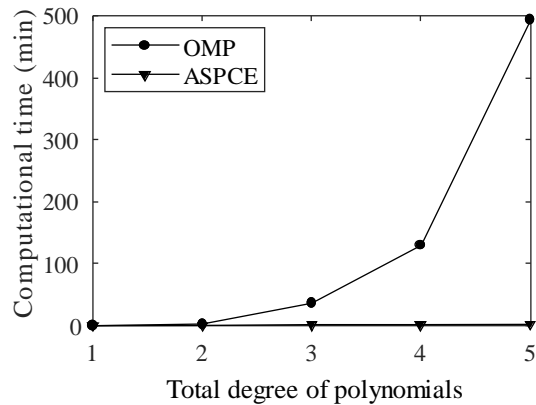
Figure 4.9 Training time of OMP and ASPCE
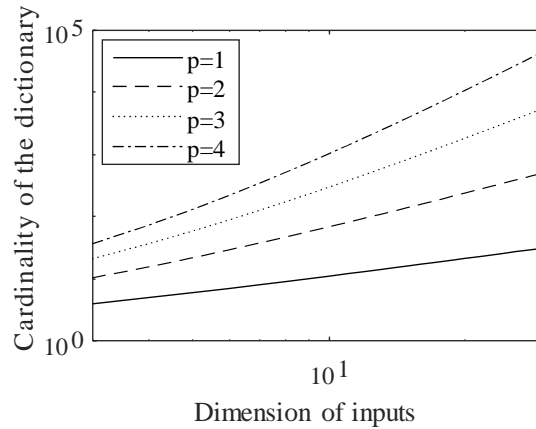
Figure 4.10 Cardinality of the PCE dictionary

To summarize the performance of the investigated surrogate models, the ASPCE has satisfying predictive ability and computational cost. The implemented three speeding-up techniques can effectively reduce the computational cost and ensure the satisfying predictive performance.

The seismic vulnerability analysis is performed using the developed surrogate model. The probabilistic input vector is generated from corresponding distributions. The surrogate models are used to compute the probabilistic demands. The probabilistic demands can be computed in seconds using the surrogate models, while the computational cost is large using the original physical models. The probabilistic capacity of a component can be computed based on corresponding distribution. Then, the seismic vulnerability of the spatially distributed bridges can be computed as indicated in Figure 4.11.
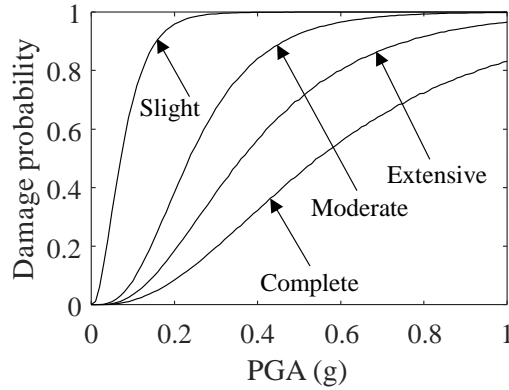
Figure 4.11 Seismic vulnerability of the spatially distributed bridges

4.6   Summary

This study presents a framework for uncertainty quantification of structural systems using sparse PCE and acceleration algorithm. Three techniques including probabilistic reduction of basis function candidates, QR decomposition, and early stopping criterion are combined to formulate an integrated acceleration algorithm for the computation of sparse PCE (ASPCE), and the computational burden of developing sparse PCE within high-dimensional engineering problems can be reduced.

Two case studies are conducted to illustrate the applicability, accuracy, and efficiency of the proposed approach. The approach is verified using MCS through a simple frame structure example. Then, the approach is applied to complex bridge structures. In general, the sparse PCE-based methods ASPCE and OMP have satisfying predictive performance compared with other investigated surrogate models. The implemented three speeding-up techniques in ASPCE can effectively reduce the computational burden compared with the greedy algorithm OMP. The training time of OMP increases significantly with the total degree of polynomials and input dimensions.

In contrast, the training time of ASPCE is independent with input dimension and the total degree of polynomials, it can be used for high-dimensional problems with reduced computational cost. The presented approaches can aid the uncertainty quantification and regional level performance assessment of spatially distributed bridges in an efficient manner.

One type of bridge is considered in this study. The sparse PCE can be applied to other types of bridges. The general procedures are summarized as follows. Based on the bridge inventory data, the probabilistic distribution of bridge input can be determined. From experimental design, bridge realizations can be generated. After performing the physical model, the training data including input and output can be obtained. The sparse PCE can be developed by performing the algorithm. By post-processing the sparse PCE model, uncertainty quantification can be achieved.

CHAPTER 5

SURROGATE-ASSISTED TWO-STAGE MULTI-CRITERIA GLOBAL SENSITIVITY ANALYSIS

5.1   Introduction

Due to the existence of uncertainty associated with the system and environment, decision-makers need to refine the database (e.g., data acquisition, investigation, and complexity reduction) for confident regional risk assessment. The global sensitivity analysis assessing the effects of the variations of input variables on the output can be used to facilitate uncertainty treatment.

The Monte Carlo method (Sobol, 2001) is a traditionally used method for global sensitivity analysis. A large number of simulations are required resulting in high computational cost. Besides the advantage of sparse PCE in efficient uncertainty quantification as introduced in chapter 4, global sensitivity analysis can be performed efficiently using the developed sparse PCE model (Sudret, 2008). The global sensitivity indices associated with different input parameters can be computed efficiently by post-processing the PCE coefficients with lower computational costs.

Traditional PCE-based global sensitivity analysis only assesses the sensitivity to an individual structural performance criterion. Assessing the global sensitivity considering multiple criteria is challenging as the sensitive parameters may not be consistent for different performance criteria. Additionally, there is not a PCE-based sensitivity analysis approach that can be adopted directly for assessing the global

sensitivity incorporating multiple structural performance criteria. To address this issue, a two-stage multi-criteria global sensitivity analysis algorithm is proposed herein by coupling the ASPCE (developed in chapter 4) and TOPSIS. A holistic global sensitivity index is proposed to identify the sensitive parameters incorporating multiple performance criteria. To illustrate the efficiency, accuracy, and applicability of the proposed approach, two illustrative cases are presented.

5.2   Global Sensitivity Analysis for the Individual Output Parameter

The contribution of uncertain input variables to the output variance can be quantified using global sensitivity analysis (Sudret, 2008). Traditionally, the global sensitivity index is computed by MCS with high computational cost especially for some complex models. By post-processing the PCE coefficients, the global sensitivity index can be computed efficiently. Let $\mathcal{H}_{i_1,\dots,i_s}$ represent the set from $\alpha \in \mathcal{A}$ where only the indices $\{i_1,\dots,i_s\}$ are non-zero, the $\mathcal{H}_{i_1,\dots,i_s}$ is expressed as

$$\mathcal{H}_{i_1,\dots,i_s} = \{\alpha \in \mathcal{A} : \alpha_v = 0 \Leftrightarrow v \notin (i_1,\dots,i_s), \forall\, v = 1,\dots,M\} \tag{5-1}$$

The PCE based sensitivity indices are derived as (Blatman & Sudret, 2010)

$$S_{i_1,\dots,i_s}^{\mathcal{A}} = \frac{\sum_{\alpha \in \mathcal{H}_{i_1,\dots,i_s}} c_\alpha{}^2}{D_{\mathcal{A}}}, \; D_{\mathcal{A}} = \sum_{\alpha \in \mathcal{A}\backslash\{0\}} c_\alpha{}^2 \tag{5-2}$$

The total sensitivity indices are computed as

$$S_i^{T,\mathcal{A}} = S_i^{\mathcal{A}} + \sum_{j<i} S_{j,i}^{\mathcal{A}} + \sum_{j<k<i} S_{j,k,i}^{\mathcal{A}} + \cdots + S_{1,\dots,M}^{\mathcal{A}} \tag{5-3}$$

The Eq. 5-3 can be rewritten as

$$S_i^{T,\mathcal{A}} = \frac{\sum_{\alpha \in \mathcal{g}_i} c_\alpha{}^2}{D_\mathcal{A}} \tag{5-4}$$

$$\mathcal{g}_i = \{\alpha \in \mathbb{N}^M : 0 \leq |\alpha| \leq p, \alpha_i \neq 0\} \tag{5-5}$$

5.3　　　Holistic Global Sensitivity Analysis

The conventional global sensitivity analysis reveals the effects of the input variable on one single output parameter. When multiple output parameters existing in a system are of interest, determining the overall sensitivity of the input with respect to multiple output parameters becomes a problem. In this study, the global sensitivity indices associated with different performance criteria are incorporated to compute the holistic global sensitivity index. The TOPSIS (Hwang & Yoon, 1981), a multi-criteria decision making technique, is extended herein to compute the holistic global sensitivity index. In this way, the overall sensitivity of input parameters considering multiple criteria could be assessed. The following part introduces the basic procedures of computing the holistic global sensitivity index. The global sensitivity indices associated with all the output parameters are formulated in a sensitivity index matrix **S** as

$$\mathbf{S} = \begin{pmatrix} S_{1,1} & \cdots & S_{1,n_c} \\ \vdots & \ddots & \vdots \\ S_{n_i,1} & \cdots & S_{n_i,n_c} \end{pmatrix} \tag{5-6}$$

where $S_{i,j}$ is the global sensitivity index of the ith input parameter with respect to the jth performance criterion; n_c is the number of performance criteria; and n_i is the number of input parameters. The global sensitivity index used in Eq. 5-6 could be first-order or total order. The total order global sensitivity index describes the contribution of an input parameter to output variance considering the effects of its interaction with other input

parameters (Blatman & Sudret, 2010; Palar et al., 2018). The choice of first-order or total order depends on the concerns and requirements of the decision makers. If the decision makers desire the information including the interaction among different variables, the total order global sensitivity index can be chosen. If the isolated impact of the input variable is of concern, the first-order global sensitivity index can be chosen. If total global sensitivity index is used in Eq. 5-6, the interaction effects among different variables are incorporated in the decision-making process.

Then, the sensitivity index matrix is normalized as

$$
\bar{\mathbf{S}} = \begin{pmatrix} \bar{S}_{1,1} & \cdots & \bar{S}_{1,n_c} \\ \vdots & \ddots & \vdots \\ \bar{S}_{n_i,1} & \cdots & \bar{S}_{n_i,n_c} \end{pmatrix}, \quad \bar{S}_{i,j} = \frac{S_{i,j}}{\sqrt{\sum_{k=1}^{n_i} S_{k,j}^2}}
\tag{5-7}
$$

where $\bar{\mathbf{S}}$ is the normalized sensitivity index matrix.

Different performance criteria could result in different importance to the system safety. The different preferences of performance criteria should be incorporated within the holistic global sensitivity index by implementing weighting factor. The weighting factor associated with different performance criteria determined by the decision maker is applied to the normalized sensitivity index matrix as

$$
\hat{\mathbf{S}} = \begin{pmatrix} \hat{S}_{1,1} & \cdots & \hat{S}_{1,n_c} \\ \vdots & \ddots & \vdots \\ \hat{S}_{n_i,1} & \cdots & \hat{S}_{n_i,n_c} \end{pmatrix}, \quad \hat{S}_{ij} = w_j \times \bar{S}_{ij}
\tag{5-8}
$$

where $\hat{\mathbf{S}}$ donates the weighted and normalized sensitivity index matrix and w_j represents the weighting factor for the jth performance criterion.

The ideal sensitivity solution is obtained by extracting the maximum values of sensitivity indices associated with all input parameters. The negative-ideal solution is obtained conversely. These two sensitivity solutions are expressed as

$$S^+ = \left\{ \hat{S}_{1+},...,\hat{S}_{n_c+} \right\} = \left\{ (\max \hat{S}_{ij}), i = 1,...,n_i, j \in J \right\} \qquad (5\text{-}9)$$

$$S^- = \left\{ \hat{S}_{1-},...,\hat{S}_{n_c-} \right\} = \left\{ (\min \hat{S}_{i,j}), i = 1,...,n_i, j \in J \right\} \qquad (5\text{-}10)$$

The distance of the sensitivity associated with each input variable to the ideal solution and negative-ideal solution can be calculated. The holistic global sensitivity index is computed based on the relative closeness as

$$hs_i = \frac{\sqrt{\sum_{j=1}^{n_c} (\hat{S}_{i,j} - \hat{S}_{j-})^2}}{\sqrt{\sum_{j=1}^{n_c} (\hat{S}_{i,j} - \hat{S}_{j+})^2} + \sqrt{\sum_{j=1}^{n_c} (\hat{S}_{i,j} - \hat{S}_{j-})^2}} \qquad (5\text{-}11)$$

where hs_i is the holistic global sensitivity index for the input valuable i.

5.4　　　　Framework of Two-stage Multi-criteria Global Sensitivity Analysis

The problem can be formulated as a multi-criteria decision-making problem when there exist the following conditions: several alternatives serve as the comparable components; multiple criteria are used to describe the status of each alternative; and multiple objectives need to be satisfied. By considering multiple conflicting criteria, there may not exist a solution that is satisfying over all criteria. A compromise solution incorporating the trade-off consideration among multiple conflicting criteria can be obtained by using multi-criteria decision making techniques (Tzeng & Huang, 2011).

For an engineering system consisting of multiple outputs, different outputs may be associated with different sensitive parameters. There may not exist one input that is most sensitive to all outputs. The trade-off among multiple outputs should be considered. In this regard, sensitivity ranking of inputs considering multiple outputs can be formulated as a compromise multi-criteria decision-making problem. Each input is considered as an alternative. For each input, the global sensitivity indices with respect to multiple outputs can be quantified and they are considered as multiple ranking criteria. The objective is to determine the sensitivity raking of inputs considering the global sensitivity indices with respect to multiple outputs. TOPSIS, a robust compromise decision making approach, is extended herein to solve this multi-criteria decision-making problem.

The basic idea of TOPSIS is to rank the alternatives based on distance, where the preferential alternative should have a long distance to the negative-ideal solution and a short distance to the ideal solution. Herein, the negative-ideal solution and ideal solution are represented as the ideal insensitive solution and ideal sensitive solution, respectively. The global sensitivity index matrix is used as a decision matrix in this study. Specifically, Eq. 5-11 is used to compute relative closeness as the last step in TOPSIS, and the ranking of alternatives is determined based on this index (Hwang & Yoon, 1981; Tzeng & Huang, 2011). The numerator in Eq. 5-11 represents the distance of an alternative to the negative-ideal solution, and the denominator in Eq. 5-11 represents the sum of the distance of an alternative to the negative-ideal solution and ideal solution (Hwang & Yoon, 1981; Tzeng & Huang, 2011). A preferential alternative

should have a large value of relative closeness computed in Eq. 5-11. In the decision making of ranking inputs, a sensitive input considering multiple outputs should have a large value of relative closeness (long distance to the ideal insensitive solution and short distance to the ideal sensitive solution). Therefore, the holistic global sensitivity index is proposed based on Eq. 5-11 in this study. The sensitivity ranking of input parameters considering multiple outputs can be determined based on the proposed holistic global sensitivity index. The proposed holistic global sensitivity index can be regarded as a holistic measure and utilized to identify the sensitive input parameters considering multiple performance criteria.

The value of holistic global sensitivity index depends on many factors such as the global sensitivity indices with respect to all outputs, the importance of different outputs, and the trade-off consideration. This expression shows one of the advantages of the proposed approach, the different importance of outputs and the trade-off can be flexibly considered within the sensitive parameter identification process in TOPSIS. In real engineering problems, different outputs could be associated with different considerations of importance, the importance of outputs represented by weighting factors in TOPSIS can be determined by judgement among experts.

The holistic global sensitivity index can be used to aid the decision makers to refine the database (e.g., data acquisition, investigation, and complexity reduction) for confident regional risk assessment. For instance, more efforts and resources can be spent on collecting and investigating holistic sensitive parameters. This index can also be used for the screening of holistic sensitive parameters considering the trade-off

among multiple outputs. Based on the proposed holistic global sensitivity index, the sensitive and insensitive input parameters considering the trade-off among multiple outputs can be identified. By constraining the number of considered sensitive parameters, the top holistic sensitive parameters can be selected based on holistic global sensitivity index. In another way, decision makers could also determine the threshold of holistic global sensitivity index based on their requirement, and the parameters associated with global sensitivity indices exceeding the threshold can be identified as holistic sensitive parameters.

Overall, the ASPCE and TOPSIS coupled two-stage multi-criteria global sensitivity analysis algorithm is proposed to incorporate multiple performance criteria. The global sensitivity is first assessed for individual performance criterion. The global sensitivity indices associated with different performance outputs are then considered as the sensitivity criteria and formulated as a sensitivity matrix. TOPSIS is used to incorporate these sensitivity criteria to compute the holistic global sensitivity indices. The detailed algorithm is illustrated in Table 5.1. Both the global sensitivity indices and holistic global sensitivity indices provide information for rational treatment of the uncertainty within input parameters.

Table 5.1 Procedures of two-stage multi-criteria global sensitivity analysis

Two-stage multi-criteria global sensitivity analysis algorithm

Stage 1: Global sensitivity analysis considering individual performance criterion

1   Determine *ni* uncertain variables and corresponding probabilistic distributions.

2   Conduct experimental design.

3   for performance criterion number *cn* = 1:*nc*

4   Formulate sparse PCE model for performance criterion *cn* using ASPCE.

5   Computed global sensitivity indices of *ni* variables with respect to the performance criterion *cn* by post-processing the PCE coefficients.

6   End

Stage 2: Holistic global sensitivity analysis considering multiple performance criteria

7   Formulate sensitivity index matrix **S.**

8   Compote normalized sensitivity matrix **NS**.

9   Determine the weighting factors of all performance criteria.

10 Compote normalized and weighted sensitivity matrix **VS**.

11 Extract ideal and negative-deal sensitivity solutions.

12 Compute the holistic global sensitivity indices based on relative closeness

5.5   Illustrative Example

In connection with the approach in chapter 4, the proposed framework of uncertainty quantification and multi-criteria global sensitivity analysis using ASPCE is illustrated in Figure 5.1. The computational procedures consist of three parts: initiation of training data; establishment of sparse PCE model; and post-processing of sparse PCE model. In the first stage, probabilistic distributions of the input variables are identified. A set of input samples is generated based on the experimental design, and the output parameters are computed by running the physical models. The sparse PCE model is obtained after performing the ASPCE. The uncertainty quantification and multi-criteria global sensitivity analysis can be accomplished efficiently. The ASPCE enable uncertainty

quantification is introduced in chapter 4. By using the same cases in chapter 4, the

ASPCE enabled global sensitivity analysis is illustrated in this section.
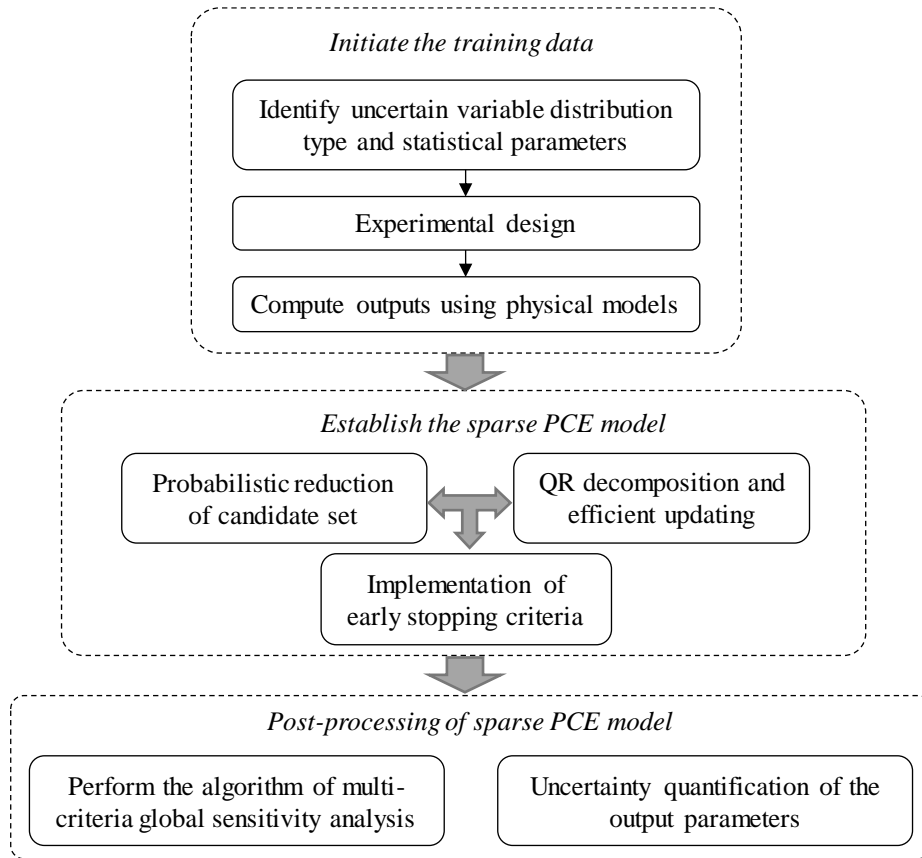
Figure 5.1 Framework of uncertainty quantification and global sensitivity analysis

5.5.1 Case 1: Global Sensitivity Analysis of a Frame Structure

The detailed description of this case is presented in chapter 4. In addition to the

uncertainty quantification, PCE can also aid efficient global sensitivity analysis. Instead

of conducting time-consuming MCS in the traditional method, the global sensitivity

indices can be computed analytically by post-processing the PCE coefficients. The

results are compared with those from MCS in Figure 5-2. The results show that the

ASPCE-derived sensitivity indices agree well with MCS-derived reference values.
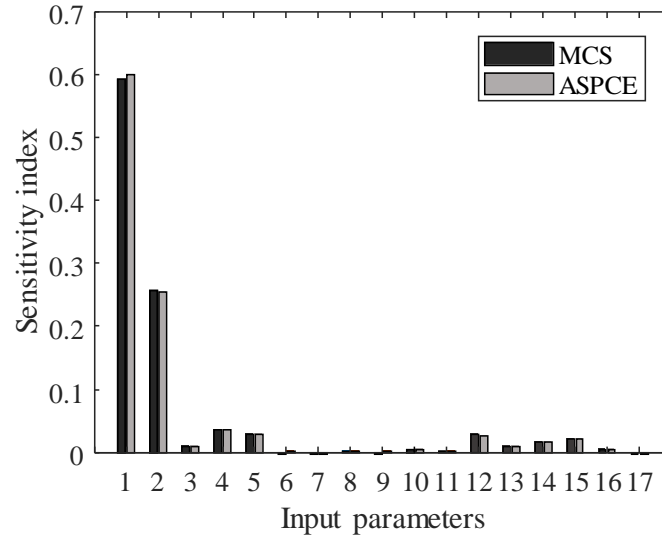
Figure 5.2 Sensitivity indices with respect to the frame displacement

The computational time of sensitivity analysis can be saved significantly by using

the ASPCE. The 400 finite element model evaluations are used in ASPCE, while a total

of $N_{MCS}(M + 2) = 10^5 \times (17 + 2) = 1.9 \times 10^6$ finite element model evaluations

are used in MCS for sensitivity analysis (Tarantola et al., 2012), where N_{MCS} is the

sample size of MCS. Within sensitivity analysis, the total computational time of MCS

is 116 hours and the total computational time ASPCE 2 minutes.

5.5.2   Case 2: Multi-criteria Global Sensitivity Analysis of Spatially Distributed Bridges Under Earthquakes

The detailed description of this case is presented in chapter 4. The seismic demand

surrogate models are obtained after performing the training algorithm. The multi-

criteria global sensitivity analysis is performed for the bridges. The seismic fragility using the information from multi-criteria global sensitivity analysis is computed.

The PCE based global sensitivity indices of the input parameters with respect to multiple demand parameters are presented in Figure 5.3. For all the structural demands, PGA is found to be the most sensitive parameter. Within the bridge parameters, the column height is the most sensitive parameter to column demand. With respect to bearing longitudinal demand, the shear modulus of elastomeric pad has the greatest influence. Apparently, the significant bridge parameters vary from component to component, and the similar observation was reported in (Jeon et al., 2019). The significant bridge parameters are not consistent for the seismic demands associated with all components. Based on sensitivity indices associated with individual seismic demand, determination of significant bridge parameters to the bridge system is challenging. Using the proposed multi-criteria global sensitivity analysis algorithm, the overall global sensitivity considering multiple structural performance criteria is assessed. Additionally, the different importance of structural performance criteria could be incorporated into the sensitivity analysis process by using weighting factor. Given different preferences of the structural performance criteria by the decision maker, the sensitivity results can be updated. The uncertainties associated with the weighting factor could also be incorporated in TOPSIS for multi-criteria global sensitivity analysis (Qian & Dong, 2020). The holistic global sensitivity indices of the bridge parameters are computed and presented in Figure 5.4. The top five most sensitive parameters of bridge input identified by multi-criteria global sensitivity analysis are

deck width, span length, shear modulus of elastomeric pad, column height, and concrete

compressive strength. The proposed holistic global sensitivity indices aid decision

maker to identify the sensitive parameters to the whole bridge system and the ranking

of the sensitive parameters can be determined.
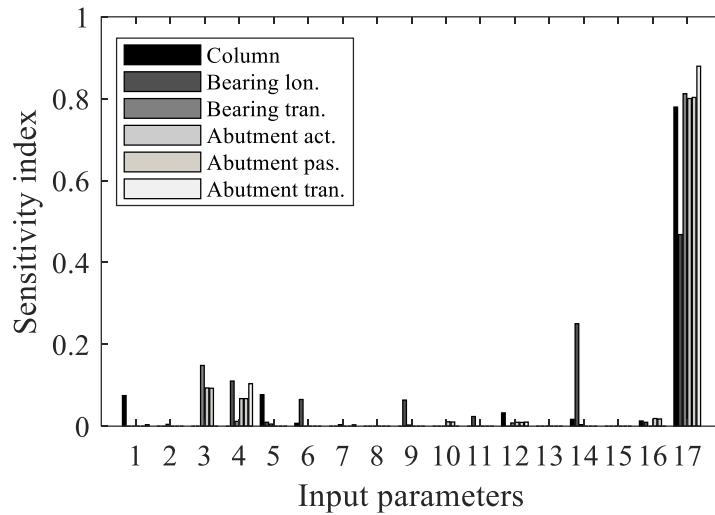
Figure 5.3 Sensitivity indices of the input parameters (Column: column demand;

Bearing lon.: bearing longitudinal demand; Bearing tran.: bearing transverse demand;

Abutment act: abutment active demand; Abutment pas.: abutment passive demand;

and Abutment tran.: abutment transverse demand)
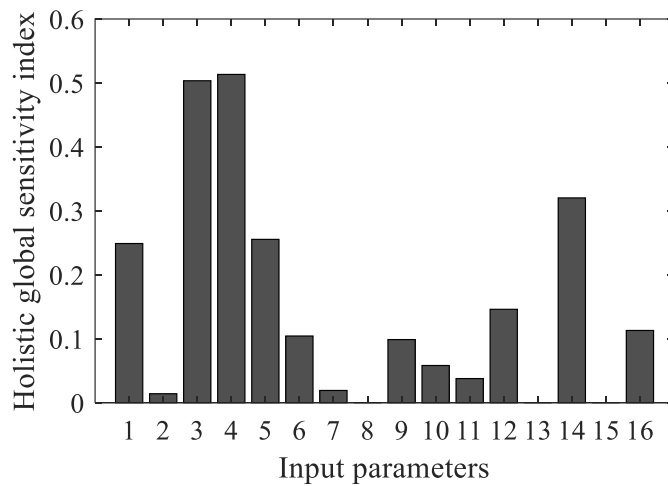
Figure 5.4 Holistic global sensitivity indices

To demonstrate the usage and decision making of the proposed holistic sensitivity index, the bridge system fragility curves computed by using different sensitive parameters are presented in Figure 5.5. By using the top five holistic sensitive input parameters identified by the proposed approach, the computed fragility is close to the one computed by using all inputs. While by using insensitive parameters identified by the proposed approach (the last five sensitive input parameters), the computed fragility deviates from the one computed by using all inputs.
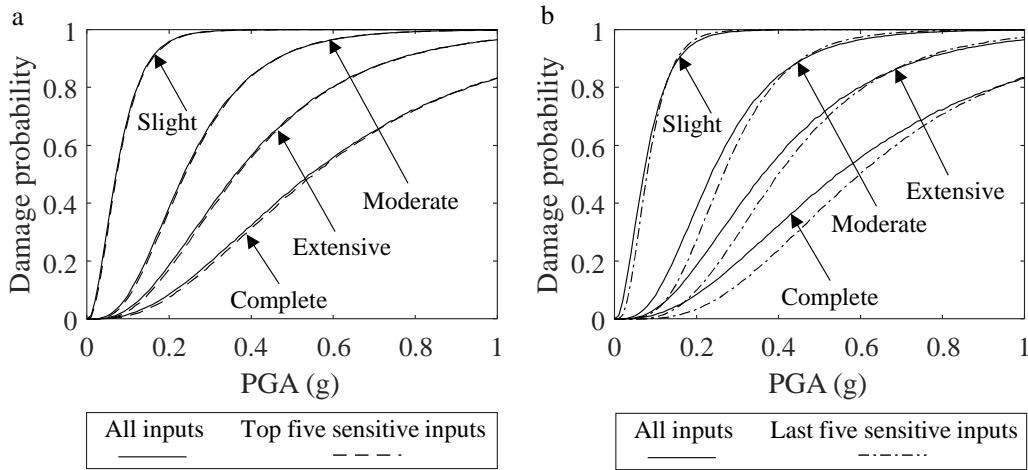
Figure 5.5 Bridge system vulnerability computed using different sensitive parameters for slight, moderate, extensive, and complete damage states

For MCS, a total of $N_{MCS}(M + 2) = 10^5 \times (17 + 2) = 1.9 \times 10^6$ FEM evaluations are required resulting in 6597 days of computational time. In this study, a total of 320 FEM evaluations are used for ASPCE to compute the global sensitivity, the time of running FEM is only 27 hours. The computational time of global sensitivity analysis for the spatially distributed bridges can be reduced significantly by using ASPCE.

5.6 Summary

A two-stage multi-criteria global sensitivity analysis algorithm is proposed in this chapter. The global sensitivity indices are first computed for the response associated with individual performance criteria. Then, holistic global sensitivity indices are computed by employing the TOPSIS. The proposed holistic global sensitivity index incorporates the trade-off among the multiple performance criteria and serves as a holistic measure. The ranking of the sensitive parameters considering multiple

structural performance criteria can be determined by the proposed holistic global sensitivity index.

Two case studies are conducted to illustrate the applicability, accuracy, and efficiency of the proposed approach. The approach is verified using MCS through a simple frame structure example. The ASPCE provides an accurate estimation of the global sensitivity index. Then, the approach is applied to complex bridge structures. The holistic global sensitivity indices indicating the overall sensitive level to the system are effectively computed by incorporating multiple criteria. By using the top five holistic sensitive input parameters identified by the multi-criteria global sensitivity analysis, the computed fragility is close to the one computed by using all inputs. These results demonstrate the applicability and effectiveness of the proposed multi-criteria global sensitivity analysis approach. The presented approaches can aid the global sensitivity analysis efficiently and holistically.

CHAPTER 6

VINE COPULA-BASED FRAMEWORK FOR SEISMIC PERFORMANCE ASSESSMENT INCORPORATING COMPLEX DEPENDENCE

6.1 Introduction

PBEE is a new generation philosophy for the assessment and decision-making of structures. In this engineering philosophy, the structures are expected to satisfy performance objectives (e.g., direct loss, indirect loss, fatality, etc.). The conventional procedures of the PBEE framework can be summarized as follows. Probabilistic seismic hazard analysis is performed to identify the potential IM levels and corresponding probabilities. A probabilistic seismic demand model can be used to predict the seismic demand under different IM levels. Vulnerability is computed based on PSDM. Then, the probabilistic performance can be computed. A general expression indicating the probability that a decision variable exceeding DV under a given IM can be written as (Zareian & Krawinkler, 2006)

$$G(DV \mid IM) = \iint G(DV \mid DM)\,dG(DM \mid EDP)\,dG(EDP \mid IM) \tag{6-1}$$

where G function is the complementary cumulative distribution function; DM represents damage measure; and EDP is the engineering demand parameter.

Improving the accuracy and efficiency of PBEE assessment is of great importance. In traditional cloud analysis, linear regression is performed in the logarithmic space of seismic IM and demand. The obtained relationship is used to predict the seismic

demand. Then, some advanced models for seismic demand prediction were developed to improve the accuracy. There exists dependence within PBEE, whereas multivariate normality of logarithmic values is widely assumed for modeling the dependence in previous studies. The linear correlation coefficients are used to compute the joint distributions. The copula model can capture complex dependence characteristics. However, in the standard copula-based approach, the same dependence structure is used for modeling all pairs of random variables for high-dimensional problems. The multiple structures and characteristics of dependence among multivariate variables in high-dimensional problems cannot be well captured by using a standard copula. In the vine copula approach, the joint distribution associated with high-dimensional problems is decomposed into marginal distributions, and the multiple dependence structures among multivariate variables are captured using a system of pair copulas.

By interconnecting the surrogate model and vine copula, this study proposes a hybrid and novel framework to improve the seismic performance assessment. The proposed framework can improve confidence while capturing more realistic dependence. The vector IM and surrogate models are coupled to predict the seismic demand. The vine copula can characterize complex nonlinear dependence structures, and it is adopted to model the dependence of demands and IMs. Then, seismic performance can be assessed. The proposed framework is illustrated on the spatially distributed bridges under seismic hazards. Additionally, the effect of dependence modeling on higher-order moments of seismic performance is investigated. The

generality and flexibility of the vine copula-based approach highlight the necessity of implementing the proposed framework.

6.2　　　　Vine Copula-based Dependence Modeling

6.2.1　Vine Copula Model

A copula is a powerful tool in characterizing the complex dependence associated with multiple variables. Let d random variables X_1, …, X_d have marginal distribution functions $F_i(x_i)$ and joint cumulative distribution function (CDF) $F(x_1, …, x_d)$, $i = 1, …, d$, the joint CDF of these variables can be expressed as (Nelsen, 2006)

$$F(x_1,...,x_d) = P[X \leq x_1,..., X_d \leq x_d] = C(F_1(x_1),..., F_d(x_d) | \boldsymbol{\theta}) = C(u_1,..., u_d | \boldsymbol{\theta}) \qquad (6\text{-}2)$$

where P[.] is the corresponding probability; $C(u_1, …, u_d|\boldsymbol{\theta})$ is the copula function with copula parameters $\boldsymbol{\theta}$; and $u_i = F(x_i)$.

The joint probability density function (PDF) of X_1, …, X_d is expressed as

$$f(x_1,...,x_d) = \frac{\partial^d C(F_1(x_1),..., F_d(x_d) | \boldsymbol{\theta})}{\partial x_1...\partial x_d} = c(F_1(x_1),..., F_d(x_d) | \boldsymbol{\theta}) \cdot \prod_{i=1}^{d} f_i(x_i) \qquad (6\text{-}3)$$

$$c(F_1(x_1),..., F_d(x_d) | \boldsymbol{\theta}) = \frac{\partial^d C(F_1(x_1),..., F_d(x_d) | \boldsymbol{\theta})}{\partial u_1...\partial u_d} \qquad (6\text{-}4)$$

where $c(u_1, …, u_d|\boldsymbol{\theta})$ represents the copula density function; and $f_i(x_i)$ is the marginal PDF of x_i.

Many copula families can be used to characterize the dependence of random variables (Joe, 1997; Nelsen, 2006). In the conventional copula approach, the same dependence structure is used for all pairs of variables, which is inflexible for describing

the different dependence structures among multiple random variables. Vine copula

(Aas et al., 2009) is used to address this issue. It is a more flexible approach to model

the complex dependence structures of high-dimensional random variables. By using

vine copula, the joint PDF is decomposed into the product of bivariant copula density

functions, thus various copula families can be used for dependence modeling of high-

dimensional variables.

The joint PDF of X_1, …, X_d can be expressed as

$$f(x_1,...,x_d) = f_1(x_1)f_{2|1}(x_2 \mid x_1)...f_{d|1,...,d-1}(x_d \mid x_1,...,x_{d-1}) \tag{6-5}$$

where $f(x|\mathbf{v})$ is the conditional PDF and can be expressed as the product of pair copulas

and conditional PDF as

$$f(x \mid \mathbf{v}) = c_{x,v_j|\mathbf{v}_{-j}}(F(x \mid \mathbf{v}_{-j}), F(v_j \mid \mathbf{v}_{-j}); \theta_{x,v_j|\mathbf{v}_{-j}})f(x \mid \mathbf{v}_{-j}) \tag{6-6}$$

where v_j is one variable of $\mathbf{v}$; $\mathbf{v}_{-j}$ is the vector excluding v_j; and $c_{x,vj/\mathbf{v}\text{-}j}(.)$ is the copula

density function. The conditional CDF can be expressed as

$$F(x \mid \mathbf{v}) = \frac{\partial C_{x,v_j|\mathbf{v}_{-j}}(F(x \mid \mathbf{v}_{-j}), F(v_j \mid \mathbf{v}_{-j}); \theta_{x,v_j|\mathbf{v}_{-j}})}{\partial F(v_j \mid \mathbf{v}_{-j})} \tag{6-7}$$

where $C_{x,vj|v\text{-}j}(.)$ is the copula function. Eq. 6-4 can be decomposed as the product of

copula density functions and marginal PDFs by using Eq. 6-5. The conditional CDF of

x on univariant v can be expressed as

$$F(x \mid v) = \frac{\partial C_{x,v}(F_x(x), F_v(v); \theta_{x,v})}{\partial F_v(v)} \tag{6-8}$$

The $F(x/v)$ can be written as h-function

$$F(x\,|\,v) = \frac{\partial C_{x,v}(u_x, u_v; \theta_{x,v})}{\partial u_v} = h(u_x, u_v; \theta_{x,v}) \tag{6-9}$$

The drawable vine (D-vine) copula and canonical vine (C-vine) copula structures are considered in this study. A vine copula consists of a set of trees, each tree consists of several nodes and edges. Each edge is represented by a pair copula function. The structures of the six-dimensional D-vine and C-vine are presented in Figure 6.1 (Okhrin et al., 2017). In the first tree T_1, the dependence of two variables is modeled based on pair copula models (e.g., $c_{1,2}$, etc.). The conditional dependence of variable is modeled in the subsequent trees based on pair copula models (e.g., $c_{1,3|2}$ and $c_{2,3|1}$, etc.). By arranging different order of variables, several different structures of vine copula can be obtained. In D-vine, the variables are considered as equivalent, while the C-vine incorporates a primary variable governing the dependence modeling (Zhou & Li, 2019). Therefore, the D-vine is suitable for dependence modeling of seismic demand (Zhou & Li, 2019). For three-dimensional case (vector IM in this study), C-vine and D-vine are equivalent, as only one conditioning variable is considered (Wang et al., 2020). The copula functions and h-functions for various copula families are provided in the literature (Nelsen, 2006). Based on the considered vine copula structure, the joint PDF of variables can be computed. The PDF of a D-vine copula is expressed as

$$f(x_1,...,x_d) = \prod_{j=1}^{d-1}\prod_{i=1}^{d-j} c_{i,i+j|i+1,...,i+j-1}(F(x_i\,|\,x_{i+1},...,x_{i+j-1}), F(x_{i+j}\,|\,x_{i+1},...,x_{i+j-1}); \theta_{i,i+j|i+1,...,i+j-1})\prod_{k=1}^{d} f(x_k)$$

(6-10)
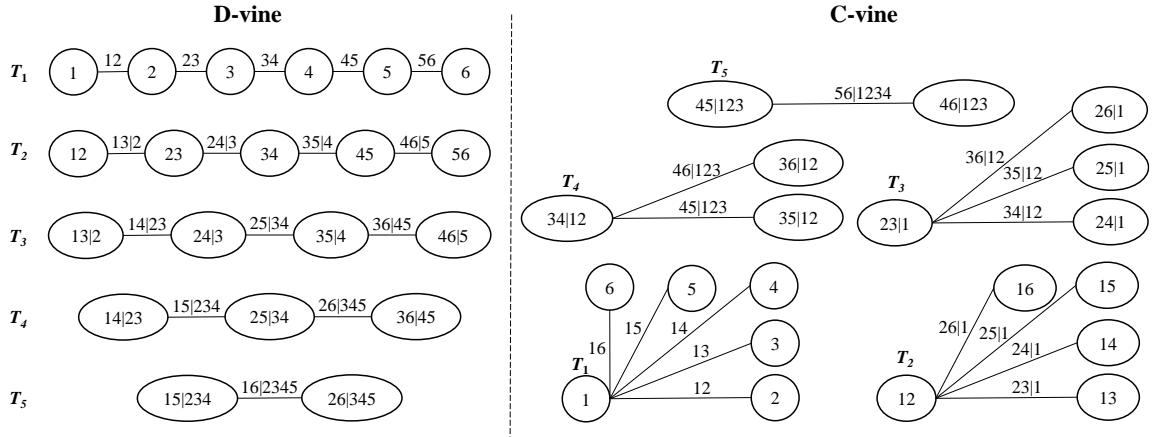
Figure 6.1 Structures of D-vine and C-vine

6.2.2 Inference of Vine Copula from Data

Given the vine copula structure and a set of samples $\mathbf{x}^{(1)}, ..., \mathbf{x}^{(N)}$, $\mathbf{x}^{(i)} = (x_1^i, ..., x_d^i)$, the parameters of vine copula can be computed using joint maximum likelihood estimation (Aas et al., 2009). The joint maximum likelihood estimation simultaneously computes all the parameters of a vine copula by maximizing the log-likelihood. The parameters of a given vine copula structure under a set of samples can be estimated as

$$\hat{\boldsymbol{\theta}} = \arg\max_{\Theta} LL(\mathbf{x}^k; \boldsymbol{\theta}) \tag{6-11}$$

where $\hat{\boldsymbol{\theta}}$ is the estimated vector of vine copula parameters; Θ is the range of copula parameters; and $LL(\mathbf{x}^k; \boldsymbol{\theta})$ is the log-likelihood for a given sample set.

The different conditioning order and copula families result in different structures of vine copulas. It is necessary to determine the optimal vine copula within the candidates. The Akaike Information Criterion (AIC) can be used to select the optimal copula (Akaike, 1974; Tang et al., 2015). For a given vine copula and sample set, the AIC is computed as

$$AIC = -2LL(\mathbf{x}^k; \hat{\boldsymbol{\theta}}) + 2np \tag{6-12}$$

where $LL(\mathbf{x}^k; \hat{\boldsymbol{\theta}})$ is the log-likelihood of the fitted vine copula; and np is the number of parameters in a vine copula.

Bayesian Information Criterion (BIC) is the other criterion to determine the optimal vine copula, it can be expressed as

$$BIC = -2LL(\mathbf{x}^k; \hat{\boldsymbol{\theta}}) + np \ln N_v \tag{6-13}$$

where N_v is the number of samples used for developing vine copula. The optimal vine copula is determined as the one associated with minimum AIC and BIC values. The criteria of AIC and BIC are considered in this study for vine copula selection. These two criteria incorporate penalty terms on the number of model parameters, thus, the overfitting problem can be prevented (Härdle et al., 2017; Torre et al., 2019a). Once the optimal vine copula is inferred, the joint distribution of multivariant variables considering dependence can be determined (Kurowicka & Cooke, 2007).

6.3   Dependence Modeling within Performance-based Earthquake Engineering

There exists dependence associated with multiple sources within PBEE. For instance, a complex system usually consists of multivariant demands, the dependence among multiple demands can affect the system vulnerability. When vector IM is used, the dependence among multiple IMs can affect the joint exceeding frequency. In this study, the dependence from two sides (e.g., IMs and demands) is considered. The joint normality of logarithmic values is widely assumed in previous studies for dependence

modeling within PBEE. However, the multivariate normal distribution cannot reflect the complex nonlinear dependence characteristics. This simple assumption may lead to inaccurate assessment and mislead decision-making of structures. The vine copula captures complex nonlinear dependence characteristics, and it is adopted in this study to model more realistic dependence structures.

6.3.1 Probabilistic Seismic Hazard Analysis for Vector IM Considering Dependence

Conventionally, scalar seismic IM is used in performance assessment (Padgett & DesRoches, 2008). Scalar IM can only reflect part of the information regarding amplitude, spectrum characteristics, and duration of ground motion. Due to the complexity of the ground motion, the demands predicted using a single seismic IM usually involve a relatively large amount of uncertainty. Compared with scalar IM, vector IM contains more information on ground motion, thus it can reduce the uncertainty of seismic demand prediction (Baker, 2007). To further improve the accuracy of seismic demand prediction, the vector IM is used in this study.

To quantify the probabilistic performance, the joint probabilistic distribution of seismic intensities should be identified, and it is achieved by probabilistic seismic hazard analysis. For given magnitude and distance, the seismic intensity is uncertain. The ground motion prediction model (GMPM) is used to predict probabilistic seismic intensity (Boore & Atkinson, 2008). The GMPM can be generally expressed as

$$\ln IM = \mu_{\ln IM}(R, M, \Omega) + \varepsilon_{IM}\sigma_{\ln IM} \tag{6-14}$$

where ln *IM* is the natural logarithm of an earthquake intensity; *M* is magnitude; *R* is the source to site distance; Ω are other parameters used to describe an earthquake scenario (e.g., region of the earthquake and shear wave velocity averaged over top 30 m, etc.); $\mu_{\ln IM}(R, M, \Omega)$ is the mean of ln *IM* for given *R*, *M*, and Ω; $\sigma_{\ln IM}$ is the standard deviation of ln *IM*; and ε_{IM} is normalized residual term.

There is dependence among IMs. The ε_{IM} represents the record-to-record aleatory variability (Baker & Cornell, 2005) and is considered to follow a standard normal distribution (Baker *et al*., 2007). By using ε_{IM}, the correlation models were developed to account for the dependence among IMs (Baker & Jayaram, 2008). The logarithmic IMs are assumed to follow a multivariate normal distribution in previous studies and the Pearson correlation coefficient is widely used (Faouzi & Nasser, 2014). As indicated previously, vine copula is a flexible approach and can capture complex dependence characteristics. This study utilizes the vine copula approach to model the dependence of IMs. By using the approach mentioned in section 3.2, the vine copula model can be inferred based on ε_{IM} and historical data. Once the vine copula model is established, the joint PDF of vector IM for given earthquake magnitude and distance $f(IM_1, IM_2, IM_3|m, r)$ can be computed based on GMPM and Eq. 6-9. The probability of IM_1, IM_2, IM_3 exceeding im_1, im_2, and im_3 for a given earthquake scenario can be expressed as

$$P_{(IM_1 > im_1, IM_2 > im_2, IM_3 > im_3|m,r)} = \iiint_{im_1, im_2, im_3} f(IM_1, IM_2, IM_3 \mid m,r)dIM_1 dIM_2 dIM_3 \qquad (6\text{-}15)$$

Considering uncertain scenarios, the joint mean rate of the three IMs exceeding im_1, im_2, and im_3 is computed based on the total probability theorem as (Faouzi & Nasser, 2014; Wang et al., 2020)

$$\lambda(im_1,im_2,im_3) = \lambda_{m_{min}} \iint P_{(IM_1>im_1,IM_2>im_2,IM_3>im_3|m,r)} f_M(m) f_R(r) dmdr \qquad (6\text{-}16)$$

where $\lambda_{m\text{min}}$ is the annual rate of occurrence of earthquakes exceeding considered minimum magnitude; and $f_M(m)$ and $f_R(r)$ are the PDFs of the magnitude and distance, respectively.

6.3.2 Joint Probabilistic Seismic Demands Considering Dependence

In this study, the relationship between the input vector $X \in \mathbb{R}^M$ and multiple outputs $[Y_1, Y_2, \ldots, Y_W]$ is established using surrogate model. Generally, multivariate surrogate model can be expressed as (A. Du & Padgett, 2020a)

$$\hat{Y} = \bar{Y}(X) + \varepsilon_S(X) \qquad (6\text{-}17)$$

where $\hat{Y} \in \mathbb{R}^W$ is the prediction from the model; $\bar{Y} \in \mathbb{R}^W$ is the estimation from a trend model; and $\varepsilon_S \in \mathbb{R}^W$ is the correlated model error.

For an engineering system, multiple seismic demands are usually of interest. It is necessary to compute the joint probabilistic demands considering dependence for system vulnerability analysis. The dependence among multiple structural demands can be described by the dependence of ε_S (Du & Padgett, 2020a). Modeling of ε_S plays an important role in uncertainty propagation and reliability analysis. It incorporates the consideration of the difference between finite element model evaluations and trend model predictions, as well as the uncertainty associated with ground motion. Normal

distribution with a mean of zero is a widely acceptable consideration for modeling the marginal distribution of ε_S (Du & Padgett, 2020a; Torre et al., 2019b). The multivariate normal distribution is widely assumed for the dependence modeling of ε_S (Du & Padgett, 2020a). In this study, the vine copula is used to model the dependence of ε_S, as it can capture more complex dependence characteristics. After establishing the SPCE, the residual of the structural demands can be computed. Then, the residual from multiple demands is used to infer the vine copula based on the method mentioned in section 6.2. The joint distribution of multivariant demands incorporating dependence can be generated from the established vine copula model. The process of dependence modeling within seismic performance assessment is presented in Figure 6.2.
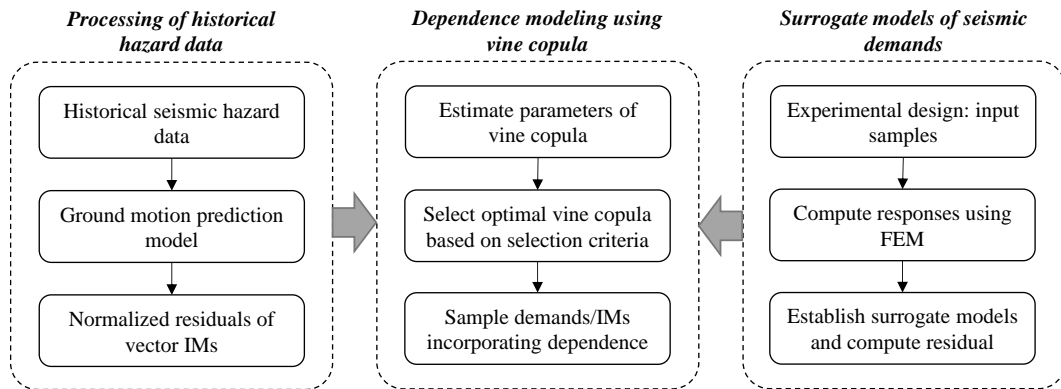
Figure 6.2 Process of dependence modeling within PBEE

6.4 Updated Framework of Seismic Performance Assessment (UFSPA)

By integrating the surrogate model and vine copula, this study proposes a framework for improved seismic performance assessment. The vector IM is adopted within the UFSPA as it reflects more information on the hazard characteristics compared with the

scalar IM. The probabilistic seismic hazard analysis is performed for vector IM. The vine copula is used to capture the complex dependence among multiple IMs. The seismic demand surrogate models incorporating vector IM are established using a learning algorithm. The vine copula is used for the second time to model the dependence among multiple demands. The system vulnerability considering dependence can be computed using the surrogate model and vine copula. Then, the seismic performance indicators can be computed. The illustration of the computational process is shown in Figure 6.3.

In this study, two vine copula models can be developed for capturing the dependence of IMs and demands. Based on the historical ground motion data, the normalized residuals are computed using the ground motion prediction model. Then, a vine copula model capturing the dependence of IMs is established using IM residuals, as indicated in section 6.2. The residuals associated with different demands are computed from the surrogate models. Then, the second vine copula model capturing the dependence of demands can be established using the residual data.

Compared with conventional PBEE, the proposed UFSPA framework has several advantages. The assumption of multivariate normality of logarithmic values can only capture one of many possible solutions and may produce severely biased results (Tang et al., 2013). In the proposed framework, two vine copula models are established for demands and IMs, respectively. More realistic dependence structures are captured by vine copula models. In addition, the uncertainty associated with seismic demand prediction is reduced by coupling SPCE and vector IM. The necessity and superiority

of the proposed approach are illustrated in the case study. The computational process

of the proposed approach is illustrated in Table 6.1. A comparison of the conventional

PBEE framework and the UFSPA is presented in Figure 6.4.

The major contribution of this chapter is to develop an updated and integrated

seismic performance assessment framework by interconnecting several novel

techniques. Confident seismic performance assessment can be accomplished by using

the developed UFSPA.

Table 6.1 Computational procedures of the UFSPA

Procedures of UFSPA
Probabilistic hazard analysis for vector IM considering vine copula captured dependence
1. Process historical earthquake data to obtain normalized residuals of considered IMs
2. Determine copula families
3. Pair copula selection
4. Compute copula parameters by performing joint maximum likelihood estimation, subjected to residual data
5. Compute AIC and BIC
6. Obtain best-fit vine copula
7. Identify seismic hazard source
8. Sample dependent residuals using established vine copula
9. Compute $\mu_{\ln IM}$ (R, M, Ω) and $\sigma_{\ln IM}$ for the corresponding scenarios using the ground motion prediction model
10. Obtain joint distribution of vector IM considering the dependence
Surrogate-assisted vulnerability assessment considering vine copula captured dependence
11. Determine probabilistic structural parameters from inventory
12. Obtain a set of structure samples
13. Perform nonlinear time history analysis for the sampled structures
14. Record the demands of interest
15. Perform leaning algorithm to establish surrogate models of all demands using structure samples, vector IMs, and recorded demands
16. Compute residuals from surrogate models
17. Establish vine copula for demands using the residuals (invoke line 2-6)
18. Compute vulnerability using surrogate model and vine copula
Performance assessment
19. Compute the probabilities of structures being in each damage state

20. Determine consequences associated with each damage state
21. Compute probabilistic performance
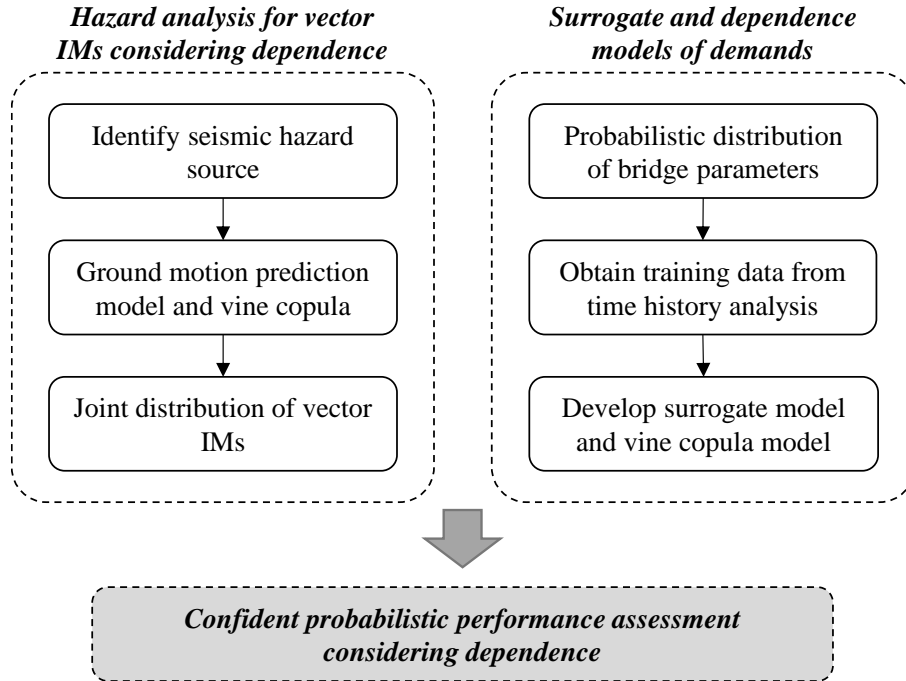
Figure 6.3 Illustration of the computational process
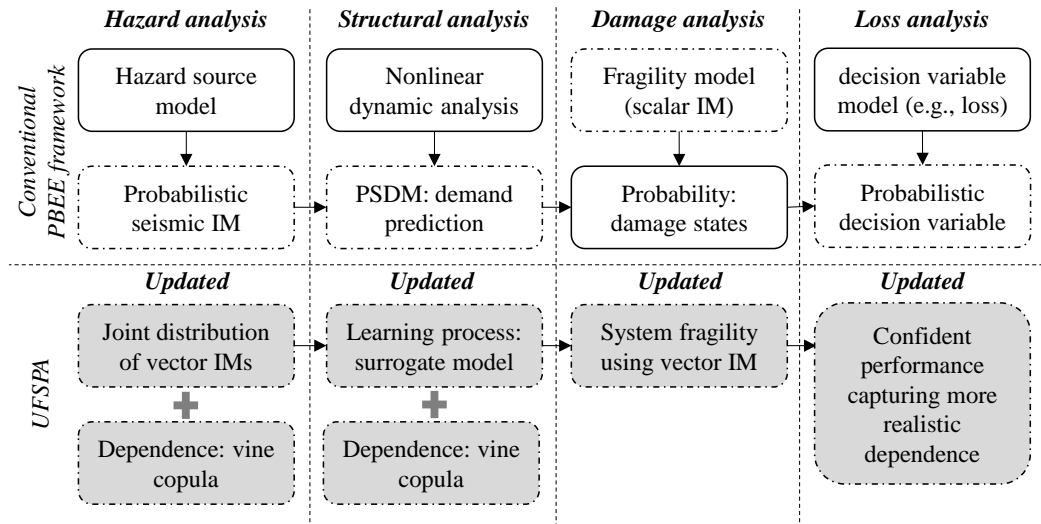
Figure 6.4 Conventional PBEE framework and updated framework of seismic

performance assessment

6.5   Illustrative Example

This study aims to facilitate seismic performance assessment of spatially distributed bridges. In this context, the uncertainties associated with bridge geometry and material parameters should be considered in the assessment process (Jeon et al., 2019). The probabilistic distributions of bridge parameters can be determined based on the bridge inventory database. Based on the probabilistic distributions of bridge parameters, a set of bridge samples accounting for uncertainties is randomly generated to facilitate regional seismic performance assessment (Jeon et al., 2019; Mangalathu et al., 2016; Mangalathu, Jeon, et al., 2018). Nonlinear time history analysis of the bridges is performed in OpenSEES to obtain the training data. Seismic demand surrogate models are established, and vine copula is used to model the dependence among multiple demands. The probabilistic seismic hazard analysis for vector IM is performed and vine copula is used to capture the dependence. Finally, system vulnerability and probabilistic performance are computed.

6.5.1   Probabilistic Seismic Hazard for Vector IM Incorporating Vine Copula Captured Dependence

The peak ground acceleration (PGA), spectral acceleration at the period of 0.2s (Sa0.2), and spectral acceleration at the period of 1.5s (Sa1.5) are used as vector IM in this example. There is dependence among multiple seismic IMs. Dependence modeling is necessary for probabilistic seismic hazard analysis for multiple IMs. Conventionally, the dependence is modeled based on the assumption of multivariate normality of logarithmic values. In this study, the dependence modeling of IMs is accomplished by using vine copula as it can capture nonlinear and complex dependence characteristics.

The historical ground motion data is needed to establish the vine copula model. The normalized residuals are computed using the ground motion prediction model (Boore & Atkinson, 2008). The marginal distribution of IM residual is considered to follow the standard normal distribution (Baker, 2007). Then, a vine copula model capturing the dependence of IMs is established using IM residuals, as indicated in section 6.2. The same set of IM residuals is used to derive the joint normal distribution and the vine copula joint distribution model to investigate the effects of dependence modeling. The Figure 6.5 shows the comparison of simulated data from vine copula and original data. The general overlapping of the simulated data and the original data is observed, which indicates the satisfying performance of the vine copula throughout the full range of data. The performance of the vine copula is quantitatively assessed by using the criterion values of AIC, BIC, and log-likelihood. These criteria indicate that the vine copula performs better than the conventionally used joint normal distribution. The detailed assessment of the performance of the vine copula is illustrated in the next section.
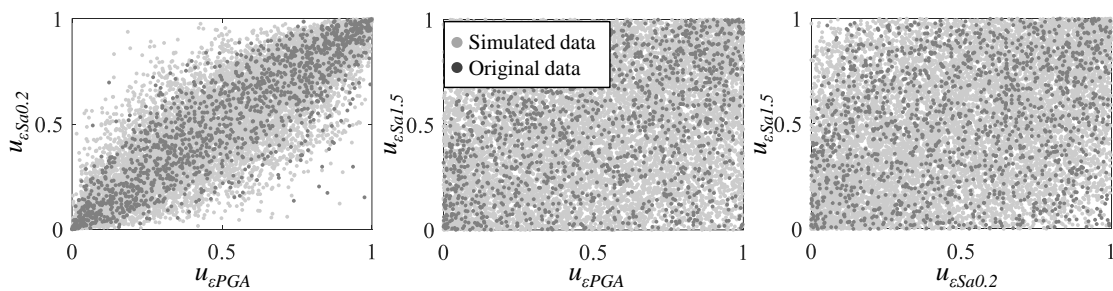
Figure 6.5 Comparison of simulated data from vine copula and original data

Given different seismic scenarios, the mean and standard deviation of ln IM can be computed using the ground motion prediction model. The ground motion prediction

model (Boore & Atkinson, 2008) used in this study was developed using a set of worldwide historical records. These historical records contain different earthquake characteristics (a wide range of distances and magnitudes etc.). This ground motion prediction model is a general model which is applicable for magnitude = 5-8, distance < 200 km. Other ground motion prediction models can be used in future implementation. The residual samples of IMs are generated from the established vine copula model, then the joint probabilistic distribution of the three IMs associated with a given scenario can be computed.

Chopra and Chintanapakdee compared the structural response under near-field and far-field earthquakes, where the earthquakes with distance values more than 12 km are considered as far-field ground motions (Chopra & Chintanapakdee, 2001). The performance of the proposed approach under near-field and far-field earthquakes is also illustrated in this study. A single source case and a multiple sources case are considered. For the single source, the magnitudes considered are 5.5-8, the distance is considered as 6 km. The source model with single fault and certain distance can be used for illustration purposes in seismic performance assessment, as it is representative for many sites which are near a single large fault (e.g., near the San Andreas or Hayward faults in northern California) (Baker & Cornell, 2005). For the multiple sources case, the magnitudes considered are 5.5-8, the distance values associated with three sources are considered as 5 km, 10 km, and 20 km respectively. Two million vector IM samples considering dependence are generated using the ground motion prediction model and vine copula. For each vector IM sample, the return period can be calculated. For a

considered return period, the target vector IM samples can be determined (Du & Padgett, 2020b). The return periods computed herein are based on a single source case (magnitudes: 5.5-8, distance: 6 km) and a multiple sources case (magnitudes: 5.5-8, the distance values associated with three sources: 5 km, 10 km, and 20 km), respectively.

6.5.2 Surrogate Models of Seismic Demands Incorporating Dependence

To establish the surrogate model of seismic demand, a set of training data should be obtained. The 320 bridge samples are generated using the Latin hypercube sampling technique (Ayyub & Lai, 1989). Each bridge realization is paired with a selected ground motion (Baker et al., 2011), and nonlinear time history analysis is performed in software OpenSEES (Dong et al., 2013; Dong & Frangopol, 2015; Qian & Dong, 2020). The demands associated with the column, bearing, and abutment are recorded. Thus, the training data set including the probabilistic input parameters and demands is obtained.

Given the training data set, the sparce PCE models of seismic demands are established using the approach indicated in chapter 4. Once the sparse PCE is established, it can be used for efficient seismic demand prediction. To illustrate the prediction performance of the proposed approach on a test sample set, the R^2 values of demand from prediction and finite element modeling are presented in Table 6.2. By implementing SPCE only, multiple bridge parameters are incorporated within demand prediction. By using this approach (SPCE with multiple bridge parameters), the average relative improvement of R^2 over all components (ARIR^2) is 13%, compared with the conventional linear regression in the logarithmic space. The R^2 values of the six

demands are further increased by incorporating vector IM in SPCE. By using vector IM in SPCE, the $ARIR^2$ is 16%, compared with the method using scalar IM and SPCE. Compared with the conventional linear regression in the logarithmic space, the relative improvement of R^2 of the proposed approach is shown in Figure 6.6, and the $ARIR^2$ is 32%. By using the developed approach, a significant improvement of R^2 is observed, indicating a significant improvement in prediction performance. The improvement of R^2 associated with the proposed approach can be interpreted from three aspects: (1) the implementation of SPCE for uncertainty propagation; (2) the incorporation of a more comprehensive description of hazard intensities by vector IM; and (3) the incorporation of multiple bridge parameters within demand prediction.

Table 6.2 R^2 of demand from prediction and finite element modeling on a test sample set

Methods	C1	C2	C3	C4	C5	C6
Linear regression in the logarithmic space	0.6443	0.3616	0.6372	0.4838	0.4845	0.6763
SPCE	0.7382	0.4924	0.7321	0.4881	0.4901	0.7500
SPCE and vector IM	0.7566	0.6616	0.7637	0.6222	0.6249	0.7706

Note: C1 is the column curvature ductility; C2 is the bearing longitudinal displacement; C3 is the bearing transverse displacement; C4 is the abutment active displacement; C5 is the abutment passive displacement; and C6 is the abutment transverse displacement.
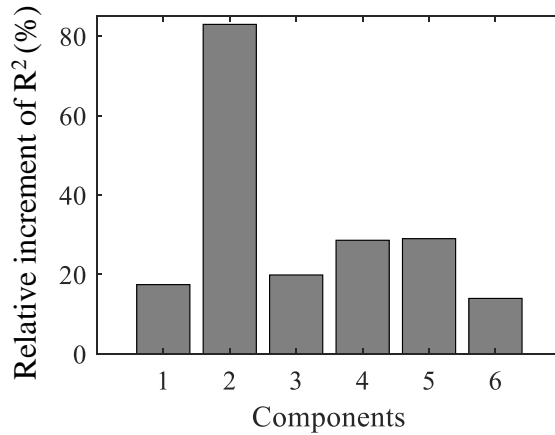
Figure 6.6 The relative improvement of R^2 comparing the proposed approach and

conventional approach

The model error is used to characterize the dependence among multiple demands.

The marginal distribution of these residuals is considered as a normal distribution with

a mean of zero (Du & Padgett, 2020a; Torre et al., 2019b). For dependence modeling,

the multivariate normal distribution is widely assumed (Du & Padgett, 2020a). This

study uses the vine copula approach to capture the complex nonlinear dependence

characteristics of seismic demands. The residuals associated with six demands are

computed from the surrogate models. Then, the vine copula model can be established

using the residual data. To illustrate the performance of the best fit vine copula, the

criterion values of AIC, BIC, and log-likelihood are shown in Figure 6.7. The best fit

vine copula is associated with minimum AIC, BIC, and maximum log-likelihood,

which indicates that the best fit vine copula performs best for the dependence modeling.

The assumption of multivariate normality of logarithmic values is widely used in

previous studies for both IMs and demands, it can be considered as a specific case in

the copula approach, where the dependence is modeled using Gaussian copula. The

120

results show that multivariate normality is not the optimal dependence structure, while vine copula performs better due to its flexibility. To further testify the necessity of using vine copula approach, it is necessary to know how much the difference in seismic performance (e.g., repair loss ratio subjected to earthquakes, it is defined in section 2) of structures calculated by conventional multivariate normality assumption and vine copula approach would be. This aspect is investigated in next section.
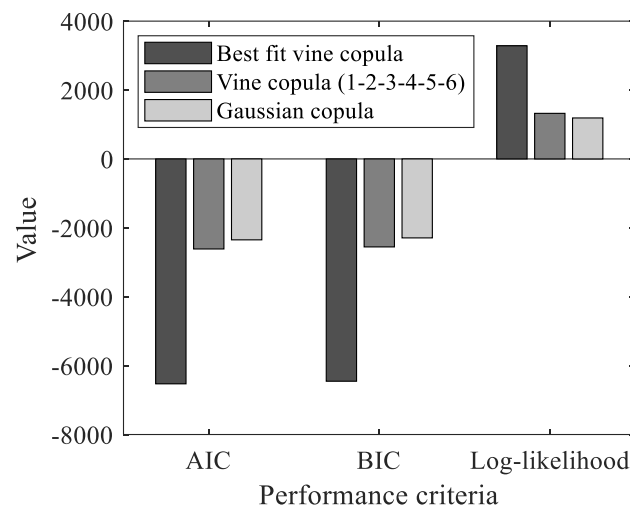
Figure 6.7 Performance of the best fit vine cupula, vine copula (1-2-3-4-5-6), and Gaussian copulas (1-2-3-4-5-6 indicates the order of variables in vine copula, the numbers correspond to the numbers of components as indicated in table 6.2: e.g., C1, C2, C3, C4, C5, and C6)

6.5.3 Probabilistic Seismic Performance

The historical data and simulated data are used to develop the vine copula joint distribution model. The same data sets are used to develop the joint normal distribution model. The seismic performance is computed by using the vine copula and joint normal distribution, respectively. In this process, the only difference is the adopted dependence

model (vine copula and joint normal distribution). In this way, the results are comparable, and the effects of dependence modeling on the seismic performance (e.g., loss ratio) can be revealed.

The surrogate model and vine copula are used to compute the seismic vulnerability of bridges. The probabilistic joint seismic demands are computed. The capacity samples are generated from corresponding distributions. Then, the bridge system vulnerability can be computed by comparing the demand and capacity samples. By repeating this process for a set of IM vectors, the vulnerability surfaces can be generated as shown in Figure 6.8.
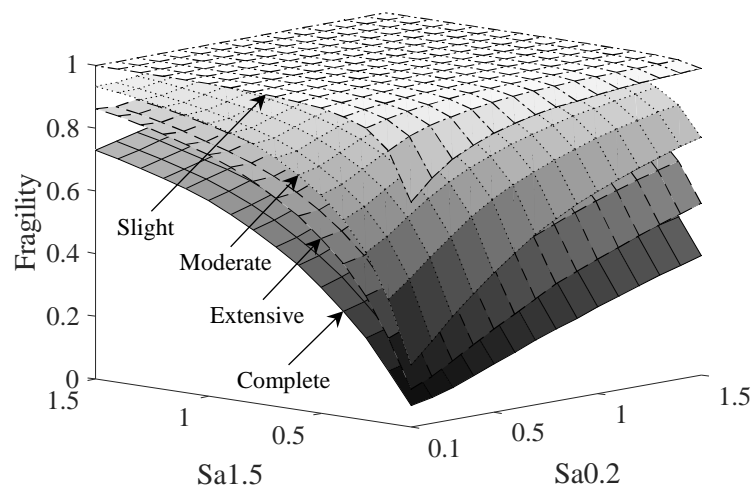
Figure 6.8 Fragility surfaces computed by SPCE and vine copula under PGA = 0.1g

Given the probabilistic distribution of the IM vector for different scenarios as computed in section 6.5.1 and vulnerability, the probabilistic loss ratio can be computed. Herein, the repair loss ratio for none, slight, moderate, extensive, and complete damage states are considered as 0, 0.03, 0.25, 0.75, and 1, respectively (Qian & Dong, 2020; Werner et al., 2006). Statistical moments of loss ratio using joint normal distribution

(widely used in previous studies) and vine copula under different scenarios are listed in Table 6.3. For the investigated scenarios, the vine copula approach and joint normal distribution approach produce similar results in terms of the mean, standard deviation (STD), and kurtosis of the loss ratio, while the significant difference is observed in skewness. The relative difference of the skewness by using the joint normal distribution approach and vine copula-based approach is 19% to 51% for the investigated scenarios. This difference may be caused by the ignorance of nonlinear dependence characteristics in the joint normal distribution.

Table 6.3 Statistical moments of loss ratio using joint normal distribution and vine copula under different scenarios

Scenario	Method	Mean	STD	Skewness	Kurtosis	The relative difference of skewness (%)
M=7.8, R=5	Vine copula	0.655	0.190	-0.393	2.452	
	Joint normality	0.668	0.185	-0.491	2.572	20
M=7.8, R=10	Vine copula	0.544	0.201	-0.050	2.216	
	Joint normality	0.556	0.200	-0.103	2.234	51
M=7.8, R=15	Vine copula	0.465	0.200	0.190	2.272	
	Joint normality	0.473	0.197	0.134	2.282	42
M=7.8, R=20	Vine copula	0.408	0.194	0.371	2.435	
	Joint normality	0.420	0.195	0.313	2.377	19

Given the distribution of the IM vector for different return periods as presented in section 6.5.1, the probabilistic loss ratio can be computed. For the single source case, the density of loss ratios computed using vine copula subjected to different return

periods is presented in Figure 6.9. For the single source case and multiple sources case, the relative difference of statistical moments of loss ratio by using joint normal distribution and vine copula is visualized in Figure 6.10. A significant difference (caused by different dependence modeling approaches) is observed for STD, skewness, and kurtosis values in both cases. As mentioned previously, higher-order moments of seismic performance indicator are essential for decision-maker to incorporate different decision attitudes. The vine copula capturing more complex dependence facilitates a confident assessment of higher-order moments of seismic performance. Thus, a vine copula-based approach is necessary to aid the rational decisions of structures under uncertainty.

The ratio of statistical moments of loss to the values associated with a return period of 75 years is presented in Figure 6.11. The density plots of loss ratios computed using joint normal distribution and vine copula subjected to return periods of 75 and 475 years are presented in Figure 6.12. The figures show that heavy and long tail behaviors are well captured by vine copula, while higher peaks of density are associated with the joint normal distribution.
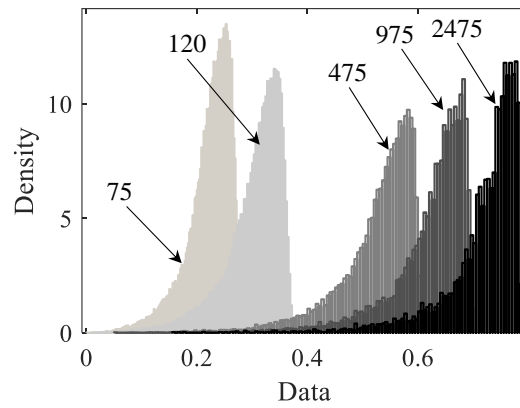
Figure 6.9 The density of loss ratios computed using vine copula subjected to return

periods of 75, 120, 475, 975, and 2475 years seismic scenario
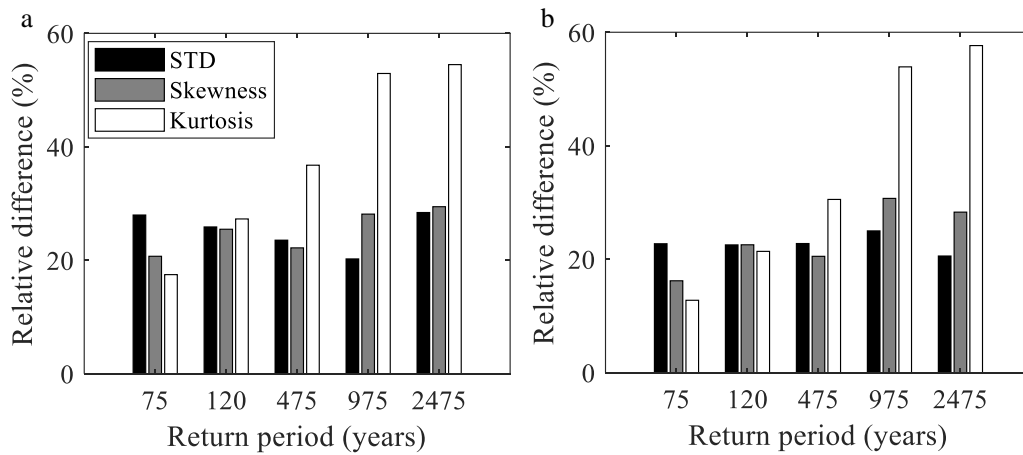
Figure 6.10 The relative difference of statistical moments of loss ratio by using joint

normal distribution and vine copula for (a) single seismic source and (b) multiple

seismic sources
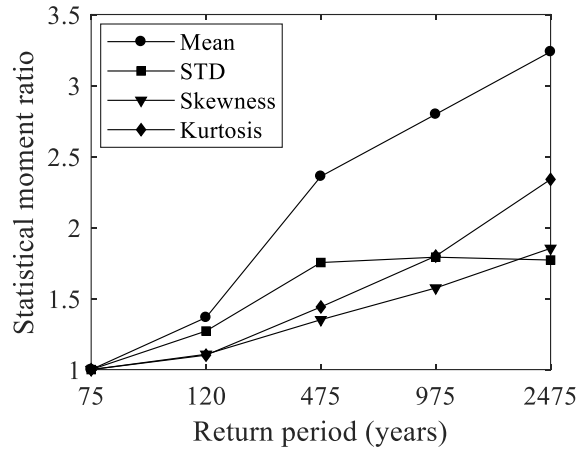
Figure 6.11 The ratio of statistical moments of loss to the values associated with a

return period of 75 years
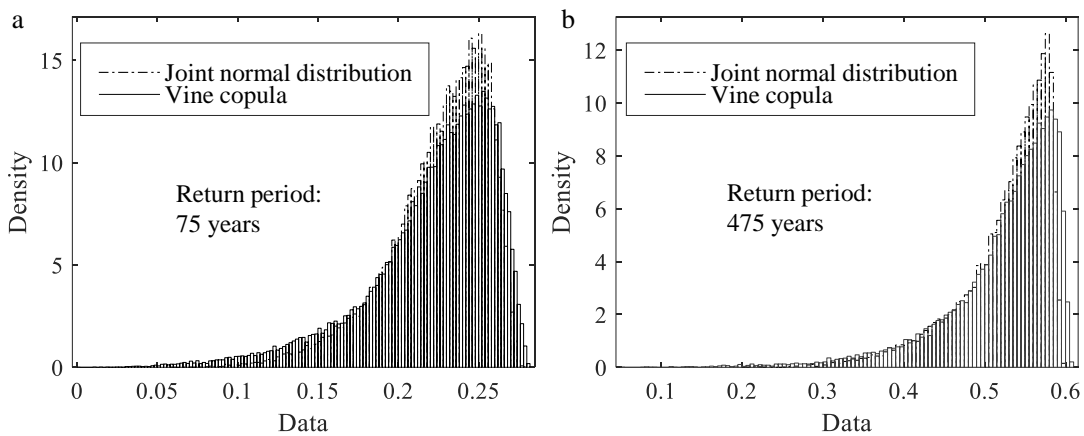
Figure 6.12 The density of loss ratios computed using the joint normal distribution

and vine copula subjected to return periods of (a) 75 years and (b) 475 years

The uncertainties associated with structural parameters, earthquake magnitudes, and intensities are considered in the investigated cases. A single source case and a three-source case with different distance values are incorporated in the analysis. Within the investigated cases, the vine copula is more appropriate to model the dependence compared with the joint normal distribution. In future practice, more cases incorporating uncertainties from different sources need to be investigated to assess the

effectiveness of vine copula and the dependence characteristics within PBEE. It is worth noting that the widely used multivariate normality can be considered as a specific case in the vine copula approach, where the pair copulas are all Gaussian copulas (Wang et al., 2020). Due to its generality, the developed vine copula-based approach can be applied in many problems to investigate and model the dependence characteristics, where the dependence structures are not well identified.

The proposed vine copula-based approach needs more technical effort for implementation compared with the conventional method. The decision makers can consider the trade-off between technical effort and assessment confidence to choose the appropriate modeling approach. When only the mean values are of interest for risk-neutral decision-makers, the multivariate normality assumption may be chosen. When higher-order moments of performance indicator are necessary for decision makers to incorporate different decision attitudes, the vine copula-based approach capturing more complex dependence is recommended. To facilitate the ease of implementation of the proposed vine copula-based approach within the PBEE framework, more studies should be conducted in the future to develop the vine copula models covering a wide range of seismic IMs and structure types.

6.6 Summary

This study proposes a hybrid framework for seismic performance assessment by interconnecting several advanced techniques. The sparse PCE is used as a surrogate model for seismic demand prediction. The vector IM, which contains more information on the hazard compared with scalar IM, is incorporated into the surrogate model to

further improve the accuracy of prediction. The dependence from both the IM side and demand side is modeled using a vine copula. The seismic performance can be computed using the proposed hybrid framework. The framework is applied to some illustrative examples. Several conclusions are drawn.

- Compared with the conventional method, SPCE and vector IM coupled approach can improve the accuracy of seismic demand prediction significantly within the investigated cases. By using SPCE, a complex relationship of the input and demand can be captured, and multiple uncertain parameters can be incorporated into uncertainty propagation. The use of vector IM incorporates more hazard information in the analysis compared with scalar IM, and the prediction confidence can be further improved.

- The multivariate normality of logarithmic values is a widely used assumption for dependence modeling within PBEE. Compared with the multivariate normality of logarithmic values, the performance criteria show that vine copula performs better to capture complex dependence associated with both IMs and demands within the investigated cases. More studies can be conducted in the future to investigate the effectiveness of the vine copula-based approach and dependence characteristics within PBEE.

- From the observation of the investigated cases, the difference between the higher-order moments of loss derived from the widely used multivariate normality assumption and the proposed vine copula-based approach is large.

Due to the generality and flexibility, the vine copula-based approach can be applied in many problems where the dependence structures are not well identified.

- The proposed approach updates the existing performance assessment framework from two aspects: improving confidence and capturing a more realistic dependence structure. It can contribute to the rational assessment and decision-making of engineering systems under seismic hazards.

CHAPTER 7

LIFE-CYCLE SUSTAINABILITY AND RESILIENCE OF STEEL-SHAPE MEMORY ALLOY (SMA) REINFORCED BRIDGE UNDER COMPOUND EARTHQUAKES AND DETERIORATION

7.1   Introduction

Resilience describes the capability of systems to withstand, adapt and recover from extreme events (Timmerman, 1981). Sustainability covers the performance metrics including social, economic, and environmental aspects. Accurate long-term sustainability and resilience assessment of bridges are of paramount importance to aid rational decision-making under seismic hazards.

Within the service life of structures, the deterioration can continuously affect the seismic performance of structures over time resulting in time-dependent performance, and multiple earthquakes can occur with stochastic occurrence time, stochastic number, and stochastic hazard intensity. Multiple earthquakes may lead to accumulated consequences in terms of sustainability and resilience. The previous corrosion-based sustainability analysis focused on time-dependent consequences, the sustainability was computed at a given time (e.g., at year 25, year 50, and year 75) under certain hazard scenarios. The two important performance criteria sustainability and resilience have not been coupled into an integrated life-cycle framework. To the authors' best knowledge,

a simulation-based life-cycle multi-criteria (e.g., accumulated sustainability and resilience) assessment framework incorporating the uncertainties associated with the corrosion, the occurrence time of earthquakes, the number of earthquakes, and hazard intensity has not been well developed.

Different strategies have been studied for seismic mitigation. Considering the ground born vibration attenuation, scholars pointed out that appropriate afforestation can effectively mitigate the earthquake hazards in a region (Muhammad, Wu and Lim, 2020; Muhammad and Lim, 2021). The built-up steel sections can be used as barriers to mitigate seismic hazards (Muhammad, Lim, and Reddy, 2019). For seismic-resistant structures, the self-centering capability is an important feature (Zhu & Zhang, 2008). The shape memory alloy (SMA) is a promising material with self-centering and corrosion-resistant characteristics. This study considers the steel-SMA reinforced concrete bridge as a potential alternative to mitigate the consequences induced by earthquakes and functional deterioration within its service life.

Despite the advantages of SMA-steel reinforced bridge in terms of self-centering and corrosion-resistant characteristics, the construction of an SMA-steel reinforced bridge is associated with higher cost and carbon dioxide emissions compared with a conventional bridge. The life-cycle cost-benefit analysis of SMA-steel reinforced bridges under earthquakes and deterioration remains a research gap. Previous studies regarding the performance of SMA-steel reinforced bridges focus on limited performance criteria (fragility or economic loss) under certain earthquake scenarios. The life-cycle sustainability (e.g., fatality and carbon dioxide emission), as well as

resilience, have not been well investigated for the SMA-steel reinforced bridge under stochastic earthquakes and deterioration. Under the background of achieving carbon neutrality and resilient city, the investigation of sustainability and resilience is an important aspect. Moreover, the deterioration has not been well incorporated to compare the life-cycle seismic performance of the SMA-steel reinforced bridge and the conventional bridge.

In this chapter, a simulation-based probabilistic life-cycle sustainability and resilience assessment framework is developed. The earthquake process and deterioration process are coupled to compute the life-cycle accumulated sustainability and resilience. The earthquake process is used to model the stochastic occurrence time of the earthquakes. The deterioration process is used to model the time-dependent performance. Finally, the life-cycle sustainability and resilience of the bridges can be computed by accumulating the consequences arising from all hazards within an investigated time horizon. Additionally, a holistic investigation of SMA-steel reinforced bridge is provided using the developed framework. Compared with previous studies, this study incorporates multiple criteria including sustainability (e.g., social, economic, and environmental metrics) and resilience, involves the effects of deterioration, and extends to assess the accumulated consequences in a life-cycle context by coupling stochastic earthquake renewal process and corrosion process. The uncertainties associated with the corrosion, the occurrence time of earthquakes, the number of earthquakes, and hazard intensity are considered in the investigation. The new insights on the life-cycle cost and benefit of sustainability and resilience of SMA-

steel reinforced bridges are provided, which can aid the decision-making of bridges considering multiple criteria under compound earthquakes and deterioration in a life-cycle context.

7.2　　　　Deterioration Process

To assess seismic sustainability and resilience from a long-term perspective, understanding the mechanism of deterioration is necessary. The deterioration is a continuous process occurring within the service life of structures. The corrosion induced by the chloride exposure environment can continuously affect the performance and resilience of structures (Akiyama et al., 2020).

7.2.1 Chloride Exposure Environment

The practical chloride exposure conditions typically include marine atmospheric environment, marine splash environment, and deicing salt environment (Ghosh & Padgett, 2012). Corrosion initiation time and rate of corrosion under these three exposure conditions are introduced in this study.

Coastal bridges are exposed to the marine environment. Due to the existence of capillary pores within concrete material, suction of chloride solution in concrete structural components can happen. Then, the concentration of chlorides can be increased from water evaporation and corrosion is initiated when these chlorides penetrate through cover concrete and contact with steel (Choe et al., 2008; Shekhar et al., 2018). A diffusion model can be adopted to compute corrosion initiation time $T_{i,marine}$ with respect to marine exposure as (Engelund et al., 2000)

$$T_{i,marine} = \left\{ \frac{x^2}{4k_e k_c D_{cl,0}(t_0)^{n_{cl}}} \left[erf^{-1}\left(\frac{C_s - C_{cr}}{C_s} \right) \right]^{-2} \right\}^{\frac{1}{(1-n_{cl})}} \qquad (7\text{-}1)$$

where x is the depth of cover concrete; $D_{cl,0}$ represents reference diffusion coefficient; k_c is the curing factor; k_e represents the environment factor; t_0 is the concrete age at the time of conducting compliance test; n_{cl} is the variable incorporating the densification of material; C_s represents the equilibrium chloride concentration at the concrete surface; C_{cr} is the critical chloride concentration; and the erf is the Gaussian error function.

After the initiation of corrosion, the area of steel starts to reduce. The corrosion rate is associated with uncertainties and it depends on different environments (Frangopol et al., 1997). A time-variant corrosion rate model under marine exposure is expressed as (Vu & Stewart, 2000)

$$r_{corr}(0) = 0.0116 i_{corr}(0) = 0.0116 \times \frac{37.8(1 - w/c)^{-1.64}}{x} \qquad (7\text{-}2)$$

$$r_{corr}(t_p) = 0.85 r_{corr}(0) t_p^{-0.29} \qquad (7\text{-}3)$$

where $i_{corr}(0)$ is the initial corrosion rate in current density (in the unit of $\mu A/cm^2$); w/c is the water-cement ratio of concrete material; $r_{corr}(0)$ is the initial corrosion rate (in the unit of mm/year), and $r_{corr}(t_p)$ is the mean corrosion rate at the time t_p after initiating corrosion.

In addition to marine atmospheric and marine splash environment, structures can be exposed to deicing salt. For the transportation networks located in frozen regions, deicing salts are spread on road networks to eliminate snow to ensure operational safety. Compared with the marine environment, deicing salt can normally cause severer

corrosion of structures due to its higher content of chlorides (Ghosh & Padgett, 2010).

The corrosion initiation time with respect to deicing salt environment can be expressed

as (Enright & Frangopol, 1998)

$$T_{i,deicing} = \frac{x^2}{4D_C} \left[erf^{-1}(\frac{C_s - C_{cr}}{C_s}) \right]^{-2} \tag{7-4}$$

where D_C is the diffusion coefficient for the deicing salt environment. The corrosion

rate for this environment can be obtained from experiments and observational

measurements. The probabilistic distribution of corrosion rate under deicing salt

environment can be found in Enright and Frangopol (1998).

7.2.2 Effects of Corrosion

The effects of corrosion within reinforced concrete structures can be summarized as

area reduction of steel and secondary effects. After the chlorides penetrate the concrete

cover and contact with steel, area loss of steel commences. Uniform corrosion and

pitting corrosion are two widely adopted models to characterize the area loss of steel.

For uniform corrosion, area loss of reinforcing steel is considered as uniform around

the circumference of reinforcing steel. Under this consideration, the residual area of

rebar can be computed as (Enright & Frangopol, 1998; Shekhar et al., 2018)

$$A_U(t) = \begin{cases} \dfrac{\pi}{4} D_i^2 & \text{for } t \leq T_i \\[2ex] \dfrac{\pi}{4} \left[D_i - 2\int_{T_i}^{t} r_{corr}(t_p)dt_p \right]^2 & \text{for } 2\int_{T_i}^{t} r_{corr}(t_p)dt_p < D_i \\[3ex] 0 & \text{for } D_i \leq 2\int_{T_i}^{t} r_{corr}(t_p)dt_p \end{cases} \tag{7-5}$$

where D_i is the diameter of pristine reinforcing steel and T_i represents the time of corrosion initiation for a specific scenario.

In addition to uniform corrosion, deep pits along the length of corroded reinforcing steel were reported in previous studies. The area loss due to pitting corrosion can be significantly larger than the area loss induced by uniform corrosion (Zandi Hanjari et al., 2011). Thus, pitting corrosion should be appropriately modelled within the corrosion process accompanied by uniform corrosion. The residual rebar area subjected to pitting corrosion can be computed using a hemispherical pit model as follows (Ghosh & Sood, 2016)

$$A_p(t) = \left[1 - \frac{w_p(t)}{2D_i}\right]\left[A_U(t) - \frac{\pi}{4}D_i^2\right] + A_{DP}(t) \tag{7-6}$$

where $w_p(t)$ is the width of the pit excluding uniform corrosion; and $A_{DP}(t)$ is the residual area of pit excluding uniform corrosion. These two parameters can be calculated using pit depth based on geometric relationships.

The pit depth is calculated as

$$p(t) = R\int_{T_i}^{T} r_{corr}(t_p)dt_p \tag{7-7}$$

where $p(t)$ is the pit depth; and R is the pitting factor. The relationship between uniform corrosion (the depth of uniform corrosion) and pitting corrosion (the maximum pit depth) can be described using the pitting factor. The spatial variability of pitting corrosion can be modelled through the consideration of spatially variant pitting factors. The probabilistic distribution of pitting factors can be determined from experiments.

For instance, Extreme Value Type I Gumbel distribution was found to be appropriate to describe the probabilistic distribution of maximum pit depth within every 100 mm length rebar (Stewart & Al-Harthy, 2008).

In addition to area loss of steel, there exist some secondary corrosion effects on reinforced concrete components (Shekhar et al., 2018). For instance, the production of rust lead to an increased volume of corroded steel, the crack of cover concrete appears due to expansion, and loss of cover concrete strength occurs. Similarly, loss of core concrete strength can occur as a result of the corrosion of transverse tie steel. Previous studies found that pitting corrosion can lead to the reduction of yield and ultimate strength of steel (Du et al., 2005; Kashani et al., 2013). The effects of corrosion on structures including loss of area of steel and other secondary effects can be modelled using finite element models. In addition to corrosion, the effects of multiple hazards on structures can also be modelled using finite element models (Li et al. 2020a; Argyroudis and Mitoulis 2021).

7.3   Seismic Hazard Processes

In addition to the corrosion process, the seismic hazard can also affect functionality and resilience within the service life of structures. For long-term performance assessment, earthquakes accruing during the service life of structures should be considered. Within the seismic hazard process, there exist uncertainties associated with both the arrival time of earthquakes and hazard intensities. Earthquake occurrence time can be described using a stochastic process based on historical events (e.g., the Poisson process). The probabilistic intensity of the hazard can be computed from ground motion

prediction models. In this section, two stochastic process models of earthquakes including both stationary and nonstationary arrival processes are introduced.

The homogeneous Poisson process with stationarity is widely adopted to model the occurrence of earthquakes (Rackwitz, 2002). In this process, the mean occurrence rate is considered as a constant. The probability of n events occurring within the time horizon t_{int} can be expressed as

$$P[N(t_{int}) = n] = \frac{(\lambda t_{int})^n \exp(-\lambda t_{int})}{n!}, \ n = 0, 1, 2, ... \tag{7-8}$$

where λ is the occurrence rate of the event. The homogeneous Poisson process can be considered as a special case of the renewal process. A renewal process can be regarded as a homogeneous Poisson process if an exponential distribution is used to describe the stochastic inter-arrival time, namely the homogeneous Poisson renewal process. In this case, the probability density function (PDF) of waiting time between two successive events is

$$f_W(x_w) = \lambda \exp(-\lambda x_w) \tag{7-9}$$

The homogeneous Poisson renewal process adopts the assumption of a constant mean occurrence rate with the time-independent occurrence of hazards. However, there can exist time-dependent features within the occurrence of earthquakes. For instance, a rupture can occur when the stochastic load state process arrives at a certain failure state. The energy is released through the earthquake, and a new cycle of energy accumulation starts. Due to the energy accumulation and release process, the occurrence of

earthquakes is associated with time-dependent characteristics. In such a situation, the

Brownian passage-time (BPT) renewal process with nonstationary features can be used

to predict the long-term occurrence of earthquakes in a time-dependent manner (Li et

al. 2020b; Matthews, Ellsworth, and Reasenberg 2002). The BPT distribution is used

to represent probabilistic inter-arrival time, the PDF of BPT distribution is

$$f_W(x_w) = (\frac{\mu}{2\pi\alpha^2 t^3})^{1/2} \exp\left\{-\frac{(t-\mu)^2}{2\mu\alpha^2 t}\right\} \tag{7-10}$$

where μ and α are the mean and coefficient of variation, respectively.

In addition to the uncertainty associated with the arrival of earthquakes, the

earthquake intensity can be uncertain for each event (Qian & Dong, 2020). For a given

magnitude, the seismic intensities are considered to follow lognormal distribution

(Boore et al., 2014). The ground motion prediction models (GMPMs) are widely

adopted to predict the probabilistic hazard intensity levels. The GMPMs provide

medians and standard deviations conditioned on earthquake scenario parameters, such

as distance, magnitude, rupture mechanism, and others.

7.4 Long-Term Sustainability and Resilience Under Compound Earthquake and Deterioration Processes

In this study, two critical metrics sustainability and resilience are considered to assess

performance of bridges. Analysis of damage conditions of the bridge under different

hazard intensities is the basis of consequence evaluation. A probabilistic seismic

demand model can be used to compute the exceeding probabilities associated with

different damage states. Seismic performance should be computed time-dependently as the corrosion can affect the performance of bridges over time. The quantification methods of sustainability and resilience are introduced. Then, the accumulated sustainability and resilience loss within the service life of the bridge can be assessed.

7.4.1 Time-dependent Sustainability

A decision is regarded as sustainable if it can meet the present generation's requirements without hindering future generations to meet their goals (Adams, 2006). Sustainability covers the consequences in terms of sociality, economy, and environment. The bridge is considered less sustainable if the relevant consequences are relatively severe after earthquakes. In this section, the metrics of sustainability in terms of social, economic, and environmental consequences are introduced. Considering the stochastic occurrence of earthquakes and time-dependent corrosion, sustainability should be updated over time.

The social metric is considered to be the number of fatalities. The top priority should be given to the life safety of people for decision making. The time-dependent expected number of fatalities under earthquakes can be computed as (Dong et al., 2013)

$$NF(t, IM) = \sum_{i=1}^{4} P_{DS_i}(t, IM) \cdot NF_{DS_i} \tag{7-12}$$

where $NF(t, IM)$ is the expected number of fatalities at time t given IM; $P_{DSi}(t, IM)$ is the probability of being damage state i; and N_{DSi} is the number of fatalities for given damage state i.

The economic metric is considered to be the monetary loss. The repair cost of the damaged bridge is considered to be the direct economic loss. Due to the damage to the bridge, the traffic capacity can be reduced, the users may spend more time and running cost arrive at their destinations. The running cost and time loss are converted to monetary values and are considered as indirect economic loss. The total economic loss is the sum of direct and indirect loss.

The time-dependent repair cost of the bridges can be computed as

$$C_{REP}(t, IM) = \sum_{i=1}^{4} P_{DS_i}(t, IM) \cdot RCR_i \cdot RBC \tag{7-13}$$

where RCR_i id the repair cost ratio associated with damage state i and RBC is the rebuilding cost of the bridge.

Due to the closure of the damaged bridge, the traffic may follow the detour to the destination (Stein et al., 1999). The running cost of the traffic can be expressed as

$$C_{Run}(t, IM) = \sum_{i=1}^{4} P_{DS_i}(t, IM) \left[c_{Run,car}(1-T) + c_{Run,truck}T \right] D_l ADTD_{DS_i} d_{DS_i} \tag{7-14}$$

where $c_{Run,car}$ is the unit cost for running cars; $c_{Run,truck}$ represents the unit cost for running trucks; T is the average daily truck traffic ratio; D_l is the detour length; $ADTD_{DSi}$ is the daily traffic following detour for damage state i; and d_{DSi} represents the time of detour for damage state i.

Due to the damage to the bridge, the speed of the traffic remaining on the link can be reduced, and some users may follow the detour to destinations, leading to time loss (Stein et al., 1999). The time loss for the users is computed as monetary value as

$$C_{TL}(t,IM) =$$

$$\sum_{i=1}^{4} P_{DS_i}(t,IM)\left[c_{AW} \cdot o_{car}(1-T) + c_{ATC} \cdot o_{truck} \cdot T\right]\left[\frac{D_l \cdot ADTD_{DS_i}}{S} + ADTE_{DS_i}(\frac{l}{S_{d,DS_i}} - \frac{l}{S_0})\right]d_{DS_i}$$

(7-15)

where c_{AW} is the wage per hour; c_{ATC} represents the compensation per hour; $ADTE_{DSi}$ is the daily traffic following damaged link for a damage state i; o_{car} and o_{truck} are the vehicle occupancies for cars and trucks, respectively; S_0 and $S_{d,DSi}$ are the speed on the intact link and damaged link, respectively; l is the length of the link; and S is the detour speed. The total economic loss under an earthquake event is the sum of the direct (e.g., repair cost) and indirect loss (e.g., running cost and time loss).

The environmental metric is considered as the carbon dioxide emission. The repair of the damaged bridge can emit carbon dioxide causing direct emissions. Due to the downtime of the damaged bridge, the traffic following the detour can emit additional carbon dioxide causing indirect emissions. The total carbon dioxide emission considered herein is the sum of emissions from repair and detour traffic. Carbon dioxide is a greenhouse gas and is the cause of global warming. Carbon neutrality is a worldwide mission to mitigate the relevant environmental issues. Compared with steel, alloy production can be associated with significantly higher carbon dioxide emissions. On the other hand, the accumulated carbon dioxide emissions from repair and detours

may be reduced within the service life of the bridge if the implementation of SMA can mitigate the damage to the bridge. In trade-off analysis, it is important to assess the long-term carbon dioxide emissions of the SMA-steel reinforced bridge under hazards. The carbon dioxide emitted from the detour traffic can be expressed as

$$EN_{DT}(t, IM) = \sum_{i=1}^{4} P_{DS_i}(t, IM) \cdot ADTD_{DS_i} \cdot D_l \cdot d_{DS_i} \cdot \left[Enp_{car} \cdot (1-T) + Enp_{Truck} \cdot T \right]$$

(7-16)

where Enp_{car} and Enp_{Truck} represent the carbon dioxide emitted per unit distance for cars and trucks, respectively. The carbon dioxide emitted from the reconstruction and repair of the damaged bridges is calculated as proportional to the damage ratios for different damage states.

7.4.2 Time-dependent Resilience

Resilience assessment focuses on the residual functionality after the hazard and the recovery patterns over time (Timmerman, 1981). Considering the time-dependent corrosion and stochastic occurrence of earthquakes, the resilience should be updated over time. By using the definition of resilience loss (Bocchini et al., 2014; Yang & Frangopol, 2019), the time-dependent resilience loss index can be computed as (Qian et al., 2022)

$$R_L(t, IM) = \frac{t_h \cdot 100\% - \int_{t_i}^{t_i+t_h} Q(t_r \mid t) dt_r}{t_h}$$

(7-17)

where t_h represents the investigated recovery time horizon; $Q(t_r|t)$ represents the time-dependent functionality of the bridge after the earthquake disruption. The time-

144

dependent functionality is the basis of assessing resilience. The restoration functions developed by HAZUS (FEMA, 2020) can be adopted. A normal cumulative distribution function characterized by a mean and standard deviation can be used to model the post-hazard functionality of bridges. In this restoration model, the post-hazard functionality is dependent on the damage states of the bridges. The bridge under a severer damage state is associated with less residual functionality and requires more time to recover to a certain level. For each damage state, the restoration function is developed by fitting the survey data from experts. By considering the effects of deterioration as indicated in section 7.2 (e.g., reduction of steel area and concrete strength), the time-dependent seismic vulnerability can be computed. The expected post-hazard functionality is computed as the sum of post-hazard functionalities for different damage states weighted by corresponding time-dependent damage state probabilities. Then, resilience loss can be quantified by Eq. 7-17.

7.5   Framework of Life-cycle Sustainability and Resilience

Within the service life of the bridge, corrosion and earthquakes induce compound effects on the sustainability and resilience of bridges in a time-dependent manner. By expanding the time horizon, this study assesses the accumulated sustainability and resilience from a long-term perspective.

The computational framework of long-term sustainability and resilience loss under earthquake and deterioration processes is presented in Figure 7-1. The developed framework consists of three modules including the deterioration process module,

earthquake process module, and long-term sustainability and resilience module. In the deterioration process module, the exposure environment should be identified. Then, the structural parameters and environmental parameters associated with corrosion should be determined. The corrosion effects on structures (e.g., loss of steel area and reduction of the strength of concrete) can be modeled subsequently. In the earthquake process module, the earthquake source and investigated scenarios are identified. The earthquake process models describing the stochastic occurrence of earthquakes and corresponding parameters are determined. The ground motion perdition model is used to compute the uncertain hazard intensities. In the long-term sustainability and resilience module, the earthquake events with stochastic occurrence time and intensity are simulated based on the earthquake process module. The seismic sustainability and resilience loss under the simulated earthquake events are computed time-dependently based on the deterioration process module. Finally, the long-term sustainability and resilience loss are computed by accumulating the relevant induced consequences within the investigated time horizon.

From a long-term perspective, the non-monetary sustainability and resilience loss can be computed as (Yang & Frangopol, 2019)

$$L_N = \sum_{k=1}^{N_h(t_L)} L_{N,k}(t_k) \tag{7-18}$$

where L_N is the long-term non-monetary sustainability or resilience loss; t_L is the considered time horizon; $N_h(t_L)$ is the number of disruptions within t_L; and $L_{N,k}(t_k)$ is the non-monetary sustainability or resilience loss associated with event k at time t_k.

146

The long-term monetary sustainability in terms of economic loss is computed as (Zheng et al., 2018)

$$L_M = \sum_{k=1}^{N_h(t_L)} L_{M,k}(t_k) \cdot e^{-rt_k} \qquad (7\text{-}19)$$

where L_M is the long-term monetary sustainability (e.g., economic loss); $L_{M,k}(t_k)$ is the monetary sustainability induced by event k at time t_k; and r is the monetary discount rate.

Sustainability and resilience are considered in this chapter. As the climate change impacts on different areas may differ, it is necessary to extend the sustainability and resilience assessment to different areas. Different areas are associated with different weather and hazard conditions. For the earthquake hazard, the stochastic renewal process describing the occurrence of earthquakes can be updated using the historical earthquake events data in a specific area. For instance, the probabilistic distribution of the inter-arrival time of earthquakes can be updated given the regional observation data. The probabilistic seismic hazard analysis can be performed based on the local fault and site conditions using the ground motion attenuation relationship (Baker, 2013). For the deterioration process, the model can be updated based on the exposure conditions associated with different areas. In general, the deicing salt, marine atmosphere, and marine splash are three widely observed exposure conditions of structures. The deterioration process models of these three different conditions can be found in (Shekhar et al., 2018). The deterioration process parameters of a specific area under specific weather and hazard conditions can be further refined based on experiments and

field measurements. For the consequence assessment, the input parameters (e.g., repair cost, traffic demand, detour length, compensation, etc.) can be updated for different areas considering relevant recovery resources, traffic conditions, economic conditions, and network topology, among others. Overall, the developed framework can be updated for different areas/weather/hazard conditions by updating the earthquake process module, the deterioration process module, and the consequence module based on historical, observational, and experimental data.
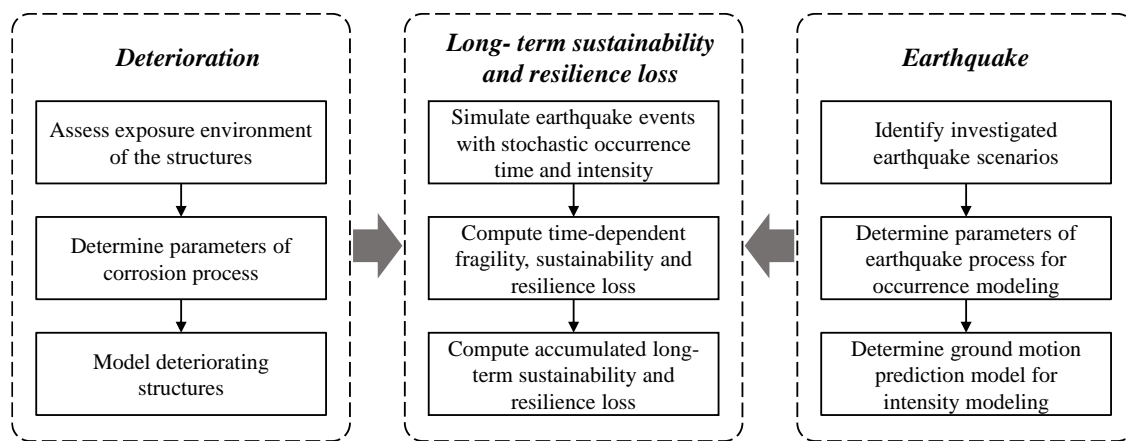
Figure 7.1 Computational framework of long-term sustainability and resilience loss under earthquakes and function deterioration

7.6   Steel-shape Memory Alloy (SMA) Reinforced Bridges

SMA material is characteristic of its shape memory effect (SME) and superelasticity (SE). SME is exhibited when the SMA is at a temperature below the martensite finish temperature M_f, where a residual strain takes place upon loading, but this residual strain can be fully recovered once the temperature later increases above the austenite finish temperature A_f. SE occurs when the SMA is stressed at a temperature above A_f, where

the induced strain can be recovered immediately upon unloading. SMA bars exhibit a flag-shaped stress-strain hysteretic behavior upon loading and unloading effects at room temperature. In other words, the SMA bar can almost recover to the pre-event position with appropriate energy dissipation feature after experiencing large nonlinear deformation (Xiang et al., 2020). The constitutive material model of the SMA bar includes two parts, i.e., tension and compression regions, as shown in Figure 7.2 (Zheng et al., 2018). In the tension region, the envelope curves associated with strain-stress (ε-σ) relationships are composed of seven paths (i.e., OB, BC, CS, SC, CD, DA, AO), where E is the elastic modulus of the SMA bar; k_1 and k_2 are discount coefficients of the elastic modulus; ε_{Ms} and σ_{Ms} are the strain and stress of the SMA bar at martensite-to-austenite transformation start; ε_{Mf} and σ_{Mf} are the strain and stress of the SMA bar at martensite transformation finish; ε_{As} and σ_{As} are the strain and stress of the SMA bar at austenite-to-martensite transformation start; ε_{Af} and σ_{Af} are the strain and stress of the SMA bar at austenite transformation finish. Similar to the tension region, the envelope curves associated with strain-stress relationships in the compression zone also include seven paths (i.e., OB', B'C', C'S', S'C', C'D', D'A', A'O).
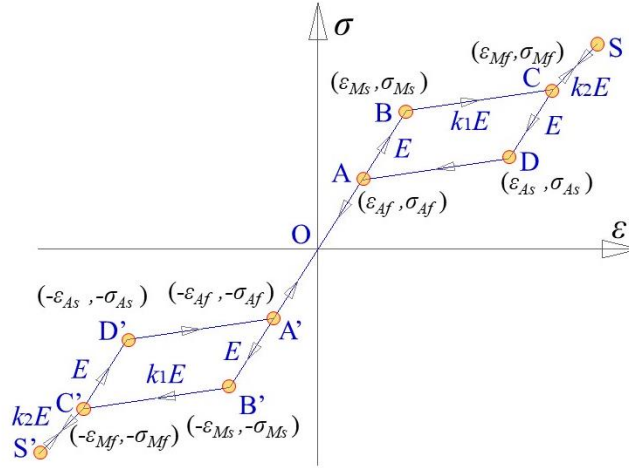
Figure 7.2 Flag-shaped constitutive model of SMA bars

Additionally, environmental corrosion can remarkably increase the vulnerability of steel-reinforced structures (Shekhar et al., 2018), SMA bars, as a kind of corrosion-resistant material, can be used to replace the conventional rebars in vulnerable regions (e.g., plastic hinge zones) for corrosion resistance (Billah & Alam, 2012). Due to the self-centering capacity, energy dissipation characteristics, and corrosion resistance, SMA bars are superior materials that can be incorporated into structures to mitigate damage under earthquakes and corrosion.

Despite the abovementioned advantages, the production of the alloy is associated with significantly higher costs and carbon dioxide emissions compared with the production of steel. Carbon dioxide is the major greenhouse gas from human activities and can cause global warming. The cost and benefit analysis should be extended to a life-cycle context to give a holistic evaluation (Dong & Frangopol, 2017). To understand the trade-off between cost and benefits in such circumstances, this study investigates the long-term sustainability and resilience of the SMA-steel reinforced

concrete bridge under deterioration and earthquake processes.

7.7   Illustrative Example

In this study, long-term sustainability and resilience loss of the steel-SMA reinforced concrete bridge under earthquake and functional deterioration processes are assessed. By considering earthquake and functional deterioration processes, long-term sustainability and resilience loss are computed. The long-term direct and indirect consequences are compared and analyzed. The effects of SMA embodied carbon dioxide emission on long-term emissions are investigated.

A conventional RC bridge and a novel SMA-steel reinforced concrete bridge are investigated, respectively. The two bridges are both two-span continuous bridges. The total length of each bridge is 40 m. The box girder is built using C40 concrete (i.e., compressive strength is 40 MPa at 28 days). The pier is composed of two columns, of which the height and diameter are 6 m and 1.2 m, respectively. C40 concrete is also used for the pier. For the SMA-steel reinforced concrete bridge, the SMA bars are employed as reinforcement in the plastic hinge of the column. The plastic hinge length can be calculated according to the experimental formula in the reference (Alam et al., 2008).

The finite element models of the conventional bridge and the SMA-steel reinforced bridge are both established in an open system for earthquake engineering simulation, namely OpenSEES (Mazzoni et al., 2006). The SMA bar is modeled using a flag-shaped self-centering material (Tremblay et al., 2008). The properties of the

SMA bar are tabulated in Table 7.1. The finite element model of the bridge is presented in Figure 7.3. Apart from the SMA bar, the parameters of other materials are also presented in Table 7.1. A set of ground motions (Baker et al., 2011) is selected to perform the nonlinear time history analysis.
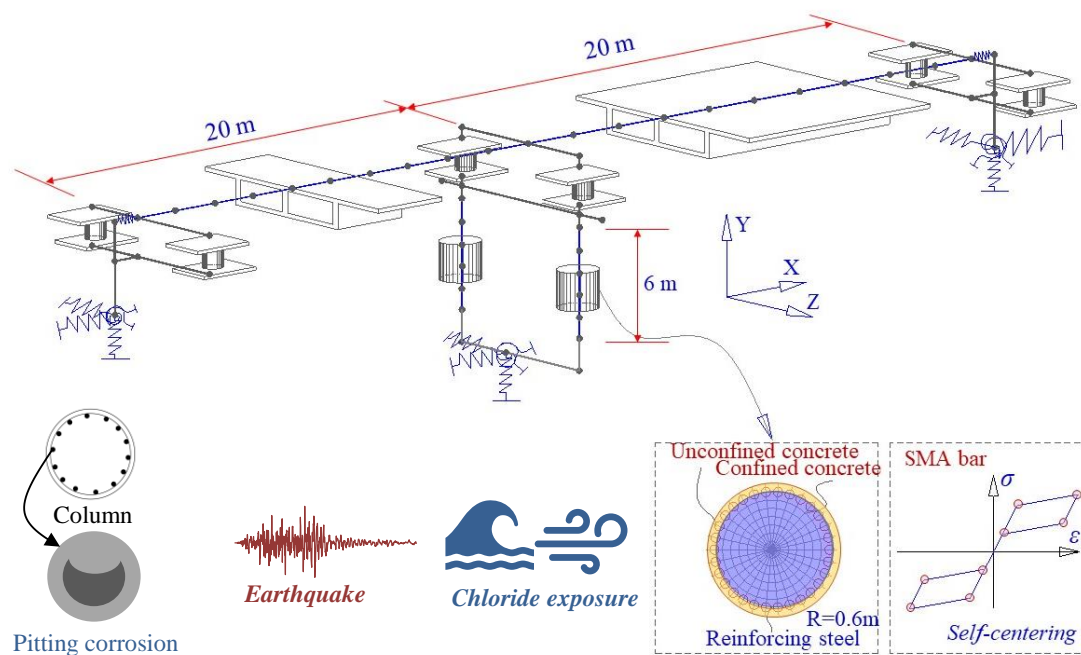
Figure 7.3 Finite element model of the bridge

Table 7.1 Parameters of materials

Material	Parameter	Value
Concrete	Compressive strength (MPa) at 28 days	40.0
	Strain at peak stress (%)	0.3
SMA	Elastic Modulus (GPa)	58.8
	Austenite-to-martensite start stress (MPa)	460.0
	Martensite finish stress (MPa)	523.7
	Martensite-to-austenite start stress (MPa)	366.8
	Austenite finish stress (MPa)	302.8

	Elastic modulus (GPa)	200.0
	Yield stress (MPa)	330.0
Steel	Ultimate stress (MPa)	455.0
	Ultimate strain (%)	9.0

7.7.1 Life-cycle Sustainability and Resilience Under Earthquakes and Deterioration

The earthquakes and deterioration are considered in this study to assess the long-term sustainability and resilience of the SMA-steel reinforced concrete bridge and the conventional bridge. The earthquakes are associated with stochastic occurrence time and intensity. The BPT renewal process is used to model the occurrence of earthquakes. For the corresponding parameters of the BPT model are determined based on (Pandey & Van Der Weide, 2017). The corrosion process can continuously reduce the area of steel and the strength of concrete, thus affecting the performance of bridges. Based on the environmental exposure parameters (Shekhar et al., 2018), the time-dependent structural parameters including the residual area of steel and concrete strength can be computed. For a given year, deteriorated bridge realizations can be generated. The corresponding performance in the given year can be computed.

Figure 7.4 illustrates the simulation process of long-term sustainability and resilience loss under earthquake and functional deterioration processes. As indicated, three planes, including deterioration, vulnerability, and sustainability or resilience are connected through the earthquake process. The upper plan is projected to the lower plan in terms of the occurrence time of the extreme events. The probabilistic inter-arrival time W_1, W_2, W_3,…, and W_k are generated from the earthquake process model, the

probabilistic hazard intensity can be generated from the ground motion prediction model. The seismic vulnerability of the corroded bridge under simulated earthquake events is computed. Based on the simulated earthquake events and seismic vulnerability, the sustainability is computed in terms of the number of fatalities, economic loss, and carbon dioxide emission. The resilience loss is computed based on the approach introduced in section 7.4. The long-term sustainability and resilience loss are computed by accumulating the corresponding consequences induced within an investigated time horizon.
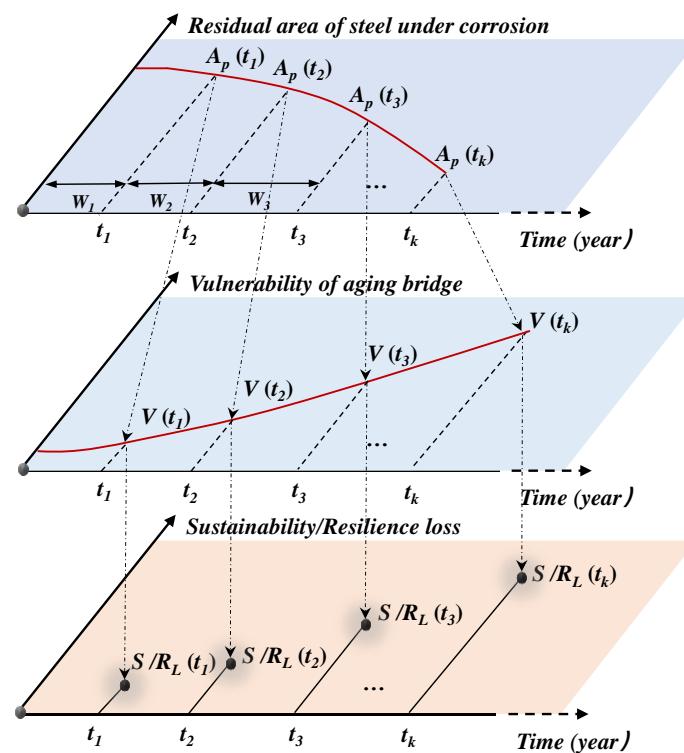
Figure 7.4 Illustration of simulating long-term sustainability and resilience loss under earthquake and functional deterioration processes

In this study, 5×10^5 simulations are performed, and the parameters for consequence assessment are listed in Table 7.2. The long-term sustainability and

resilience loss of the SMA-steel reinforced concrete bridge and the conventional bridge are presented in Figure 7.5. Compared with the conventional bridge, the SMA-steel reinforced concrete bridge is associated with a lower expected number of fatalities, economic loss, and carbon dioxide emission, which indicates the SMA-steel reinforced concrete bridge is more sustainable. Additionally, the long-term resilience loss for the SMA-steel reinforced concrete bridge is lower than that of the conventional bridge. With the increase of time, there is an increasing trend of the difference of sustainability and resilience loss, comparing the two bridges. The relative difference in long-term sustainability and resilience loss of the two bridges at the year 75 is presented in Figure 7.6. The relative difference values for the number of fatalities, economic loss, carbon dioxide emissions, and resilience loss are 47%, 29%, 26%, and 35%, respectively. For the investigated case, the implementation of SMA can make the structure more sustainable and resilient in a long-term perspective.
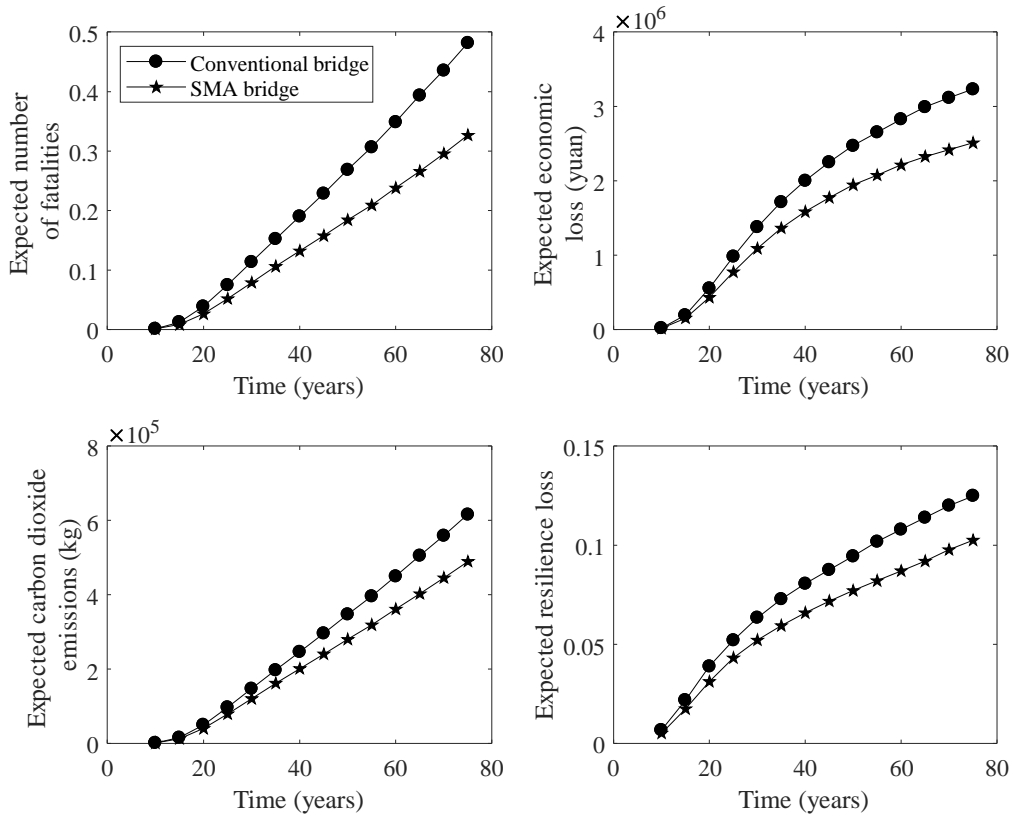
Figure 7.5 Long-term sustainability and resilience loss under earthquake and

deterioration processes
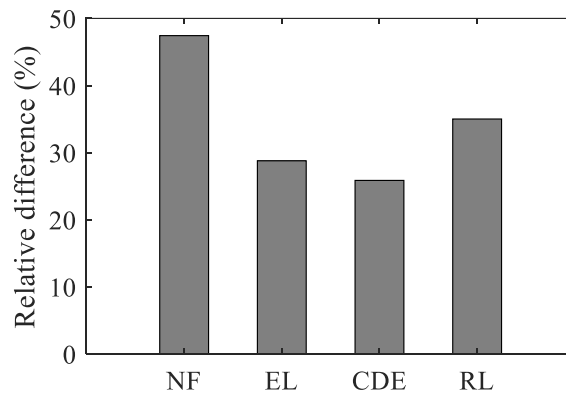
Figure 7.6 The relative difference in long-term sustainability and resilience at the

year 75 comparing conventional and SMA-steel reinforced bridges (NF: number of

fatalities; EL: economic loss; CDE: carbon dioxide emissions; and RL: resilience

loss)

7.7.2   Life-cycle Direct and Indirect Consequences

In sustainability assessment, the repair of the damaged bridge can induce carbon dioxide emissions and economic loss, which are known as direct consequences. Due to the reduced functionality of the damaged bridge, the speed of the vehicles remaining on the damaged link may be reduced, and some vehicles may follow the detour to their destinations. The traffic-induced time loss, operational cost, and carbon dioxide emissions are considered to be indirect consequences.

The long-term direct and indirect consequences of the two bridges under earthquake and functional deterioration processes are illustrated in Figure 7.7. For the two bridges, the indirect consequences are significantly larger than the direct consequences. The direct consequences associated with the SMA-steel reinforced concrete bridge and the conventional bridge are closely spaced. There exists a relatively larger difference in the indirect consequences associated with the two bridges. For the investigated case, the implementation of SMA can especially reduce the long-term indirect consequences (indirect carbon dioxide emissions and economic loss).

Compared with the conventional bridge, the cost and carbon dioxide emission of constructing the SMA-steel reinforced concrete bridge are increased by 0.25 million RMB and 2.6 tons, respectively, while the long-term economic loss and carbon dioxide emission associated with the SMA-steel reinforced concrete bridge are decreased by 0.72 million RMB and 126.6 tones, respectively (for a time horizon of 75 years). The increased values of the cost and carbon dioxide emission associated with the construction of the SMA-steel reinforced concrete bridge are relatively small, while

significant benefits can be achieved in terms of long-term sustainability (e.g., the number of fatalities, economic loss, and carbon dioxide emission) and resilience. The amount of SMA used in the plastic hinge region is relatively small compared with other construction materials (e.g., steel and concrete). The use of SMA can mitigate the damage and maintain the functionality of the bridge after hazards, thus reducing the indirect economic loss and indirect carbon dioxide emission from traffic. As mentioned previously, the indirect consequences account for most of the total consequences.
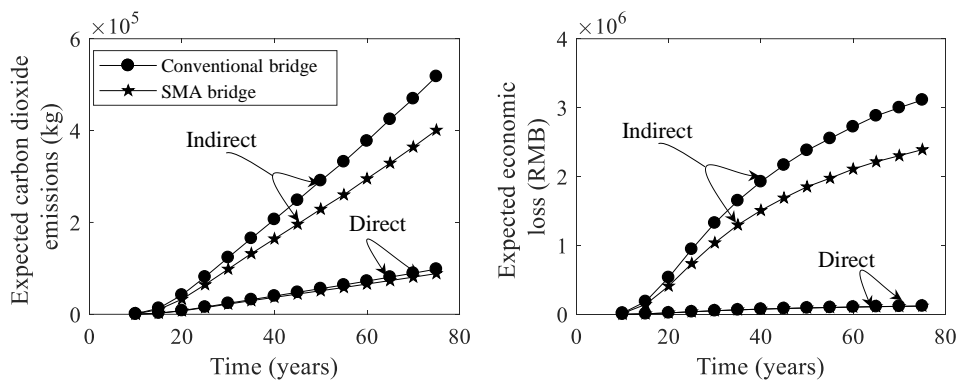
Figure 7.7 Long-term direct and indirect consequences under earthquake and functional deterioration processes

The carbon dioxide emissions of producing one-ton nickel alloy, titanium, and steel are 14, 10, and 1.2 tons, respectively (Tapia et al., 2011; NINMR 2021; Wei et al., 2020). To consider different materials and production processes of SMA, the effects of SMA embodied carbon dioxide emission on long-term emissions are assessed. As presented in Figure 7.8, the unit SMA embodied carbon dioxide emissions (SMAUCE) 12, 15, and 20 t/t are considered to compute the long-term emissions. By increasing the

SMAUCE, the direct and total long-term carbon dioxide emissions are close. The influence of different SMAUCE on long-term carbon dioxide emissions is negligible due to the small amount of the SMA used in the plastic hinge regions and the relatively small direct consequence.
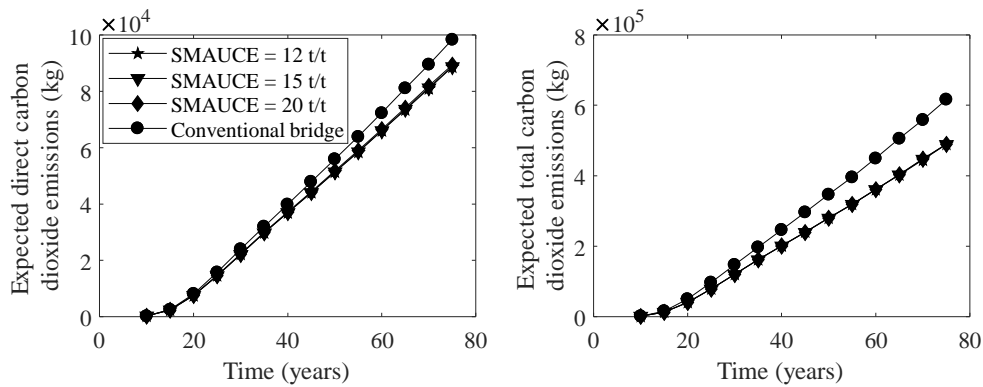
Figure 7.8 Impact of unit SMA embodied carbon dioxide emission on long-term

direct and total carbon dioxide emissions

7.8 Summary

This study develops a framework for life-cycle sustainability and resilience assessment of structures under seismic and deterioration processes. The time-variant performance can be computed considering the deterioration process. The stochastic earthquake renewal process models are introduced. The probabilistic occurrence time and intensity of earthquakes within the investigated time horizon can be simulated from the stochastic renewal process model and ground motion prediction model, respectively. Sustainability is quantified in terms of the number of fatalities, economic loss, and

carbon dioxide emissions. By accumulating the consequences within the investigated time horizon, the life-cycle sustainability and resilience loss of structures can be assessed. The obtained results can benefit decision-making and adaptation measures in real-life problems. In the design stage, structures can be optimized based on the considered long-term sustainability and resilience threshold. In the operational stage, the decision can be made to select the optimal adaptation measure (e.g., retrofit) based on quantified life-cycle sustainability and resilience. The developed approach contributes to the sustainability and resilience assessment from a life-cycle perspective. The uncertainties associated with the occurrence time of hazard, hazard intensity, deterioration, and structural damage are incorporated into the developed framework.

The long-term sustainability and resilience loss of an SMA-steel reinforced concrete bridge and a conventional bridge are assessed and compared. The results can aid the sustainable and resilient design of bridges under compound hazards. Several conclusions are drawn as follows.

- Compared with the conventional bridge, the cost and carbon dioxide emission associated with the construction of the SMA-steel reinforced concrete bridge increase slightly, while significant benefits can be achieved in terms of long-term sustainability (e.g., the number of fatalities, economic loss, and carbon dioxide emission) and resilience. For the investigated conventional bridge and steel-SMA reinforced concrete bridge, the relative difference values for the number of fatalities, economic loss, carbon dioxide emissions, and resilience loss are 47%, 29%, 26%, and 35%, respectively.

- The corrosion resistance, self-centering capacity, and energy dissipation are superior characteristics of SMA, which can mitigate the damage thus reducing the consequences under compound earthquake and corrosion processes.

- The implementation of SMA can enhance the post-hazard functionality of the bridge, and the traffic following detours can be reduced. The long-term indirect economic loss and carbon dioxide emissions from traffic can be reduced significantly. The indirect consequences account for most of the total consequences.

- The reduction of enormous long-term carbon dioxide emissions by implementing an SMA-steel reinforced concrete bridge can contribute the carbon neutrality, which is an urgent need of society to mitigate the adverse global warming issues.

CHAPTER 8
CONCLUSIONS AND FUTURE WORK

8.1 Conclusions

This thesis proposes a surrogate-enabled seismic performance analysis framework for spatially distributed bridges. An approach is developed to select the appropriate IM incorporating the trade-off among multiple criteria. The surrogate models with acceleration algorithms are developed. The surrogate models are used for uncertainty quantification and global sensitivity analysis, respectively. The surrogate models are used to compute the seismic vulnerability of bridges. A two-stage multi-criteria global sensitivity analysis algorithm coupling surrogate model and decision technique is developed for identifying the holistic sensitive parameters to the whole system. A vine copula-based approach is developed to model the complex dependence within the PBEE. The developed approaches including the multi-criteria IM selection, advanced surrogate model for uncertainty quantification, multi-criteria global sensitivity analysis, and vine copula-based dependence model can jointly improve the confidence of PBEE. Moreover, the sustainability and resilience assessment is extended to a life-cycle context considering earthquakes and deterioration. The life-cycle performance of a hazard mitigation measure is assessed. The developed framework can aid the confident design and management of spatially distributed bridges under earthquakes. The major conclusions of this thesis are summarized.

1. An approach for seismic IM selection under multiple criteria and uncertainty is

developed. A multi-criteria decision-making (MCDM) approach by incorporating stochastic multi-criteria acceptability analysis (SMAA) with the technique for order preference by similarity to ideal solution (TOPSIS) is proposed to solve the stochastic decision-making problem. The multiple performance criteria are evaluated for the investigated structural components, and the decision matrix is formulated based on the criteria of each IM alternative. The importance of the component to system reliability is quantified and used as the weighting factors in MCDM. The holistic acceptability indices indicating the overall acceptability levels of IMs are computed. Additionally, the effects of different IMs on probabilistic performance are investigated to further support the IM selection.

2. A surrogate-based performance analysis approach is developed. The sparse PCE is used as a surrogate model to emulate the response of the physical model. The acceleration techniques are integrated to formulate an algorithm for the efficient computation of sparse PCE (ASPCE). The integrated algorithm can improve the efficiency of the computational process compared with conventional greedy algorithms while ensuring satisfying predictive performance. Once the sparse PCE model is obtained, uncertainty quantification can be achieved efficiently. By using ASPCE, a complex relationship of the input and demand can be captured, and multiple uncertain parameters can be incorporated into uncertainty propagation.

3. A two-stage multi-criteria global sensitivity analysis algorithm is proposed by coupling ASPCE and the technique for order preference by similarity to the ideal solution (TOPSIS). A holistic global sensitivity index is proposed to identify the sensitive parameters incorporating multiple performance criteria. The sensitivity indices for individual output are computed based on the developed surrogate model in an efficient manner. The global sensitivity indices associated with different performance outputs are then considered as the sensitivity criteria and formulated as a sensitivity matrix. TOPSIS is used to incorporate these sensitivity criteria to compute the holistic global sensitivity indices. The holistic global sensitivity index can be used to aid the decision-makers to refine the database (e.g., data acquisition, investigation, and complexity reduction) for confident regional risk assessment.

4. A vine copula-based seismic performance assessment framework is developed. The vector IM and surrogate models are coupled to predict the seismic demand. The vine copula is used to model the dependence of demands and IMs. Then, seismic performance can be assessed. The proposed framework is illustrated on bridges under seismic hazards. For the investigated cases, the proposed framework can improve confidence significantly and better capture complex dependence. Within the investigated cases, the large difference in higher-order moments of seismic performance is observed by using conventional assumptions and vine copula. Due to its generality, the developed vine copula-based approach can be applied to many problems to investigate and model the

dependence characteristics, where the dependence structures are not well identified.

5. An approach for assessing the life-cycle sustainability and resilience of bridges under compound earthquakes and deterioration is proposed. The stochastic renewal process is used to model the occurrence of earthquakes. The effects of deterioration on bridges are modeled through the time-dependent reduction of steel area and strength of concrete. The bridge seismic performance can be computed in a time-variant manner considering deterioration. Subsequently, long-term bridge sustainability (e.g., fatality, economic loss, and carbon dioxide emission) and resilience are computed by considering earthquakes and deterioration occurring during the entire service life of bridges. The developed approach incorporates the uncertainties associated with deterioration, structural damage, earthquake occurrence, and hazard intensity.

6. The life-cycle sustainability and resilience of the steel-SMA reinforced concrete bridge are assessed. The earthquake and deterioration processes are considered in the assessment. By accumulating the consequences within the investigated time horizon, the long-term sustainability and resilience loss of structures can be assessed. The results are compared with those of the conventional bridge. The comparison results confirm that the steel-SMA reinforced concrete bridge is more sustainable and resilient under earthquakes and functional deterioration in a long-term perspective. The corrosion resistance, self-centering capacity, and energy dissipation are superior characteristics of SMA, which can mitigate

the damage thus maintaining functionality and reducing the consequences under compound earthquakes and deterioration.

8.2 Future Work

Some future work can be conducted to further contribute to the relevant field.

The life-cycle sustainability and resilience assessment can incorporate multiple hazards, fatigue, and climate change. The occurrence of hazards is complex. The prediction of long-term hazards can directly affect confidence in life-cycle assessment. There exist uncertainties associated with the occurrence time and intensity. The occurrence mechanisms of hazards should be further revealed. The hazards prediction models including the stochastic process models and intensity prediction models can be refined by incorporating the occurrence mechanisms of hazards.

The life-cycle sustainability and resilience assessment can be conducted at a transportation network level considering urbanization and complex traffic conditions. Extreme events can affect the functionality of the transportation network resulting in complex traffic conditions. Besides, urbanization can affect traffic conditions in a life-cycle context. The regional probabilistic hazard analysis considering spatial correlation should be performed to compute the hazard map for the investigated regions. Then, the vulnerability analysis of the components within the transportation network should be performed. The advanced method should be used to predict the time-dependent traffic conditions after the earthquakes considering urbanization in a life-cycle context. Historical traffic data can be used to develop and update traffic condition prediction

models. Based on traffic analysis, the post-hazard time-dependent functionality of the transportation network can be assessed. Finally, the long-term sustainability and resilience assessment can be achieved by considering the network-level indicators.

The transportation network facilitates social and economic activities. The functionality of a community depends on the functionality of the transportation network. The performance assessment at the community scale can incorporate the post-hazard functionality of the transportation network. The interaction between the transportation network and the community can be considered in the performance assessment.

The conventional resilience assessment in a structure community mainly focused on the physical damage and operational functionality, household well-being, a comprehensive and human-oriented measure, is seldom considered. In the future, the approaches for assessing the sustainability and resilience of the interdependent transportation network from a household well-being perspective should be developed through interdisciplinary research. Scholars from social science, economy, and engineering fields are encouraged to collaborate to develop a holistic assessment framework.

There exist uncertainties within each step of PBEE. The occurrence of earthquakes, structural behavior, and consequence evaluation are complex problems. Efficient and confident uncertainty treatment and quantification are challenging for the real-world application of PBEE. The physical and social mechanisms should be further revealed through real events and simulation. Advanced techniques should be developed for

efficient and confident uncertainty quantification. The physical laws guided machine learning and artificial intelligence techniques should be developed to aid the assessment and management of structures under hazards. Specifically, data-driven machine learning and artificial intelligence techniques can be developed for seismic demand prediction, traffic flow analysis, and post-hazard functionality analysis. The data sets from simulation and real events are used to develop the artificial intelligence model, while the inferred physical laws should be used for guidance and constraint within the model development process. Machine learning and artificial intelligence techniques can be used for the assessment and management of structures efficiently and confidently.

Due to the limited available data, the verification of PBEE using real data is still challenging. In the future, a comprehensive database regarding hazards, damage, and consequences should be developed. The PBEE can be verified and updated based on the multi-sources database.

APPENDIX

FINITE ELEMENT MODEL OF THE BRIDGE

Table A Summary of the finite element model

Component	Element	Material
Superstructure	Elastic beam-column element	Elastic
Bearing	Zero-length element	Steel01
Column	Nonlinear beam-column element	Concrete01 and Steel01
Abutment	Zero-length element	Quad-linear and tri-linear materials

REFERENCES

Aas, K., Czado, C., Frigessi, A., & Bakken, H. (2009). Pair-copula constructions of multiple dependence. *Insurance: Mathematics and Economics*, *44*(2), 182–198.

Adam, C., Kampenhuber, D., Ibarra, L. F., & Tsantaki, S. (2017). Optimal spectral acceleration-based intensity measure for seismic collapse assessment of P-delta vulnerable frame structures. *Journal of Earthquake Engineering*, *21*(7), 1189–1195.

Adams, W. M. (2006). The future of sustainability: Re-thinking environment and development in the twenty-first century. *Report of the IUCN Renowned Thinkers Meeting*, *29*, 31.

Akaike, H. (1974). A new look at the statistical model identification. *IEEE Transactions on Automatic Control*, *19*(6), 716–723.

Akiyama, M., Frangopol, D. M., & Ishibashi, H. (2020). Toward life-cycle reliability-, risk-and resilience-based design and assessment of bridges and bridge networks under independent and interacting hazards: emphasis on earthquake, tsunami and corrosion. *Structure and Infrastructure Engineering*, *16*(1), 26–50.

Alam, M. S., Youssef, M. A., & Nehdi, M. (2008). Analytical prediction of the seismic behaviour of superelastic shape memory alloy reinforced concrete elements. *Engineering Structures*, *30*(12), 3399–3411.

Anderson, K., & Peters, G. (2016). The trouble with negative emissions. *Science*, *354*(6309), 182–183.

Anwar, G. A., Dong, Y., & Li, Y. (2020). Performance-based decision-making of buildings under seismic hazard considering long-term loss, sustainability, and resilience. *Structure and Infrastructure Engineering*, 1–17.

Anwar, G. A., Dong, Y., & Zhai, C. (2020). Performance-based probabilistic framework for seismic risk, resilience, and sustainability assessment of reinforced concrete structures. *Advances in Structural Engineering*, *23*(7), 1454–1472. https://doi.org/10.1177/1369433219895363

Argyroudis, S. A., & Mitoulis, S. A. (2021). Vulnerability of bridges to individual and multiple hazards-floods and earthquakes. *Reliability Engineering & System Safety*, *210*, 107564.

Argyroudis, S. A., Mitoulis, S. A., Hofer, L., Zanini, M. A., Tubaldi, E., & Frangopol, D. M. (2020). Resilience assessment framework for critical infrastructure in a multi-hazard environment: Case study on transport assets. *Science of The Total Environment*, *714*, 136854.

Asadi, E., Salman, A. M., & Li, Y. (2019). Multi-criteria decision-making for seismic

   resilience and sustainability assessment of diagrid buildings. *Engineering*

   Structures, *191*, 229–246.

Ayyub, B. M., & Lai, K.-L. (1989). Structural reliability assessment using latin

   hypercube sampling. *Structural Safety and Reliability*, 1177–1184.

Baker, J. W. (2007). Probabilistic structural response assessment using vector-valued

   intensity measures. *Earthquake Engineering & Structural Dynamics*, *36*(13),

   1861–1883.

Baker, J. W. (2011). Conditional mean spectrum: Tool for ground-motion selection.

   Journal of Structural Engineering, *137*(3), 322–331.

Baker, J. W. (2013). An introduction to probabilistic seismic hazard analysis. *White*

   Paper Version, *2*(1), 79.

Baker, J. W., & Allin Cornell, C. (2005). A vector-valued ground motion intensity

   measure consisting of spectral acceleration and epsilon. *Earthquake Engineering*

   & Structural Dynamics, *34*(10), 1193–1217.

Baker, J. W., & Bradley, B. A. (2017). Intensity measure correlations observed in the

   NGA-West2 database, and dependence of correlations on rupture and site

   parameters. *Earthquake Spectra*, *33*(1), 145–156.

Baker, J. W., & Cornell, C. A. (2008). Uncertainty propagation in probabilistic

   seismic loss estimation. *Structural Safety*, *30*(3), 236–252.

Baker, J. W., & Jayaram, N. (2008). Correlation of spectral acceleration values from

NGA ground motion models. *Earthquake Spectra*, *24*(1), 299–317.

Baker, J. W., Lin, T., Shahi, S. K., & Jayaram, N. (2011). New ground motion

selection procedures and selected motions for the PEER transportation research

program. *PEER Report*, *3*.

Baker, J. W. (2007). Correlation of ground motion intensity parameters used for

predicting structural and geotechnical response. *Tenth International Conference*

on Application of Statistics and Probability in Civil Engineering, *8*.

Baptista, R., Stolbunov, V., & Nair, P. B. (2019). Some greedy algorithms for sparse

polynomial chaos expansions. *Journal of Computational Physics*, *387*, 303–325.

https://doi.org/10.1016/j.jcp.2019.01.035

Beyer, K., & Bommer, J. J. (2006). Relationships between median values and

between aleatory variabilities for different definitions of the horizontal

component of motion. *Bulletin of the Seismological Society of America*, *96*(4A),

1512–1522.

Bianchini, M., Diotallevi, P., & Baker, J. W. (2009). Prediction of inelastic structural

response using an average of spectral accelerations. *10th International*

Conference on Structural Safety and Reliability (ICOSSAR09), *1317*, 2164–

2171.

Billah, A. H. M. M., & Alam, M. S. (2012). Seismic performance of concrete columns reinforced with hybrid shape memory alloy (SMA) and fiber reinforced polymer (FRP) bars. *Construction and Building Materials*, *28*(1), 730–742.

Blatman, Géraud, & Sudret, B. (2010). An adaptive algorithm to build up sparse polynomial chaos expansions for stochastic finite element analysis. *Probabilistic Engineering Mechanics*, *25*(2), 183–197. https://doi.org/10.1016/j.probengmech.2009.10.003

Blatman, Géraud, & Sudret, B. (2011). Adaptive sparse polynomial chaos expansion based on least angle regression. *Journal of Computational Physics*, *230*(6), 2345–2367. https://doi.org/10.1016/j.jcp.2010.12.021

Blatman, Graud, & Sudret, B. (2010). Efficient computation of global sensitivity indices using sparse polynomial chaos expansions. *Reliability Engineering and System Safety*, *95*(11), 1216–1229. https://doi.org/10.1016/j.ress.2010.06.015

Bocchini, P., Frangopol, D. M., Ummenhofer, T., & Zinke, T. (2014). Resilience and sustainability of civil infrastructure: Toward a unified approach. *Journal of Infrastructure Systems*, *20*(2), 4014004.

Boore, D. M. (2010). Orientation-independent, nongeometric-mean measures of seismic intensity from two horizontal components of motion. *Bulletin of the Seismological Society of America*, *100*(4), 1830–1835.

Boore, D. M., & Atkinson, G. M. (2008). Ground-motion prediction equations for the average horizontal component of PGA, PGV, and 5%-damped PSA at spectral periods between 0.01 s and 10.0 s. *Earthquake Spectra*, *24*(1), 99–138.

Boore, D. M., & Kishida, T. (2017). Relations between some horizontal-component ground-motion intensity measures used in practice. *Bulletin of the Seismological Society of America*, *107*(1), 334–343.

Boore, D. M., Stewart, J. P., Seyhan, E., & Atkinson, G. M. (2014). NGA-West2 equations for predicting PGA, PGV, and 5% damped PSA for shallow crustal earthquakes. *Earthquake Spectra*, *30*(3), 1057–1085.

Candès, E. J., Wakin, M. B., & Boyd, S. P. (2008). Enhancing sparsity by reweightedℓ1 minimization. *Journal of Fourier Analysis and Applications*, *14*(5–6), 877–905. https://doi.org/10.1007/s00041-008-9045-x

Catto, J. L., & Dowdy, A. (2021). Understanding compound hazards from a weather system perspective. *Weather and Climate Extremes*, *32*, 100313.

Cha, E. J., & Ellingwood, B. R. (2013). Seismic risk mitigation of building structures: the role of risk aversion. *Structural Safety*, *40*, 11–19.

Choe, D.-E., Gardoni, P., Rosowsky, D., & Haukaas, T. (2008). Probabilistic capacity models and seismic fragility estimates for RC columns subject to corrosion. *Reliability Engineering \& System Safety*, *93*(3), 383–393.

Chopra, A. K., & Chintanapakdee, C. (2001). Comparing response of SDF systems to
near-fault and far-fault earthquake motions in the context of spectral regions.
Earthquake Engineering & Structural Dynamics, *30*(12), 1769–1789.

Chu, Z., Cheng, M., & Yu, N. N. (2021). A smart city is a less polluted city.
Technological Forecasting and Social Change, *172*, 121037.

Cimellaro, G. P., Reinhorn, A. M., & Bruneau, M. (2010). Seismic resilience of a
hospital system. *Structure and Infrastructure Engineering*, *6*(1–2), 127–144.

Cordova, P. P., Deierlein, G. G., Mehanny, S. S. F., & Cornell, C. A. (2000).
Development of a two-parameter seismic intensity measure and probabilistic
assessment procedure. *The Second US-Japan Workshop on Performance-Based
Earthquake Engineering Methodology for Reinforced Concrete Building
Structures*, 187–206.

Cornell, C. A., Jalayer, F., Hamburger, R. O., & Foutch, D. A. (2002). Probabilistic
basis for 2000 SAC federal emergency management agency steel moment frame
guidelines. *Journal of Structural Engineering*, *128*(4), 526–533.

Daniel, J. W., Gragg, W. B., Kaufman, L., & Stewart, G. W. (1976).
Reorthogonalization and stable algorithms for updating the Gram-Schmidt ??
factorization. *Mathematics of Computation*, *30*(136), 772–795.

Decò, A., Bocchini, P., & Frangopol, D. M. (2013). *A probabilistic approach for the
prediction of seismic resilience of bridges*. *January*, 1469–1487.
https://doi.org/10.1002/eqe

Dong, Y., & Frangopol, D. M. (2015). Risk and resilience assessment of bridges

under mainshock and aftershocks incorporating uncertainties. *Engineering

Structures*, *83*, 198–208. https://doi.org/10.1016/j.engstruct.2014.10.050

Dong, Y., & Frangopol, D. M. (2016a). Performance-based seismic assessment of

conventional and base-isolated steel buildings including environmental impact

and resilience. *Earthquake Engineering & Structural Dynamics*, *45*(5), 739–756.

Dong, Y., & Frangopol, D. M. (2016b). Probabilistic time-dependent multihazard life-

cycle assessment and resilience of bridges considering climate change. *Journal

of Performance of Constructed Facilities*, *30*(5), 4016034.

Dong, Y., & Frangopol, D. M. (2017). Probabilistic life-cycle cost-benefit analysis of

portfolios of buildings under flood hazard. *Engineering Structures*, *142*, 290–

299.

Dong, Y., Frangopol, D. M., & Sabatino, S. (2015). Optimizing bridge network

retrofit planning based on cost-benefit evaluation and multi-attribute utility

associated with sustainability. *Earthquake Spectra*, *31*(4), 2255–2280.

Dong, Y., Frangopol, D. M., & Saydam, D. (2013). Time-variant sustainability

assessment of seismically vulnerable bridges subjected to multiple hazards.

Earthquake Engineering & Structural Dynamics, *42*(10), 1451–1467.

Dong, Y., Frangopol, D. M., & Saydam, D. (2014). Sustainability of highway bridge

networks under seismic hazard. *Journal of Earthquake Engineering*, *18*(1), 41–

66.

Doostan, A., & Owhadi, H. (2011). A non-adapted sparse approximation of PDEs with stochastic inputs. *Journal of Computational Physics*, *230*(8), 3015–3034. https://doi.org/10.1016/j.jcp.2011.01.002

Du, A., & Padgett, J. E. (2020a). Investigation of multivariate seismic surrogate demand modeling for multi-response structural systems. *Engineering Structures*, *207*(January). https://doi.org/10.1016/j.engstruct.2020.110210

Du, A., & Padgett, J. E. (2020b). Multivariate return period-based ground motion selection for improved hazard consistency over a vector of intensity measures. *Earthquake Engineering and Structural Dynamics*, *March*, 1–21. https://doi.org/10.1002/eqe.3338

Du, A., Padgett, J. E., & Shafieezadeh, A. (2019). A posteriori optimal intensity measures for probabilistic seismic demand modeling. *Bulletin of Earthquake Engineering*, *17*(2), 681–706.

Du, Y. G., Clark, L. A., & Chan, A. H. C. (2005). Residual capacity of corroded reinforcing bars. *Magazine of Concrete Research*, *57*(3), 135–147.

Dueñas-Osorio, L., & Padgett, J. E. (2011). Seismic reliability assessment of bridges with user-defined system failure events. *Journal of Engineering Mechanics*, *137*(10), 680–690.

Eads, L., Miranda, E., & Lignos, D. G. (2015). Average spectral acceleration as an intensity measure for collapse risk assessment. *Earthquake Engineering & Structural Dynamics*, *44*(12), 2057–2073.

Ebad Sichani, M., & Padgett, J. E. (2019). Surrogate modelling to enable structural assessment of collision between vertical concrete dry casks. *Structure and Infrastructure Engineering*, *15*(9), 1137–1150. https://doi.org/10.1080/15732479.2019.1618878

Engelund, S., Edvardsen, C., & Mohr, L. (2000). General guidelines for durability design and redesign. *Report R15 of EU-Brite EuRam III Project BE95-1347 DuraCrete. Probabilistic Performance Based Durability Design of Concrete Structures*.

Enright, M. P., & Frangopol, D. M. (1998). Probabilistic analysis of resistance degradation of reinforced concrete bridge beams under corrosion. *Engineering Structures*, *20*(11), 960–971.

Fang, C., Liang, D., Zheng, Y., & Lu, S. (2022). Seismic performance of bridges with novel SMA cable-restrained high damping rubber bearings against near-fault ground motions. *Earthquake Engineering & Structural Dynamics*, *51*(1), 44–65.

Fang, C., Liang, D., Zheng, Y., Yam, M. C. H., & Sun, R. (2020). Rocking bridge piers equipped with shape memory alloy (SMA) washer springs. *Engineering Structures*, *214*, 110651.

Fang, C., Ping, Y., Zheng, Y., & Chen, Y. (2021). Probabilistic economic seismic loss estimation of steel braced frames incorporating emerging self-centering technologies. *Engineering Structures*, *241*, 112486.

Fang, C., Wang, W., He, C., & Chen, Y. (2017). Self-centring behaviour of steel and

steel-concrete composite connections equipped with NiTi SMA bolts.

Engineering Structures, *150*, 390–408.

Fang, C., Wang, W., Qiu, C., Hu, S., MacRae, G. A., & Eatherton, M. R. (2022).

Seismic resilient steel structures: A review of research, practice, challenges and

opportunities. *Journal of Constructional Steel Research*, *191*, 107172.

Fang, C., Yam, M. C. H., Lam, A. C. C., & Xie, L. (2014). Cyclic performance of

extended end-plate connections equipped with shape memory alloy bolts.

Journal of Constructional Steel Research, *94*, 122–136.

Faouzi, G., & Nasser, L. (2014). Scalar and vector probabilistic seismic hazard

analysis: Application for Algiers City. *Journal of Seismology*, *18*(2), 319–330.

https://doi.org/10.1007/s10950-013-9380-5

FEMA. (2020). Hazus Earthquake Model Technical Manual. *Federal Emergency

Management Agency*, *October*, 1–436.

FEMA, P. *58. Seismic performance assessment of buildings, Vol. 1--2. Washington,

D. C., September; 2012*.

Frangopol, D. M., & Bocchini, P. (2011). Resilience as optimization criterion for the

rehabilitation of bridges belonging to a transportation network subject to

earthquake. *Structures Congress 2011*, 2044–2055.

Frangopol, D. M., Lin, K.-Y., & Estes, A. C. (1997). Reliability of reinforced

concrete girders under corrosion attack. *Journal of Structural Engineering*,

123(3), 286–297.

Gautam, D., & Dong, Y. (2018). Multi-hazard vulnerability of structures and lifelines

due to the 2015 Gorkha earthquake and 2017 central Nepal flash flood. *Journal

of Building Engineering*, *17*, 196–201.

Gencturk, B., Hossain, K., & Lahourpour, S. (2016). Life cycle sustainability

assessment of RC buildings in seismic regions. *Engineering Structures*, *110*,

347–362.

Georgiou, G., Manan, A., & Cooper, J. E. (2012). Modeling composite wing

aeroelastic behavior with uncertain damage severity and material properties.

Mechanical Systems and Signal Processing, *32*, 32–43.

Ghosh, J., & Padgett, J. E. (2010). Aging considerations in the development of time-

dependent seismic fragility curves. *Journal of Structural Engineering*, *136*(12),

1497–1511.

Ghosh, J., & Padgett, J. E. (2012). Impact of multiple component deterioration and

exposure conditions on seismic vulnerability of concrete bridges. *Earthquakes

and Structures*, *3*(5), 649–673.

Ghosh, J., Padgett, J. E., & Dueñas-Osorio, L. (2013). Surrogate modeling and failure

surface visualization for efficient seismic vulnerability assessment of highway

bridges. *Probabilistic Engineering Mechanics*, *34*, 189–199.

https://doi.org/10.1016/j.probengmech.2013.09.003

Ghosh, J., & Sood, P. (2016). Consideration of time-evolving capacity distributions

and improved degradation models for seismic fragility assessment of aging

highway bridges. *Reliability Engineering & System Safety*, *154*, 197–218.

Giouvanidis, A., & Dong, Y. (2020). Seismic loss and resilience assessment of single-

column rocking bridges. *BULLETIN OF EARTHQUAKE ENGINEERING*.

Giovenale, P., Cornell, C. A., & Esteva, L. (2004). Comparing the adequacy of

alternative ground motion intensity measures for the estimation of structural

responses. *Earthquake Engineering & Structural Dynamics*, *33*(8), 951–979.

Goda, K, & Hong, H. P. (2006). Optimal seismic design considering risk attitude,

societal tolerable risk level, and life quality criterion. *Journal of Structural

Engineering*, *132*(12), 2027–2035.

Goda, Katsuichiro, & Tesfamariam, S. (2015). Multi-variate seismic demand

modelling using copulas: Application to non-ductile reinforced concrete frame in

Victoria, Canada. *Structural Safety*, *56*, 39–51.

Golub, G. H., & Van Loan, C. F. (1996). Matrix Computations Johns Hopkins

University Press. *Baltimore and London*.

Gordon, E. (2002). A Seismic Risk Model for A Designated Highway System: Comparing Predicted Actual Damage from the Loma Prieta Earthquake. *Mid-America Earthquake Center*.

Guo, H.-Y., Dong, Y., Gardoni, P., & Gu, X.-L. (2021). Time-Dependent Reliability Analysis Based on Point-Evolution Kernel Density Estimation: Comprehensive Approach with Continuous and Shock Deterioration and Maintenance. *ASCE-ASME Journal of Risk and Uncertainty in Engineering Systems, Part A: Civil Engineering*, *7*(3), 4021032.

Guo, H., Dong, Y., Bastidas-Arteaga, E., & Gu, X.-L. (2021). Probabilistic failure analysis, performance assessment, and sensitivity analysis of corroded reinforced concrete structures. *Engineering Failure Analysis*, *124*, 105328.

Guo, X., Dias, D., Carvajal, C., Peyras, L., & Breul, P. (2018). Reliability analysis of embankment dam sliding stability using the sparse polynomial chaos expansion. *Engineering Structures*, *174*(February), 295–307.

Han, Q., Du, X., Liu, J., Li, Z., Li, L., & Zhao, J. (2009). Seismic damage of highway bridges during the 2008 Wenchuan earthquake. *Earthquake Engineering and Engineering Vibration*, *8*(2), 263–273.

Härdle, W. K., Chen, C. Y.-H., & Overbeck, L. (2017). *Applied quantitative finance*. Springer.

Hariri-Ardebili, M A, & Saouma, V. E. (2016). Probabilistic seismic demand model and optimal intensity measure for concrete dams. *Structural Safety*, *59*, 67–85.

Hariri-Ardebili, Mohammad Amin, & Sudret, B. (2020). Polynomial chaos expansion

    for uncertainty quantification of dam engineering problems. *Engineering*

    Structures, *203*(June). https://doi.org/10.1016/j.engstruct.2019.109631

Hwang, C.-L., & Yoon, K. (1981). Methods for multiple attribute decision making. In

    Multiple attribute decision making (pp. 58–191). Springer.

Jakeman, J. D., Eldred, M. S., & Sargsyan, K. (2015). Enhancing ℓ1-minimization

    estimates of polynomial chaos expansions using basis selection. *Journal of*

    Computational Physics, *289*, 18–34. https://doi.org/10.1016/j.jcp.2015.02.025

Jalayer, F., & Cornell, C. A. (2009). Alternative non-linear demand estimation

    methods for probability-based seismic assessments. *Earthquake Engineering &*

    Structural Dynamics, *38*(8), 951–972.

Jalayer, F., De Risi, R., & Manfredi, G. (2015). Bayesian Cloud Analysis: efficient

    structural fragility assessment using linear regression. *Bulletin of Earthquake*

    Engineering, *13*(4), 1183–1203.

Jeon, J. S., Mangalathu, S., Song, J., & Desroches, R. (2019). Parameterized Seismic

    Fragility Curves for Curved Multi-frame Concrete Box-Girder Bridges Using

    Bayesian Parameter Estimation. *Journal of Earthquake Engineering*, *23*(6), 954–

    979. https://doi.org/10.1080/13632469.2017.1342291

Joe, H. (1997). *Multivariate models and multivariate dependence concepts*. CRC

    Press.

Kang, W.-H., Song, J., & Gardoni, P. (2008). Matrix-based system reliability method and applications to bridge networks. *Reliability Engineering \& System Safety*, *93*(11), 1584–1593.

Kashani, M. M., Crewe, A. J., & Alexander, N. A. (2013). Nonlinear stress--strain behaviour of corrosion-damaged reinforcing bars including inelastic buckling. *Engineering Structures*, *48*, 417–429.

Kazantzi, A. K., & Vamvatsikos, D. (2015). Intensity measure selection for vulnerability studies of building classes. *Earthquake Engineering & Structural Dynamics*, *44*(15), 2677–2694.

Kiremidjian, A. A., & Basöz, N. I. (1997). Evaluation of bridge damage data from recent earthquakes. In *Bulletin NCEER* (Vol. 11, Issue 2, pp. 1–7). US National Center for Earthquake Engineering Research.

Kohrangi, M., Bazzurro, P., & Vamvatsikos, D. (2016). Vector and scalar IMs in structural response estimation, Part I: Hazard analysis. *Earthquake Spectra*, *32*(3), 1507–1524.

Kong, J., & Simonovic, S. P. (2019). Probabilistic multiple hazard resilience model of an interdependent infrastructure system. *Risk Analysis*, *39*(8), 1843–1863.

Kurowicka, D., & Cooke, R. M. (2007). Sampling algorithms for generating joint uniform distributions using the vine-copula method. *Computational Statistics & Data Analysis*, *51*(6), 2889–2906.

Lahdelma, R., & Salminen, P. (2001). SMAA-2: Stochastic multicriteria acceptability analysis for group decision making. *Operations Research*, *49*(3), 444–454.

Lee, T.-H., & Mosalam, K. M. (2006). *Probabilistic seismic evaluation of reinforced concrete structural components and systems*. Pacific Earthquake Engineering Research Center.

Li, S., Wang, J., & Alam, M. S. (2021). Seismic performance assessment of a multispan continuous isolated highway bridge with superelastic shape memory alloy reinforced piers and restraining devices. *Earthquake Engineering & Structural Dynamics*, *50*(2), 673–691.

Li, Y., Dong, Y., Frangopol, D. M., & Gautam, D. (2020a). Long-term resilience and loss assessment of highway bridges under multiple natural hazards. *Structure and Infrastructure Engineering*, *16*(4), 626–641. https://doi.org/10.1080/15732479.2019.1699936

Li, Y., Dong, Y., Frangopol, D. M., & Gautam, D. (2020b). Long-term resilience and loss assessment of highway bridges under multiple natural hazards. *Structure and Infrastructure Engineering*, *16*(4), 626–641.

Li, Y., Dong, Y., & Qian, J. (2020). Higher-order analysis of probabilistic long-term loss under nonstationary hazards. *Reliability Engineering and System Safety*, *203*(June), 107092. https://doi.org/10.1016/j.ress.2020.107092

Liang, D., Zheng, Y., Fang, C., Yam, M. C. H., & Zhang, C. (2020). Shape memory alloy (SMA)-cable-controlled sliding bearings: development, testing, and system behavior. *Smart Materials and Structures*, *29*(8), 85006.

Muhammad & Lim, C. W. (2021). Natural seismic metamaterials: the role of tree branches in the birth of Rayleigh wave bandgap for ground born vibration attenuation. *Trees*, *35*(4), 1299–1315.

Muhammad, Lim, C. W., & Reddy, J. N. (2019). Built-up structural steel sections as seismic metamaterials for surface wave attenuation with low frequency wide bandgap in layered soil medium. *Engineering Structures*, *188*, 440–451.

Liu, M., Wen, Y. K., & Burns, S. A. (2004). Life cycle cost oriented seismic design optimization of steel moment frame structures with risk-taking preference. *Engineering Structures*, *26*(10), 1407–1421.

Mangalathu, S., Heo, G., & Jeon, J. S. (2018). Artificial neural network based multi-dimensional fragility development of skewed concrete bridge classes. *Engineering Structures*, *162*(January), 166–176.

Mangalathu, S., Jeon, J. S., & DesRoches, R. (2018). Critical uncertainty parameters influencing seismic performance of bridges using Lasso regression. *Earthquake Engineering and Structural Dynamics*, *47*(3), 784–801.

Mangalathu, S., Jeon, J. S., Padgett, J. E., & DesRoches, R. (2016). ANCOVA-based grouping of bridge classes for seismic fragility assessment. *Engineering Structures*, *123*, 379–394. https://doi.org/10.1016/j.engstruct.2016.05.054

Marelli, S., & Sudret, B. (2015). UQLab user manual--Polynomial chaos expansions. *Chair of Risk, Safety & Uncertainty Quantification, ETH Zürich, 0.9-104 Edition*, 97–110.

Matthews, M. V, Ellsworth, W. L., & Reasenberg, P. A. (2002). A Brownian model for recurrent earthquakes. *Bulletin of the Seismological Society of America*, *92*(6), 2233–2250.

Mazzoni, S., McKenna, F., Scott, M. H., Fenves, G. L., & others. (2006). OpenSees command language manual. *Pacific Earthquake Engineering Research (PEER) Center*, *264*, 137–158.

Miller, M., & Baker, J. (2015). Ground-motion intensity and damage map selection for probabilistic infrastructure network risk assessment using optimization. *Earthquake Engineering & Structural Dynamics*, *44*(7), 1139–1156.

Minaie, E., & Moon, F. (2017). Practical and simplified approach for quantifying bridge resilience. *Journal of Infrastructure Systems*, *23*(4), 1–11.

Morgan, J. N., & Sonquist, J. A. (1963). Problems in the analysis of survey data, and a proposal. *Journal of the American Statistical Association*, *58*(302), 415–434.

Mosalam, K. M., Alibrandi, U., Lee, H., & Armengou, J. (2018). Performance-based engineering and multi-criteria decision analysis for sustainable and resilient building design. *Structural Safety*, *74*, 1–13.

Muhammad, Wu, T., & Lim, C. W. (2020). Forest trees as naturally available seismic metamaterials: low frequency rayleigh wave with extremely wide bandgaps. *International Journal of Structural Stability and Dynamics*, *20*(14), 2043014.

Muntasir Billah, A. H. M., & Alam, M. S. (2015). Seismic fragility assessment of concrete bridge pier reinforced with superelastic shape memory alloy. *Earthquake Spectra*, *31*(3), 1515–1541.

Nelsen, R. B. (2006). An Introduction to Copulas. Springer, New York. *MR2197664*.

Ni, P., Xia, Y., Li, J., & Hao, H. (2019). Using polynomial chaos expansion for uncertainty and sensitivity analysis of bridge structures. *Mechanical Systems and Signal Processing*, *119*, 293–311.

Nielson, B. G. (2005). *Analytical fragility curves for highway bridges in moderate seismic zones*. Georgia Institute of Technology.

Nielson, B. G., & DesRoches, R. (2007). Seismic fragility methodology for highway bridges using a component level approach. *Earthquake Engineering & Structural Dynamics*, *36*(6), 823–839.

Okhrin, O., Ristig, A., & Xu, Y.-F. (2017). *Copulae in High Dimensions: An Introduction* (Issue August).

Padgett, Jamie E, & DesRoches, R. (2008). Methodology for the development of analytical fragility curves for retrofitted bridges. *Earthquake Engineering & Structural Dynamics*, *37*(8), 1157–1174.

Padgett, Jamie E, Nielson, B. G., & DesRoches, R. (2008). Selection of optimal

intensity measures in probabilistic seismic demand models of highway bridge

portfolios. *Earthquake Engineering & Structural Dynamics*, *37*(5), 711–725.

Padgett, Jamie E, & Tapia, C. (2013). Sustainability of natural hazard risk mitigation:

Life cycle analysis of environmental indicators for bridge infrastructure. *Journal

of Infrastructure Systems*, *19*(4), 395–408.

Padgett, Jamie Ellen. (2007). *SEISMIC VULNERABILITY ASSESSMENT OF

RETROFITTED BRIDGES USING PROBABILISTIC METHODS*.

Palar, P. S., Zuhal, L. R., Shimoyama, K., & Tsuchiya, T. (2018). Global sensitivity

analysis via multi-fidelity polynomial chaos expansion. *Reliability Engineering

and System Safety*, *170*(October 2017), 175–190.

Pandey, M. D., & Van Der Weide, J. A. M. (2017). Stochastic renewal process

models for estimation of damage cost over the life-cycle of a structure.

Structural Safety, *67*, 27–38.

Qian, J., & Dong, Y. (2020). Multi-criteria decision making for seismic intensity

measure selection considering uncertainty. *Earthquake Engineering and

Structural Dynamics*, *March*, 1–20. https://doi.org/10.1002/eqe.3280

Qian, J., Dong, Y., & Frangopol, D. M. (2022). Probabilistic long-term resilience of

bridges under seismic and deterioration processes. *Proceedings of the Institution

of Civil Engineers-Bridge Engineering, (Ahead of Print)*.

Rackwitz, R. (2002). Optimization and risk acceptability based on the life quality index. *Structural Safety*, *24*(2–4), 297–331.

Rasmussen, C. E., & Williams, C. K. I. (2006). Gaussian Processes for Machine Learning the MIT Press. *Cambridge, Mass*.

Rokach, L., & Maimon, O. Z. (2008). *Data mining with decision trees: theory and applications* (Vol. 69). World scientific.

Salehi, S., Raisee, M., Cervantes, M. J., & Nourbakhsh, A. (2017). Efficient uncertainty quantification of stochastic CFD problems using sparse polynomial chaos and compressed sensing. *Computers and Fluids*, *154*, 296–321.

Saltelli, A., Ratto, M., Andres, T., Campolongo, F., Cariboni, J., Gatelli, D., Saisana, M., & Tarantola, S. (2008). *Global sensitivity analysis: the primer*. John Wiley & Sons.

Santa-Cruz, S., Córdova, G. F. de, Rivera-Holguin, M., Vilela, M., Arana, V., & Palomino, J. (2016). Social sustainability dimensions in the seismic risk reduction of public schools: a case study of Lima, Peru. *Sustainability: Science, Practice and Policy*, *12*(1), 34–46.

Shekhar, S., Ghosh, J., & Padgett, J. E. (2018). Seismic life-cycle cost analysis of ageing highway bridges under chloride exposure conditions: Modelling and recommendations. *Structure and Infrastructure Engineering*, *14*(7), 941–966.

Shome, N. (1999). *Probabilistic seismic demand analysis of nonlinear structures*. Stanford University.

Shrestha, B., & Hao, H. (2016). Parametric study of seismic performance of super-elastic shape memory alloy-reinforced bridge piers. *Structure and Infrastructure Engineering*, *12*(9), 1076–1089.

Sinou, J.-J., & Jacquelin, E. (2015). Influence of Polynomial Chaos expansion order on an uncertain asymmetric rotor system response. *Mechanical Systems and Signal Processing*, *50*, 718–731.

Smola, A. J., & Schölkopf, B. (2000). *Sparse greedy matrix approximation for machine learning*.

Sobol, I. M. (2001). Global sensitivity indices for nonlinear mathematical models and their Monte Carlo estimates. *Mathematics and Computers in Simulation*, *55*(1–3), 271–280.

Stanford, L. (1998). *The Northridge Earthquake: Vulnerability and Disaster*. Taylor & Francis.

Stein, S. M., Young, G. K., Trent, R. E., & Pearson, D. R. (1999). Prioritizing scour vulnerable bridges using risk. *Journal of Infrastructure Systems*, *5*(3), 95–101.

Stewart, M. G., & Al-Harthy, A. (2008). Pitting corrosion and structural reliability of corroding RC structures: Experimental data and probabilistic analysis. *Reliability Engineering & System Safety*, *93*(3), 373–382.

Sudret, B. (2008). Global sensitivity analysis using polynomial chaos expansions. *Reliability Engineering and System Safety*, *93*(7), 964–979.

Takahashi, Y., Kiureghian, A. Der, & Ang, A. H.-S. (2004). Life-cycle cost analysis based on a renewal model of earthquake occurrences. *Earthquake Engineering & Structural Dynamics*, *33*(7), 859–880.

Tang, X.-S., Li, D.-Q., Zhou, C.-B., & Phoon, K.-K. (2015). Copula-based approaches for evaluating slope reliability under incomplete probability information. *Structural Safety*, *52*, 90–99.

Tang, X.-S., Li, D.-Q., Zhou, C.-B., Phoon, K.-K., & Zhang, L.-M. (2013). Impact of copulas for modeling bivariate distributions on system reliability. *Structural Safety*, *44*, 80–90.

Tapia, C., Ghosh, J., & Padgett, J. E. (2011). Life cycle performance metrics for aging and seismically vulnerable bridges. *Structures Congress 2011*, 1937–1948.

Tarakji, G. (1992). Lessons not Learned from 1989 Loma Prieta Earthquake. *Journal of Professional Issues in Engineering Education and Practice*, *118*(2), 132–138.

Tarantola, S., Becker, W., & Zeitz, D. (2012). A comparison of two sampling methods for global sensitivity analysis. *Computer Physics Communications*, *183*(5), 1061–1072.

Tierney, K. J. (1997). Business impacts of the Northridge earthquake. *Journal of Contingencies and Crisis Management*, *5*(2), 87–97.

Timmerman, P. (1981). Vulnerability resilience and collapse ofsociety. *A ReviewofModels and Possible Climatic Appli-Cations. Toronto, Canada. Institute for Environmental Studies, University of Toronto*.

Titanium extraction technology, Northwest Institute For Non-ferrous Metal Research.

Torre, E., Marelli, S., Embrechts, P., & Sudret, B. (2019a). A general framework for data-driven uncertainty quantification under complex input dependencies using vine copulas. *Probabilistic Engineering Mechanics*, *55*(August 2018), 1–16.

Torre, E., Marelli, S., Embrechts, P., & Sudret, B. (2019b). Data-driven polynomial chaos expansion for machine learning regression. *Journal of Computational Physics*, *388*, 601–623.

Towhata, I. (2013). Long-term effects of earthquake-induced slope failures. *Proceedings of the 7th International Conference on Case Histories in Geotechnical Engineering, Chicago*, *10*.

Tremblay, R., Lacerte, M., & Christopoulos, C. (2008). Seismic response of multistory buildings with self-centering energy dissipative steel braces. *Journal of Structural Engineering*, *134*(1), 108–120.

Triantaphyllou, E. (2000). Multi-criteria decision making methods. In *Multi-criteria decision making methods: A comparative study* (pp. 5–21). Springer.

Tu, B., Dong, Y., & Fang, Z. (2019). Time-dependent reliability and redundancy of corroded prestressed concrete bridges at material, component, and system levels. *Journal of Bridge Engineering*, *24*(9), 4019085.

Tzeng, G.-H., & Huang, J.-J. (2011). *Multiple attribute decision making: methods and applications*. CRC press.

Vamvatsikos, D., & Cornell, C. A. (2002). Incremental dynamic analysis. *Earthquake Engineering & Structural Dynamics*, *31*(3), 491–514.

Vu, K. A. T., & Stewart, M. G. (2000). Structural reliability of concrete bridges including improved chloride-induced corrosion models. *Structural Safety*, *22*(4), 313–333.

Wakabayashi, H., & Kameda, H. (1992). Network performance of highway systems under earthquake effects: A case study of the 1989 Loma Prieta earthquake. *Proceedings of the US-Japan Workshop on Earthquake Disaster Prevention for Lifeline Systems. Tsukuba Science City, Japan*, *215232*.

Wan, H. P., Ren, W. X., & Todd, M. D. (2020). Arbitrary polynomial chaos expansion method for uncertainty quantification and global sensitivity analysis in structural dynamics. *Mechanical Systems and Signal Processing*, *142*, 106732.

Wang, B., Zhu, S., Casciati, F., Chen, K., & Jiang, H. (2021). Cyclic behavior and deformation mechanism of superelastic SMA U-shaped dampers under in-plane and out-of-plane loadings. *Smart Materials and Structures*, *30*(5), 55009.

Wang, B., Zhu, S., Chen, K., & Huang, J. (2020). Development of superelastic SMA angles as seismic-resistant self-centering devices. *Engineering Structures*, *218*, 110836.

Wang, C., Zhang, H., Ellingwood, B. R., Guo, Y., Mahmoud, H., & Li, Q. (2020). Assessing post-hazard damage costs to a community's residential buildings exposed to tropical cyclones. *Structure and Infrastructure Engineering*, *17*(4), 443–453.

Wang, F., Harindintwali, J. D., Yuan, Z., Wang, M., Wang, F., Li, S., Yin, Z., Huang, L., Fu, Y., Li, L., & others. (2021). Technologies and perspectives for achieving carbon neutrality. *The Innovation*, *2*(4), 100180.

Wang, J. P., Tang, X.-S., Wu, Y.-M., & Li, D.-Q. (2018). Copula-based earthquake early warning decision-making strategy. *Soil Dynamics and Earthquake Engineering*, *115*, 324–330.

Wang, M.-X., Huang, D., Wang, G., Du, W., & Li, D.-Q. (2020). Vine Copula-Based Dependence Modeling of Multivariate Ground-Motion Intensity Measures and the Impact on Probabilistic Seismic Slope Displacement Hazard Analysis. *Bulletin of the Seismological Society of America*.

Wang, M., Zhang, H., Dai, H., & Shen, L. (2022). A deep learning-aided seismic fragility analysis method for bridges. *Structures*, *40*, 1056–1064.

Wang, X., Shafieezadeh, A., & Ye, A. (2018). Optimal intensity measures for probabilistic seismic demand modeling of extended pile-shaft-supported bridges

in liquefied and laterally spreading ground. *Bulletin of Earthquake Engineering*, *16*(1), 229–257.

Wang, Z., Dueñas-Osorio, L., & Padgett, J. E. (2014). Influence of scour effects on the seismic response of reinforced concrete bridges. *Engineering Structures*, *76*, 202–214.

Wei, W., Samuelsson, P. B., Tilliander, A., Gyllenram, R., & Jönsson, P. G. (2020). *Energy Consumption and Greenhouse Gas Emissions of Nickel Products*.

Werner, S. D., Taylor, C. E., Cho, S., Lavoie, J.-P., Huyck, C. K., Eitzel, C., Chung, H., & Eguchi, R. T. (2006). *Redars 2 methodology and software for seismic risk analysis of highway systems*.

Wiener, N. (1938). The homogeneous chaos. *American Journal of Mathematics*, *60*(4), 897–936.

Wu, L. Z., Li, S. H., Zhang, M., & Zhang, L. M. (2019). A new method for classifying rock mass quality based on MCS and TOPSIS. *Environmental Earth Sciences*, *78*(6), 1–11.

Wu, S. Q., & Law, S. S. (2012). Evaluating the response statistics of an uncertain bridge--vehicle system. *Mechanical Systems and Signal Processing*, *27*, 576–589.

Xiang, N., Chen, X., & Alam, M. S. (2020). Probabilistic seismic fragility and loss

    analysis of concrete bridge piers with superelastic shape memory alloy-steel

    coupled reinforcing bars. *Engineering Structures*, *207*(April 2019), 110229.

Xie, Y. (2017). *Seismic modeling, quantifying and protection of highway bridges*

    considering shaking and lateral spreading. UCLA.

Xie, Y., Zheng, Q., Yang, C.-S. W., Zhang, W., DesRoches, R., Padgett, J. E., &

    Taciroglu, E. (2019). Probabilistic models of abutment backfills for regional

    seismic assessment of highway bridges in California. *Engineering Structures*,

    180, 452–467.

Yang, D. Y., & Frangopol, D. M. (2019). Life-cycle management of deteriorating

    civil infrastructure considering resilience to lifetime hazards: A general approach

    based on renewal-reward processes. *Reliability Engineering & System Safety*,

    183, 197–212.

Yang, Y., Wu, Q., Wang, Y., Qin, W. & Lu, K. (2019). Dynamic characteristics of

    cracked uncertain hollow-shaft. *Mechanical Systems and Signal Processing*, *124*,

    36–48.

Zandi Hanjari, K., Kettil, P., & Lundgren, K. (2011). Analysis of mechanical behavior

    of corroded reinforced concrete structures. *ACI Structural Journal*, *108*(5), 532–

    541.

Zareian, F., & Krawinkler, H. (2006). *Simplified performance-based earthquake*

    engineering. Stanford University Stanford, CA.

Zeng, D., Zhang, H., & Wang, C. (2020). Modelling correlated damage of spatially

distributed building portfolios under scenario tropical cyclones. *Structural

Safety*, *87*, 101978.

Zhao, X., Ma, X., Chen, B., Shang, Y., & Song, M. (2022). Challenges toward carbon

neutrality in China: Strategies and countermeasures. *Resources, Conservation

and Recycling*, *176*, 105959.

Zhao, X., Shang, Y., & Song, M. (2020). Industrial structure distortion and urban

ecological efficiency from the perspective of green entrepreneurial ecosystems.

Socio-Economic Planning Sciences, *72*, 100757.

Zheng, Y., & Dong, Y. (2019). Performance-based assessment of bridges with steel-

SMA reinforced piers in a life-cycle context by numerical approach. *Bulletin of

Earthquake Engineering*, *17*(3), 1667–1688.

Zheng, Y., Dong, Y., & Li, Y. (2018). Resilience and life-cycle performance of smart

bridges with shape memory alloy (SMA)-cable-based bearings. *Construction and

Building Materials*, *158*, 389–400.

Zheng, Y., Fang, C., Liang, D., & Sun, R. (2021). An innovative seismic-resilient

bridge with shape memory alloy-washer-based footing rocking RC piers. *Journal

of Intelligent Material Systems and Structures*, *32*(5), 549–567.

Zhou, T., & Li, A. Q. (2019). Seismic fragility assessment of highway bridges using

D-vine copulas. *Bulletin of Earthquake Engineering*, *17*(2), 927–955.

Zhu, S., & Zhang, Y. (2008). Seismic analysis of concentrically braced frame systems with self-centering friction damping braces. *Journal of Structural Engineering*, *134*(1), 121–131.